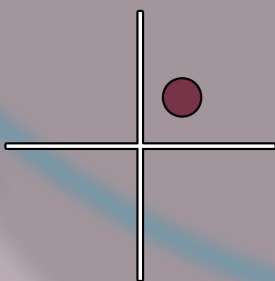
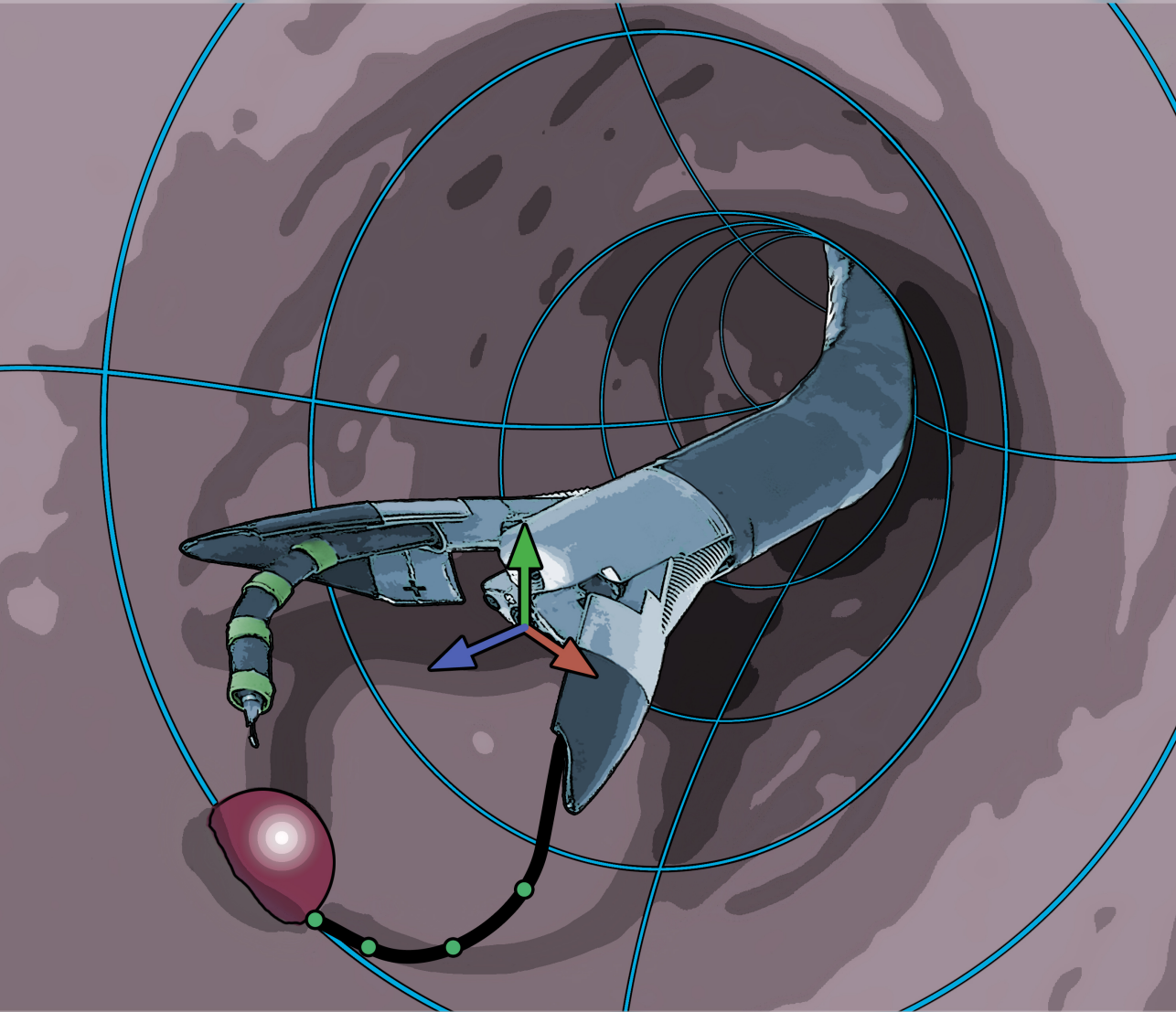


Image-Based Robotic Steering of Advanced Flexible Endoscopes and Instruments

Rob Reilink



x: 11.7
y: 26.4
z: 25.9

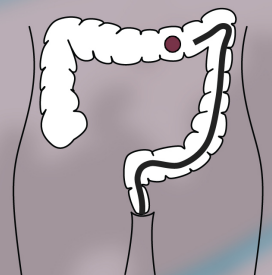


Image-Based Robotic Steering
of Advanced Flexible Endoscopes and Instruments

Rob Reilink

Dissertation committee:

Chairman:

prof. dr. ir. A. J. Mouthaan University of Twente

Promotors:

prof. dr. ir. S. Stramigioli University of Twente

prof. dr. I.A.M.J. Broeders University of Twente

Assistant promotor:

dr. S. Misra University of Twente

Members:

prof. S. Hutchinson M.Sc. Ph.D. University of Illinois at Urbana-Champaign

prof. dr. J. Dankelman Delft University of Technology

prof. dr. ir. M. Steinbuch Eindhoven University of Technology

prof. dr. ir. F.J.A.M. van Houten University of Twente

dr. ir. F. van der Heijden University of Twente

This research has been conducted at the Robotics and Mechatronics group of the University of Twente, within the TeleFLEX project. The research was funded by the Dutch Ministry of Economic Affairs and the Province of Overijssel, within the Pieken in de Delta (PIDON) initiative. The Anubis endoscopic instrument was provided by Karl Storz GmbH & Co. KG, Tuttlingen, Germany. The Olympus endoscope was provided by Olympus Corp., Tokyo, Japan.

The cover illustration shows the Anubis flexible endoscope within the gastrointestinal tract. Illustration by Derk Reilink.

ISBN: 978-90-365-3526-7

DOI: 10.3990/1.9789036535267

Printed by Wöhrmann Print Service, Zutphen, The Netherlands.

Copyright 2013, Rob Reilink, Enschede, The Netherlands.

IMAGE-BASED ROBOTIC STEERING
OF ADVANCED FLEXIBLE ENDOSCOPES AND INSTRUMENTS

PROEFSCHRIFT

ter verkrijging van
de graad van doctor aan de Universiteit Twente,
op gezag van de rector magnificus,
prof. dr. H. Brinksma,
volgens besluit van het College voor Promoties
in het openbaar te verdedigen
op vrijdag 26 april 2013 om 16:45 uur

door

Rob Reilink

geboren op 6 oktober 1983

te Waspik

Dit proefschrift is goedgekeurd door:

prof. dr. ir. S. Stramigioli, promotor
prof. dr. I.A.M.J. Broeders, promotor
dr. S. Misra, assistent-promotor

Samenvatting

Flexibele endoscopie stelt de arts in staat om de holle organen van de patiënt te bekijken op een minimaal invasieve manier. Er worden geavanceerde flexibele endoscopen en instrumenten ontwikkeld, die de arts in staat zullen stellen om interventies uit te voeren die niet mogelijk zijn met conventionele flexibele endoscopen. Deze endoscopen en instrumenten zijn echter moeilijk te gebruiken, omdat ze niet intuïtief en niet ergonomisch zijn, en omdat meerdere artsen nodig zijn om een procedure uit te voeren. Een mogelijke oplossing hiervoor is een robotisch systeem, dat één enkele arts in staat zal stellen om een geavanceerde flexibele endoscoop en de instrumenten te bedienen. Hierbij bestuurt de arts alle vrijheidsgraden vanuit een chirurgische console. In dit proefschrift worden verschillende aspecten van robotische besturing van de endoscoop en de instrumenten behandeld.

Voor de endoscoop is het sturen van de tip met behulp van een haptische joystick onderzocht. In dit onderzoek hebben beginners en ervaren endoscopisten een endoscoop bestuurd en daarmee een gesimuleerde colonoscopie uitgevoerd. De haptische terugkoppeling die werd gegeven hielp de proefpersoon om de endoscoop in de richting van het lumen te sturen. De locatie van het lumen werd bepaald op basis van beeldverwerking. Deze aansturingmethode werd vergeleken met conventionele besturing van de endoscoop en met aansturing zonder haptische terugkoppeling. De resultaten tonen aan dat een haptische joystick een geschikt alternatief kan zijn voor het aansturen van geavanceerde flexibele endoscopen. De resultaten geven een indicatie dat het gebruik van haptische terugkoppeling de pijn van de patiënt kan verminderen.

Voor het besturen van de endoscopische instrumenten is de hysteresis die in het systeem aanwezig is een belangrijk probleem. Deze hysteresis wordt veroorzaakt door wrijving, flexibiliteit en speling. De systeemparemeters zijn in het algemeen onbekend, aangezien zij veranderen tijdens de procedure. Het is daarom gewenst dat deze parameters on-line geschat worden om vervolgens de hysteresis te verminderen. Deze parameterschatting vereist dat de actuele positie van de tip van het instrument bekend is. Het is echter lastig om sensoren toe te voegen om deze positie te meten, aangezien de beschikbare ruimte in de tip zeer beperkt is, en omdat de instrumenten bestand moeten zijn tegen sterilisatie. Daarom wordt een methode aangedragen die de positie van de tip kan schatten op basis van de endoscopische beelden. Dit is gerealiseerd middels een 'virtual visual servoing'-benadering. Hierbij wordt een model van het instrument continue aangepast zodat het model overeenkomt met het werkelijke instrument dat in de endoscopische beelden zichtbaar is. Twee methoden worden vergeleken: één met en één zonder het gebruik van visuele markeringen op het instrument. De twee methoden presteren vergelijkbaar, en zijn in staat om de positie van de tip te schatten met een RMS fout van minder dan 1.8mm horizontaal, verticaal en

in de richting van de optische as van de camera.

Er wordt een systeem aangedragen dat de hysteresis schat en compenseert op basis van de endoscopische beelden, om zo de hysteresis die aanwezig is in de endoscopische instrumenten terug te dringen. In een experimentele validatie is aangetoond dat dit systeem de hysteresis met ongeveer 75% kan verminderen in alle vrijheidsgraden van het instrument.

Afsluitend is tele-operatie van een hysteresis-gecompenseerd instrument geëvalueerd. Deze methode wordt vergeleken met de handmatige bedieningsgreep die oorspronkelijk gebruikt werd om het instrument aan te sturen. Proefpersonen hebben met beide methoden een taak uitgevoerd waarbij ze punten moesten aantikken. De resultaten tonen aan dat de tijd die nodig is om de taak te volbrengen significant wordt verminderd met 67% bij het gebruik van tele-operatie.

De resultaten van deze studies tonen aan dat het aansturen van geavanceerde flexibele endoscopen en hun instrumenten vanuit een chirurgische console mogelijk is. Dit zal één enkele arts in staat stellen om met een flexibele endoscoop interventies uit te voeren die tot op heden niet mogelijk zijn.

Summary

Flexible endoscopy allows the physician to examine the internal body cavities of the patient in a minimally invasive way. Advanced flexible endoscopes and instruments are being developed, which will enable the physician to perform interventions that are not possible using conventional endoscopes. However, these endoscopes and instruments are difficult to use, because they are not ergonomic, their control is not intuitive, and multiple physicians are required to work together to perform the procedure. In order to allow a single physician to control the advanced flexible endoscope and the instruments in an intuitive way, a robotic solution is envisioned, in which the physician controls all degrees of freedom from a surgical console. In this thesis, several aspects of the robotic steering of the endoscope and the instruments are investigated.

For the endoscope, steering the tip with a haptic device is evaluated. In this study, novices and experienced endoscopists steer the endoscope to perform a simulated colonoscopy. Haptic feedback is provided to help the subject to steer the endoscope towards the lumen. The lumen position is detected from the endoscopic images using image processing. This steering method was compared to conventional endoscope steering, and to steering without haptic feedback. The results show that using a haptic device may be a viable alternative method for the steering of advanced flexible endoscopes. The results suggest that the use of haptic cues may reduce patient discomfort.

For the steering of the instruments, hysteresis that is present in the system is a major issue. This is caused by friction, compliance, and free play. The system parameters are in general unknown, since they change during the procedure. Thus, online estimation of the system parameters is desired in order to reduce the hysteresis effect. This estimation requires knowing the position of the tip of the endoscopic instrument. However, adding sensors to measure the tip position is difficult, since the space at the tip is very limited and because of sterilization issues. Therefore, estimation of the tip position from the endoscopic images is proposed. This is realized using a virtual visual servoing approach. A model of the instrument is updated to match the actual instrument that is observed in the endoscopic images. Two methods are compared: with and without adding visual markers to the endoscopic instrument. The two methods perform similarly, and are able to estimate the position of the tip with an RMS error of less than 1.8mm in the horizontal, vertical, and away-from-camera directions.

The developed tip position estimation algorithm is used to improve the control of the endoscopic instruments. A hysteresis estimation and compensation system is proposed which uses the estimated instrument tip position to reduce the hysteresis that is present. In an experimental validation, it is shown that the proposed system can reduce the hysteresis by approximately 75% for all degrees of freedom of the instrument.

Finally, tele-operated steering of the hysteresis-compensated instrument is evaluated. The method is compared to the manual control handle that was originally used to steer the instrument. Subjects performed a tapping task using both methods. The results show a reduction of the average task completion time by 67% when using the tele-operated steering.

The results from these studies show that steering an advanced flexible endoscope and its instruments from a surgical console is viable. This would enable a single physician to perform interventions using a flexible endoscope that are currently not yet possible.

Contents

1	Introduction	1
1.1	Advanced endoscopic procedures	3
1.1.1	Mechanical advanced flexible endoscopes	4
1.1.2	Robotic advanced flexible endoscopes	4
1.2	Objectives	6
1.3	Contributions	7
1.4	Outline	9
2	Flexible endoscope steering using haptic guidance	11
2.1	Introduction	12
2.1.1	Steering using haptic guidance	13
2.1.2	Evaluation	14
2.1.3	Outline	14
2.2	Materials and Methods	14
2.2.1	Endoscope control using haptic guidance	14
2.2.2	Experimental conditions	18
2.2.3	Survey	19
2.2.4	Experimental methods	20
2.2.5	Evaluation criteria	20
2.2.6	Test setup	21
2.2.7	Tip control	22
2.2.8	Procedure	22
2.2.9	Subjects	23
2.3	Results	24
2.4	Discussion	26
3	3D position estimation of flexible instruments	29
3.1	Introduction	30
3.2	Materials and Methods	31
3.2.1	Kinematics model of the instrument	32
3.2.2	Endoscopic camera model	33
3.2.3	Feature detection	34
3.2.4	State estimation	35
3.2.5	Experimental evaluation	40
3.3	Results	43
3.4	Discussion	46

4	Image-based hysteresis reduction for the control of flexible instruments	47
4.1	Introduction	48
4.2	Hysteresis Compensation and Estimation	49
4.2.1	Compensation	50
4.2.2	Estimation	51
4.3	Kinematics and Camera Models	51
4.3.1	Kinematics Model of the Instrument	53
4.3.2	Camera Model	53
4.4	Image-based State Estimation	54
4.4.1	Image Processing	54
4.4.2	State Estimation	55
4.5	Evaluation	55
4.5.1	Experimental Setup	57
4.5.2	Experimental Plan	57
4.5.3	Results	58
4.6	Conclusion	60
5	Evaluation of robotically controlled advanced endoscopic instruments	61
5.1	Introduction	62
5.2	Materials and Methods	62
5.2.1	Advanced flexible endoscopic instruments	63
5.2.2	Robotic control of the endoscopic instrument	63
5.2.3	Experimental methods	65
5.2.4	Experimental conditions	66
5.2.5	Procedure	69
5.2.6	Subjects	69
5.3	Results	70
5.4	Discussion	71
6	Conclusions	73
A	Derivation of the forward kinematics of the instrument model	77
	Bibliography	80
	Nawoord	87

Flexible endoscopy is a procedure that allows the physician to inspect the internal body cavities of the patient. Common procedures are gastroscopy (Fig. 1.1), colonoscopy, and bronchoscopy. These are inspection of the stomach, the colon, and the lungs, respectively. Dedicated endoscopes are available for each procedure, varying in length, diameter, the size and amount of instrument channels, etc. However, the key components are similar. A flexible endoscope consists of a flexible tube, with a camera at the distal tip. This tip can be articulated in one or two degrees of freedom (DOFs) by manipulating control wheels at the control handle that is located at the proximal end of the endoscope. Light is delivered to the tip through optical fibers. The endoscopic images are displayed on a monitor. One or more instrument channels may be available that allow the physician to perform interventions such as taking biopsies, or removing malignant tissue (polypectomy, mucosectomy). Furthermore, auxiliary functions such as inflation, suction, and lens flushing may be available.

Since the development of the first modern flexible endoscopes in the 1950's and 1960's, the steering method for flexible endoscopes has remained the same [60]. The control handle is held by the physician and control wheels are operated to articulate the tip of the endoscope. Yet, this design has important shortcomings that may influence the performance of the physician, especially when performing difficult procedures. The main shortcomings are the poor ergonomics and the lack of intuitiveness. In the conventional steering approach, two concentric wheels operate two orthogonal tip motions, as illustrated in Fig. 1.2. This is counterintuitive. Experienced physicians can work with this approach, but it takes significant time to learn [24].

Furthermore, the shape of the control handle makes it difficult for the physician to operate both control wheels single-handedly. For some groups of physicians (especially females), the handle is too big to reach to the inner control wheel. Thus, bimanual operation may be required. However, this means that the help of

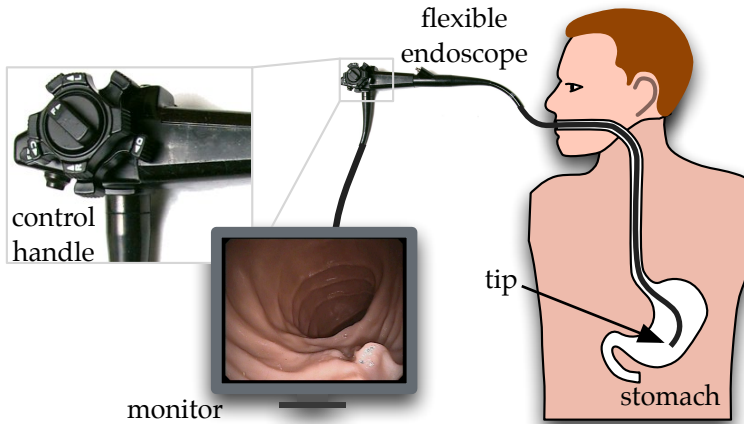


Figure 1.1: Gastroscopy: The flexible endoscope is inserted through the mouth and the esophagus into the stomach. The tip of the endoscope is controlled using the control handle. The endoscopic images are observed on a monitor.

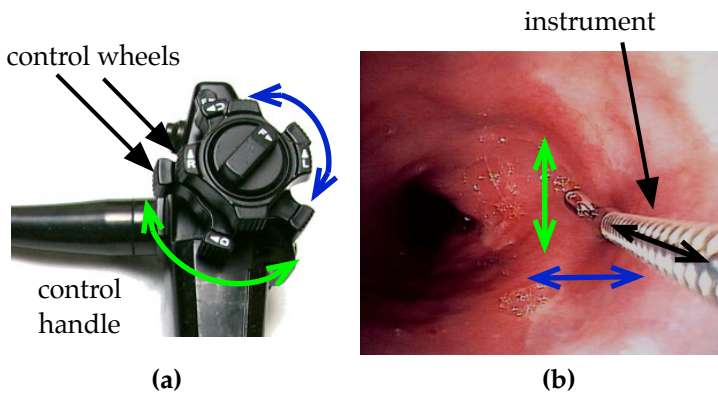


Figure 1.2: The two concentric wheels of the control handle control two orthogonal tip motions, up/down and left/right. This control is not intuitive. Endoscopic image (b) shows an endoscopic instrument that emerges from the endoscope tip and can move forward and backward in the direction of the tip.

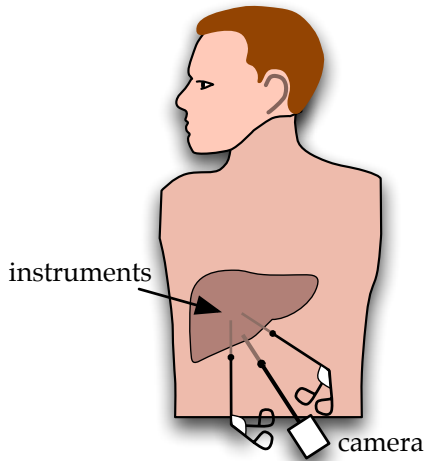


Figure 1.3: Laparoscopy: The camera and the instruments enter the abdominal cavity through ports, which are inserted through small incisions in the abdominal wall.

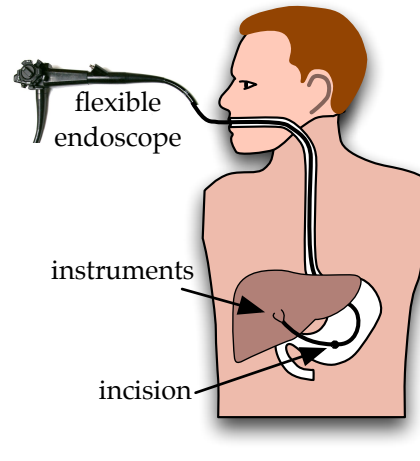


Figure 1.4: NOTES: The abdominal cavity is reached through an incision in an organ. Instruments emerge from the tip of the endoscope.

an assistant is required in order to insert the endoscope into the patient, and to operate an endoscopic instrument. It is difficult to obtain optimal coordination between the physician and the assistant.

1.1 Advanced endoscopic procedures

Over the last decade, physicians have explored the possibility to use flexible endoscopes to perform more advanced procedures such as appendectomy and cholecystectomy [15, 19, 27, 36, 43]. Currently, these procedures are generally performed laparoscopically. In laparoscopy, small incisions are made through which a rigid endoscopic camera and rigid instruments are inserted (Fig. 1.3, [12]). By using flexible endoscopes, the physician could approach the site of the intervention through one of the natural body openings (mouth, anus, or vagina), without leaving any visible external scars. This approach is called Natural Orifice Transluminal Endoscopic Surgery (NOTES, Fig. 1.4). Possible benefits of the NOTES approach over laparoscopy include the fact that there are no visible scars, reduced post-procedural pain, and shorter hospital stay [15, 27]. However, these benefits are not yet clinically proven.

An important drawback of flexible endoscopy with regard to laparoscopy is the limited triangulation. In laparoscopy, the instruments enter the workspace

from the sides (Fig. 1.3). This enables the physician to grasp tissue with one instrument, while cutting it with another instrument. In conventional flexible endoscopes, the instruments emerge from the tip in the direction of the camera (Fig. 1.2b). This limits the workspace of the instruments, and makes it difficult for the physician to perform bimanual procedures.

The development of NOTES procedures has led to new endoscopic devices, several of which will be described in this section [28, 62]. Key points of attention for NOTES devices are improved dexterity, and the realization of triangulation [62].

1.1.1 Mechanical advanced flexible endoscopes

Several endoscopes have been developed to enable NOTES procedures (Fig. 1.5). The Olympus R-scope (XGIF-2TQ160R, Olympus Corp., Japan) is a flexible endoscope with two articulated instrument channels. One of the instruments can be moved up and down, the other can be moved to the left and to the right. This functionality improves the dexterity of the instruments.

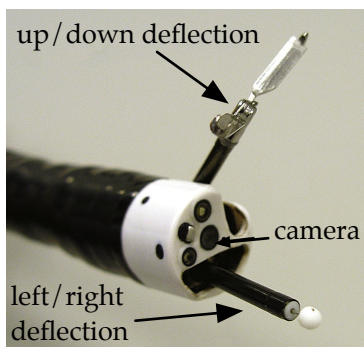
The Karl Storz ANUBIS endoscope (Karl Storz GmbH & Co. KG, Germany) is a prototype endoscope that has two instruments with improved dexterity, and one conventional instrument channel. A novel feature of this endoscope is that it has a tip that folds open. While the tip is closed, the endoscope is small enough to transverse the gastrointestinal tract, and when opened, the instruments emerge from the tip at an angle so as to provide triangulation. Each instrument is controlled with a control handle.

The Olympus EndoSamurai (Olympus Corp., Japan) is a similar prototype endoscope. It has two steerable instrument arms, and one conventional instrument channel. The instrument motions are controlled by a console, which provides the physician with two manipulators that are similar to laparoscopic instruments. The system requires at least two physicians, one for controlling the instruments and another to steer the endoscope itself.

1.1.2 Robotic advanced flexible endoscopes

Advanced flexible endoscopes have more degrees of freedom than conventional endoscopes. As such, the aforementioned endoscopes require several physicians to co-operate to steer the complete endoscope and the instruments. This is undesirable because of associated costs, and because optimal coordination between the physicians is difficult. Furthermore, the accuracy and intuitiveness of the controls are limited.

In order to overcome these shortcomings, the use of robotics to enhance the capabilities of the endoscope is considered promising [43]. In the case of rigid endoscopy, the Da Vinci robotic endoscopic system (Intuitive Surgical Inc., Sunnyvale, USA) has many advantages over conventional rigid endoscopy in terms of intuitiveness and ergonomics. For flexible endoscopy, several research groups are working on robotically actuated flexible endoscope systems (Fig. 1.6).



(a) Olympus R-Scope



(b) Karl Storz Anubis



(c) Olympus EndoSamurai



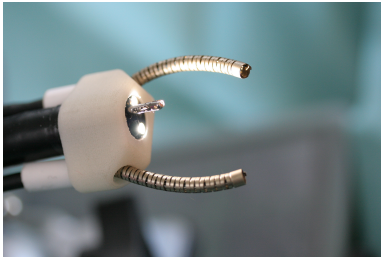
(d) EndoSamurai console

Figure 1.5: Mechanical advanced flexible endoscopes: (a) The Olympus R-scope has two deflecting instrument channels [4]. (b) The Karl Storz Anubis endoscope has a tip that folds open. (c, d) The Olympus EndoSamurai has two instruments that are operated from a console [26]. Images (a), (c), (d) reprinted with permission from Elsevier.

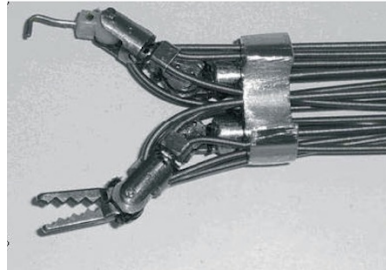
The IRCAD institute (l'Institut de Recherche contre les Cancers de l'Appareil Digestif, Strassbourg, France) has developed an experimental setup that attaches to a conventional gastroscope, and provides two additional instruments that are robotically actuated and have four degrees of freedom each. The motion of the tip of the endoscope is also actuated [5].

The MASTER (Master and Slave Translumenal Endoscopic Robot) is a system with two cable-driven instruments that attaches to the tip of a conventional flexible endoscope [41]. This system is developed by the Nanyang Technological University (Singapore). Unlike the other systems, the MASTER instruments cannot be changed during the procedure.

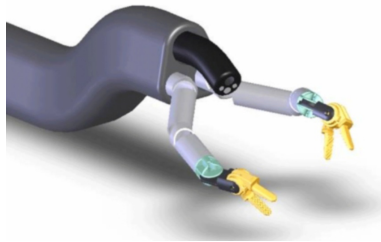
The ViaCath system is based on an overtube, that guides a flexible endoscope



(a) IRCAD endoscope attachment



(b) MASTER



(c) ViaCath

Figure 1.6: Robotic advanced flexible endoscopes: (a) The IRCAD has developed a prototype tip attachment [8] (©IEEE 2010) (b) The MASTER has articulated cable-driven instruments [42] (©2008 John Wiley & Sons, Ltd). (c) The ViaCath system uses an overtube [1] (©IEEE 2007).

and two instruments [1]. This system is developed at Purdue University (West Lafayette, USA). Both instruments with a bending tip as well as articulating instruments have been developed for this system.

All of these three systems are extensions to existing flexible endoscopes. This approach is also used for the work described in this thesis. However, the work is equally applicable to the existing mechanical advanced flexible endoscopes that were mentioned before, provided that robotic actuation is added to these endoscopes.

1.2 Objectives

The research described in this thesis is conducted within the TeleFLEX project at the University of Twente. The goal of this project is to develop a surgical tele-manipulation system that allows controlling all required flexible instruments in an intuitive way. Fig. 1.7 illustrates what such a tele-manipulation might look like in the future. Within this project, this thesis is focussed on the control systems



Figure 1.7: The TeleFLEX project focusses on an intuitive tele-manipulation system for surgical interventions with flexible instruments.

that are required to realize accurate and intuitive steering. The objectives are to realize intuitive steering of the endoscope and the instruments, and to evaluate the performance.

1.3 Contributions

The main contributions of this thesis are threefold:

- A method was developed that allows a user to steer the tip of the endoscope using a haptic device, while providing haptic guidance that is computed based on the endoscopic images.
- A state-estimation algorithm was developed that is able to estimate the position of the tip of the endoscopic instrument, based solely on the endoscopic images.
- This state-estimation algorithm was used to estimate the hysteresis that is present in the endoscopic instrument on-line, and a control strategy was developed to reduce this hysteresis.

Within the context of the thesis, the following articles were published in, or are under review for, international peer-reviewed journals.

- R. Reilink, S. Stramigioli, A. M. L. Kappers, and S. Misra. Evaluation of flexible endoscope steering using haptic guidance. *International Journal of Medical Robotics and Computer Assisted Surgery*, 7(2):178–186, 2011.
- R. Reilink, S. Stramigioli, and S. Misra. 3D position estimation of flexible instruments: marker-less and marker-based methods. *International Journal of Computer Assisted Radiology and Surgery*, 2012. Published online.

- R. Reilink, S. Stramigioli, and S. Misra. Image-based hysteresis reduction for the control of flexible endoscopic instruments. *Mechatronics*, 2013. Under review.
- R. Reilink, A. M. L. Kappers, S. Stramigioli, and S. Misra. Evaluation of robotically controlled advanced endoscopic instruments. *International Journal of Medical Robotics and Computer Assisted Surgery*, 2013. Accepted for publication.

The following papers were published at leading international peer-reviewed conferences:

- R. Reilink, G. de Bruin, M. Franken, M. A. Mariani, S. Misra, and S. Stramigioli. Endoscopic camera control by head movements for thoracic surgery. In *Proc. 3rd IEEE RAS/EMBS Int'l. Conf. on Biomedical Robotics and Biomechatronics (BioRob)*, pages 510–515, Tokyo, Japan, Sept. 2010.
- R. Reilink, S. Stramigioli, and S. Misra. Image-based flexible endoscope steering. In *Proc. IEEE/RSJ Int'l. Conf. on Intelligent Robots and Systems*, pages 2339–2344, Taipei, Taiwan, Oct. 2010.
- R. Reilink, S. Stramigioli, and S. Misra. Three-dimensional pose reconstruction of flexible instruments from endoscopic images. In *Proc. IEEE/RSJ Int'l. Conf. on Intelligent Robots and Systems (IROS)*, pages 2076–2082, San Francisco, USA, Sept. 2011.
- N. Kuperij, R. Reilink, M. P. Schwartz, S. Stramigioli, S. Misra, and I. A. M. J. Broeders. Design of a user interface for intuitive colonoscope control. In *Proc. IEEE/RSJ Int'l. Conf. on Intelligent Robots and Systems (IROS)*, pages 937–942, San Francisco, USA, Sept. 2011.
- R. Reilink, S. Stramigioli, and S. Misra. Pose reconstruction of flexible instruments from endoscopic images using markers. In *Proc. IEEE Int'l. Conf. on Robotics and Automation (ICRA)*, pages 2939–2943, St. Paul, USA, May 2012.
- R. Reilink, S. Stramigioli, and S. Misra. Image-based pose estimation of an endoscopic instrument. In *Proc. IEEE Int'l. Conf. on Robotics and Automation (ICRA)*, pages 3555–3556, St. Paul, USA, May 2012.
- N. van der Stap, R. Reilink, S. Misra, I. A. M. J. Broeders, and F. van der Heijden. The use of the focus of expansion for automated steering of flexible endoscopes. In *Proc. 4th IEEE RAS/EMBS Int'l. Conf. on Biomedical Robotics and Biomechatronics (BioRob)*, pages 13–18, Rome, Italy, June 2012.

1.4 Outline

The chapters in this thesis are adapted versions of the aforementioned articles that are published in, or under review for, international peer-reviewed journals. The thesis is outlined as follows:

Chapter 2 investigates methods for steering the tip of flexible endoscopes. The conventional steering method with two concentric wheels is compared to intuitive steering with a haptic device. Haptic feedback is given to guide the physician towards the desired direction. This desired direction is computed based on the endoscopic images. The steering methods are compared in a human subjects experiment.

Chapter 3 deals with the three-dimensional position estimation of advanced endoscopic instruments. The purpose is to reconstruct the three-dimensional tip position of the endoscopic instrument using solely the two-dimensional endoscopic images as an input. Two methods are compared: with and without adding markers to the instrument.

Chapter 4 uses the algorithms that were proposed in chapter 3 to reduce the hysteresis that is present in the actuation of endoscopic instruments. The estimated 3D tip position is used to estimate the hysteresis parameters. Using the estimated hysteresis parameters, the instrument is actuated so as to reduce the hysteresis. The hysteresis reduction is experimentally evaluated.

Chapter 5 evaluates robotic steering of the advanced endoscopic instruments. Robotic steering is compared to conventional steering in a human subjects experiment.

Finally, chapter 6 concludes and gives recommendations for future work.

Flexible endoscope steering using haptic guidance

Steering the tip of a flexible endoscope relies on the physician's dexterity and experience. For complex flexible endoscopes, the conventional controls may be inadequate. In this chapter, a steering method based on a multi-degree-of-freedom haptic device is presented. Haptic cues are generated based on the endoscopic images. The method is compared against steering using the same haptic device without haptic cues, and against conventional steering. Human-subject studies were conducted in which 12 students and 6 expert gastroenterologists participated. The results show that experts are significantly faster when using the conventional method as compared to using the haptic device, either with or without haptic cues. However, it is expected that the performance of the subjects with the haptic device will increase with experience. Thus, using a haptic device may be a viable alternative to the conventional method for the control of complex flexible endoscopes. The results suggest that the use of haptic cues may reduce the patient discomfort.

2.1 Introduction

A common endoscopic procedure is colonoscopy, the inspection of the colon via the rectum. The physician uses a flexible endoscope which is steered through the body by controlling the orientation of the endoscope tip, while manually feeding the endoscope into the patient. The tip orientation is controlled using two wheels that are positioned on the control handle (Fig. 2.1). The endoscopic images are displayed on a monitor.

During a colonoscopy, the endoscope is first introduced up to the cecum, which is at the end of the colon, and then the visual inspection is performed while the endoscope is slowly retracted. In order to maneuver the endoscope through the colon, and to ensure appropriate investigation and visualization, the physician needs to steer the tip accurately.

Usually, the physician uses one hand to operate the wheels that control the tip, while the other hand is used to feed the endoscope into the patient [60]. However, it is sometimes necessary for the physician to use both his/her hands in order to manipulate the wheels accurately. Since control of the tip requires spatial reasoning and dexterity, the introduction of the endoscope may take significant time and effort. The control of the tip orientation is also not very intuitive, as the two directions (up/down and left/right) are controlled by two concentric wheels. Therefore, experience is necessary to master this procedure [24]. This makes endoscope steering difficult, especially for less experienced physicians.

Despite the fact that current endoscopes are already difficult to steer, complex endoscopes are currently being developed, which require significantly more effort to control. These include the EndoSAMURAI (Olympus Corp., Tokyo, Japan) and the ANUBIS (Karl Storz GmbH & Co. KG, Tuttlingen, Germany). These endoscopes feature sophisticated instruments, to be used for Natural Orifice Transluminal Endoscopic Surgery (NOTES). These endoscopes can no longer be controlled by one physician. Controlling the endoscope by multiple physicians is undesirable because of the costs and the fact that this requires optimal cooperation between the physicians. A solution would be to use a multi-degree-of-freedom (DOF) steering device to control all instrument motions by one physician.

Allemann *et al.* have developed a system, where they use a joystick to control a flexible endoscope [2]. In their evaluation, both novices and experienced physicians required significantly more time to complete a given task when using a joystick compared to conventional controls. However, in their experiment, rate control was applied whereas position control might be more appropriate for this task. According to Zhai [63], rate control is suitable when the workspace is large, while position control is more suitable when accurate manipulation in a limited workspace is required. The latter is the case for endoscope steering. Furthermore, the design of the setup limited the rotation of the endoscope around its axis.

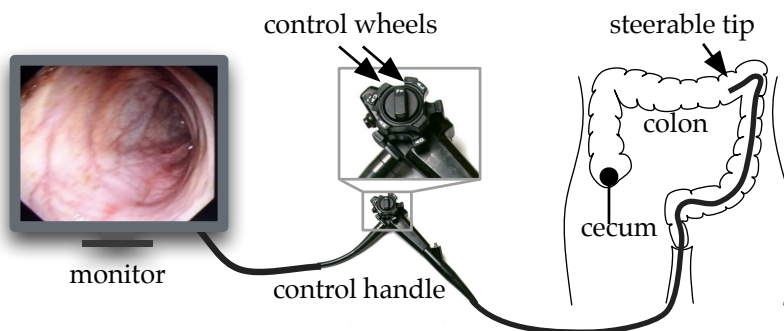


Figure 2.1: Conventional colonoscopy: The physician uses the control wheels to control the steerable tip while feeding the endoscope into the patient up to the cecum. The endoscopic images are observed on the monitor.

2.1.1 Steering using haptic guidance

In this research study, we will describe a control method that is designed to assist the physician in his/her steering task and we will evaluate its effectiveness. Our approach is to let the physician control the endoscope tip via a multi-DOF haptic device. This allows for intuitive coupling between the motion of the input device and the endoscope tip, while enabling the use of haptic guidance to steer the physician in a certain direction.

By using a multi-DOF haptic device, the control can be designed such that the movement of the endoscope tip matches the movement of the physician's hand. This will result in intuitive steering. Additionally, the haptic device can be held in one hand, as opposed to the conventional control handle which may require both hands to operate. Single-handed steering allows the physician to use his other hand to feed the endoscope into the patient without the use of an assistant, improving the quality of the endoscopy [60].

In addition to making the endoscope control intuitive, haptic cues may also be given to the physician. Haptic cues can be used to improve the physician's performance [9, 10]. They play an important role in the training of physicians using medical simulators [17]. Using haptic guidance, we aim to help the physician to steer the endoscope tip in the appropriate direction i.e., in the direction of the lumen. Implementing haptic guidance can increase the performance of the physician, and reduce the cognitive load. This increases the cognitive reserve available for the task of the inspection of the endoscopic images for abnormalities [13].

In order to apply the haptic guidance, the direction of the lumen needs to be determined. Using a purely mechanics-based approach to calculate the lumen direction would require an accurate model of the endoscope as it interacts with the soft tissue. Since the *in vivo* tissue parameters are unknown, such an approach is realistically not possible. Therefore, we will use the endoscopic images to deter-

mine the direction of the lumen.

An overview of endoscopic image processing algorithms is given by Liedlgruber [32]. However, these algorithms were not designed for use in the feedback of a control loop. As such, their performance in terms of robustness and processing speed may not be sufficient. Therefore, we will use an algorithm based on our previous work [47]. This algorithm finds the dark region of the endoscopic image, which is the part that is furthest away from the camera. This is the center of the lumen.

2.1.2 Evaluation

The endoscope steering system was evaluated using a flexible endoscopy simulator. Human-subject studies were performed in which 18 subjects, 6 experienced gastroenterologists and 12 students, performed a simulated colonoscopy. Every subject used three different control methods: a haptic device with haptic guidance, the same haptic device without haptic guidance, and a conventional endoscope. Their performance was evaluated on introduction time, patient discomfort and percentage of the colon that was visualized.

2.1.3 Outline

This chapter is structured as follows: In Section 2.2, the endoscope control method using haptic guidance will be discussed and the experiment that was designed to evaluate this control method will be described. Section 2.3 will show the results of this experiment. Section 2.4 concludes with the discussion.

2.2 Materials and Methods

2.2.1 Endoscope control using haptic guidance

During the introduction phase of the colonoscopy, the physician generally tries to steer the endoscopic camera in the direction of the lumen. In this situation, the lumen is centered in the image, as shown in Fig. 2.2. This way, the endoscopic camera stays clear of the colon wall. In order to assist the physician in this steering task, we will apply a force on the haptic device in the direction that is required to get the lumen centered. The algorithms that are used to determine the center of the lumen, and to provide the haptic guidance, are described in this section.

Lumen center detection

In order to find the preferred direction of the endoscope, the endoscopic images will be used to find the direction of the lumen. Possible approaches are optical flow-based methods and image intensity-based methods.

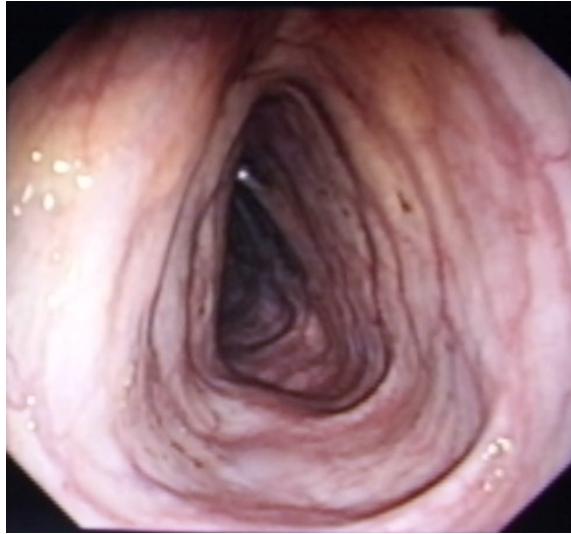


Figure 2.2: Endoscopic image within the colon: The physician tries to keep the lumen centered in the image while introducing the endoscope.

In an optical flow-based approach, subsequent images are used to determine the motion of the environment as perceived by the camera [57]. This approach was successfully used to steer mobile robots away from obstacles and through corridors [18, 37], a task which is similar to steering the endoscope through an endoluminal path. In previous work, we have successfully used such an approach in a simulated environment, which modelled the view of a camera moving through a rigid model of the colon [47]. However, we have found that in reality, the robustness suffers from the motion blur caused by sudden motions that occur when the endoscope is introduced manually.

In an image intensity-based approach, a single image is used to find the direction of the lumen. Due to the arrangement of the camera and the light source in the endoscope tip, areas that are further away from the camera appear darker in the image (Fig. 2.2). This approach was successfully used for the purpose of lumen contour detection [30, 59] and polyp detection [3, 61]. In this research, adaptive thresholding is used to obtain a binary image, which is then processed to obtain the shape of the lumen wall. However, for our purpose of finding the appropriate haptic guidance, we are not interested in an accurate description of the lumen wall shape, but more in a robust estimation of the lumen center. Moreover, the algorithm should run in real time at the speed of the vision system (25 frames per second). In order to meet these requirements, we have developed an algorithm that uses the centroid of the dark area of the image [47]. This algorithm will be briefly described in the remainder of this section.

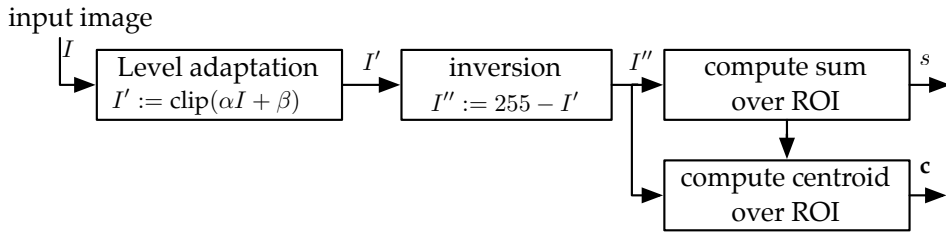


Figure 2.3: From the input image that is captured (I), the levels are adapted resulting in image I' . This image is then inverted yielding I'' . From I'' , the sum s and centroid c are computed.

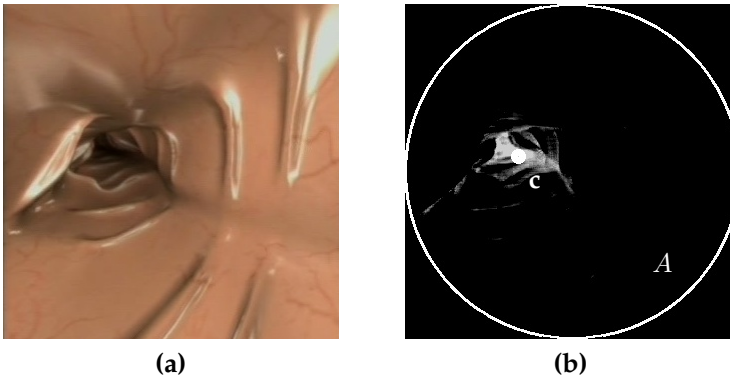


Figure 2.4: Lumen center detection: (a) Example image from the endoscopy simulator that is provided as input to the algorithm. (b) Image (a) with the levels adapted and inverted. The ROI A and the centroid c are marked.

The block diagram of the algorithm is shown in Fig. 2.3. A color image is captured, which is converted to a grayscale image $I(x, y)$, where x and y indicate the horizontal and vertical pixel positions, respectively. $x = 0, y = 0$ represents the center of the endoscopic view. $I(x, y)$ is an 8 bit image, with 0 and 255 representing black and white, respectively. An example input image is shown in Fig. 2.4a.

In order to extract the dark area of the image, first the intensity levels are adapted to increase the contrast. We define the function

$$\text{clip}(x) = \begin{cases} 0 & \text{if } x < 0 \\ x & \text{if } 0 \leq x \leq 255 \\ 255 & \text{if } x > 255 \end{cases}, \quad (2.1)$$

and adapt the intensity levels according to

$$I'(x, y) := \text{clip}(\alpha I(x, y) + \beta), \quad (2.2)$$

where $I'(x, y)$ is the resulting image, and α and β are parameters. α and β influence the contrast and the intensity levels of $I'(x, y)$, respectively. When the

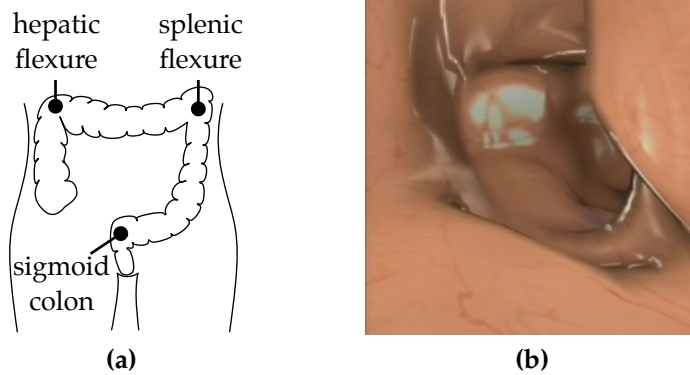


Figure 2.5: Areas where the lumen cannot be found: (a) This situation occurs in the hepatic flexure, the splenic flexure, and the sigmoid colon. (b) Example image of this situation in the hepatic flexure.

algorithm is used in a simulated environment, parameters α and β can be constant values, since the illumination will be constant. For the experiments, $\alpha = 16$ and $\beta = 0$ were used. In order to use the algorithm in a real environment, it may be necessary to automatically adapt α and β when changes in illumination condition occur. An algorithm that performs such adaptation was presented in [47].

The resulting image $I'(x, y)$ with increased contrast is inverted:

$$I''(x, y) := 255 - I'(x, y) \quad . \quad (2.3)$$

The inverted image $I''(x, y)$ (Fig. 2.4b) clearly shows the direction of the lumen. In this image, a circular region of interest (ROI) A is defined, as shown in the figure. A circular ROI is used, because the corners of the image often contain dark regions due to the lighting of the endoscope. These regions would adversely affect the algorithm. Over this region, sum s and centroid \mathbf{c} of the resulting inverted image $I''(x, y)$ are computed as:

$$s := \sum_{(x,y) \in A} I''(x, y) \quad , \quad (2.4)$$

$$\mathbf{c} := \frac{\sum_{(x,y) \in A} \begin{bmatrix} x \\ y \end{bmatrix} I''(x, y)}{s} \quad . \quad (2.5)$$

We define the resulting centroid \mathbf{c} as the direction of the lumen. The sum s will be used to determine whether the direction of the lumen could be found. When s is small, this means that the dark region is small, and the direction \mathbf{c} that was found is likely to be inaccurate. If s is smaller than a given threshold, it is assumed that the direction could not be found. This situation occurs in the 'bends' in the colon, the sigmoid colon, the hepatic flexure, and the splenic flexure, as shown in Fig. 2.5. In these cases, no haptic guidance will be given, since direction of the

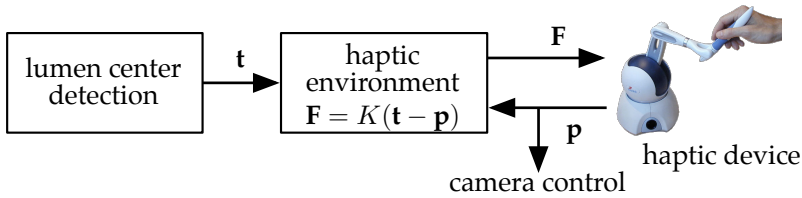


Figure 2.6: The target \mathbf{t} is computed by the lumen center detection. This is used as the equilibrium point for a linear spring model with stiffness K . The spring model is used to compute the force \mathbf{F} for a given position \mathbf{p} of the haptic device.

lumen cannot be determined reliably. Enabling and disabling the haptic guidance is done using a smooth transition in order not to present sudden force changes to the user.

Haptic guidance based on lumen position

The image processing algorithm described in the previous section computes the lumen position \mathbf{c} . This direction is used to display a haptic environment to the subject. The 2D lumen position \mathbf{c} is mapped to 3D target point \mathbf{t} on a vertical plane:

$$\mathbf{t} := \begin{bmatrix} c_x \\ c_y \\ 0 \end{bmatrix}, \quad (2.6)$$

We have implemented a linear spring model that will pull the user in the direction of the target \mathbf{t} , given by

$$\mathbf{F} = K(\mathbf{t} - \mathbf{p}), \quad (2.7)$$

where \mathbf{F} is the applied force, \mathbf{p} is the position of the haptic device and K is the stiffness. The model represents a linear spring with its equilibrium point at $\mathbf{p} = \mathbf{t}$. This is illustrated in Fig. 2.6. Position \mathbf{p} is used to steer the endoscopic camera.

The haptics loop is computed at an update rate of 1000Hz. The parameters are updated by the image processing algorithm at the frame rate of 25 frames per second. We have evaluated this steering method in a human-subject experimental study which will be described in the following sections.

2.2.2 Experimental conditions

In order to assess the value of endoscope steering using haptic guidance, we have compared it with two other endoscope steering methods. These methods are *conventional steering* and *steering without haptics*, as described in the remainder of this section.

Conventional steering

The *conventional steering* method allows the subject to control the endoscope tip using the endoscope control wheels. This method of steering is the current practice in flexible endoscopy. However, this method of steering is not very intuitive, which makes the control hard to learn [24]. We will use this method as a reference to compare the other steering methods.

Steering without haptics

The *steering without haptics* experimental condition uses the same haptic interface that is used to evaluate the *steering with haptics*, but does not provide the haptic feedback. This method is included to evaluate whether differences between the *conventional steering* and the *steering with haptics* are caused by the use of haptics, or by the difference in the interface.

Steering with haptics

The experimental condition *steering with haptics* is the steering method that was described in section 2.2.1. Haptic guidance is provided to the subject, based on the endoscopic images.

2.2.3 Survey

In order to determine an appropriate model to perform the flexible endoscopy, we conducted a survey among five gastroenterologists. Four of them were also part of our expert subject group of the experiment. We asked them to give their opinion on the anatomical model, the flexible endoscopy simulator, and the animal model. These are three models that are commonly used for flexible endoscopy training [60]. We also asked them which criteria should be used to assess how well someone performs a flexible endoscopy.

Two out of the five gastroenterologists had used an anatomical model. They indicated that the ‘feel’ of the model is better than interacting with a computer simulation, although it is different from a real patient. On the other hand, they found the images less realistic compared to a computer simulation.

Four out of the five gastroenterologists had used a prepared animal model (usually a pig’s stomach) to practice a specific skill e.g., placing a clip onto tissue. The skill to be practiced is described as realistic, but the model does not allow practicing the feeding of the endoscope. One gastroenterologist had used living animal models, these were described as being realistic.

All gastroenterologists had used a flexible endoscopy simulator. It was commonly described as being quite realistic. The subjects do not find the force-feedback that the simulator gives very realistic, but they consider this a minor limitation. Despite this limitation, they consider the simulator useful for the evaluation of basic steering skills.

Regarding the evaluation of the endoscopy, the consensus of the participants of the survey is that it is important to reach the target quickly, without too much discomfort for the patient. Subsequently, enough time should be spent to inspect the colon thoroughly during retraction. Both during introduction and retraction, it is in general important to keep the lumen well centered.

During colonoscopy, reaching the cecum (the boundary between small bowel and colon) and the time required to do so are important criteria. During retraction, the entire colonic mucosa should be visualized properly.

2.2.4 Experimental methods

Based on the survey results, we have selected to use the flexible endoscopy simulator as the model, since it is considered reasonably realistic and it is easy to use (unlike e.g. animal models). Another advantage over other models is that it outputs several metrics that can be used to evaluate the performance. These include the total procedure time, the introduction time, the insertion depth, the patient discomfort, and the percentage of the mucosa that was visualized. The latter two are not available on any of the other models. Furthermore, using a simulator ensures that the test environment is identical for all subjects and for all experimental conditions.

We have used the AccuTouch endoscopy simulator (Immersion Corp., San Jose, CA, USA). This simulator is used for training and evaluating gastroenterologists. Expert colonoscopists consider this simulator to be realistic [54]. Furthermore, its validity has been demonstrated in several trials, summarized by Carter *et al.* [14]. We have used the ‘colonoscopy introduction case 1’, since it is the easiest case. An easy case was chosen to ensure all students could complete the case. The other cases of the simulator are of a more difficult level.

2.2.5 Evaluation criteria

Based on the survey results, three metrics that could be obtained from the simulator were chosen as criteria for the experiment. These are the introduction time, the patient discomfort, and the percentage of the colonic mucosa that was visualized (the visualization performance). The first two criteria are chosen since the gastroenterologists mentioned that during introduction, the target should be reached quickly without causing too much discomfort. The visualization performance was chosen since it shows how well the subject performs the inspection. Proper inspection was mentioned as an important criterion by the participants of the survey.

The simulator does not give one single value for the discomfort of the patient, but a set of values that indicate how long the patient had mild, moderate, severe, and extreme discomfort. These represent the force levels exerted on the colon. We will denote these values as d_1 , d_2 , d_3 and d_4 , in increasing order of discomfort.

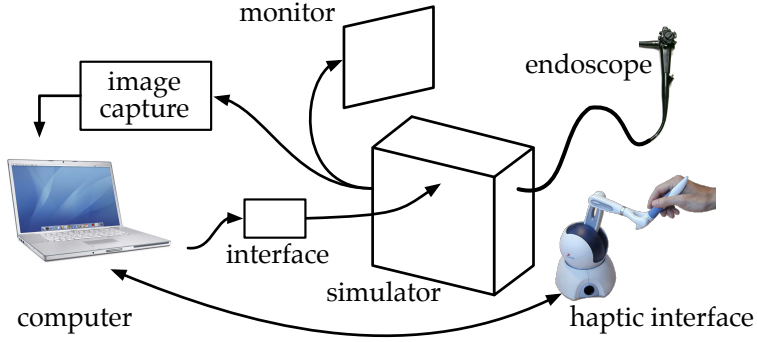


Figure 2.7: For the experiments, the simulator is not controlled by the endoscope controls, but by the control signals from the computer. The images of the simulated procedure are captured by the computer to be processed by the vision algorithm.

In order to get one value for the discomfort, we will use a linear combination:

$$d_t := \alpha_1 d_1 + \alpha_2 d_2 + \alpha_3 d_3 + \alpha_4 d_4 \quad , \quad (2.8)$$

where d_t denotes the total discomfort value. Since each higher level of discomfort is much more severe, we have chosen to use an exponential set of parameters: $\alpha_1 = 1, \alpha_2 = 2, \alpha_3 = 4, \alpha_4 = 8$. Hence, one second of extreme discomfort (d_4) is equivalent to 8 seconds of mild discomfort (d_1).

2.2.6 Test setup

A test setup was built to enable evaluation of the three control methods that were described in Section 2.2.2. An overview of this setup is shown in Fig. 2.7. An image capture device (ADVC55, GrassValley, Conflans St. Honorine, France), was used to acquire the simulated endoscopic images. These are used by the image processing algorithm. The images are also shown on a monitor. In order to control the simulator with the haptic device, an interface was developed. The simulator endoscope is not a functional endoscope, it is merely a device that reports the position of the control knobs to the simulator. The interface emulates this, and allows the computer to control the reported control knob positions. This way, the computer can control the simulation, based on the input from the haptic device. A Phantom Omni (SensAble Technologies, Inc., Woburn, MA, USA) was used as a haptic device. Fig. 2.8 shows the setup in use.

In all experimental conditions, the subjects still feed the endoscope manually into the simulator in order to move the endoscope forward through the colon. However, its controls are only used in the experiments where the *conventional steering* is evaluated.



Figure 2.8: The test setup in use by one of the gastroenterologists.

2.2.7 Tip control

Position control was implemented to steer the endoscope tip using the haptic device. The coupling between the haptic device motions and the camera motions was chosen so as to simulate the physician holding the camera in his/her hand. That is, left/right movements of the tip were coupled to horizontal camera motion, up/down movements were coupled to vertical camera motion. Subjects could control the camera rotation by rotating the endoscope itself using their right hand. This is identical to how the rotation is controlled in conventional endoscopies.

Motion towards and away from the haptic device was ignored. This motion was limited by a spring force towards a vertical plane. The orientation of the stylus of the haptic device was also ignored.

The proportional gain was chosen such that a displacement of 100mm from the neutral position corresponded to maximum camera motion. This gain was chosen based on initial experiments. It allowed the full camera motion range to be covered, given the workspace of the haptic device.

2.2.8 Procedure

In order to be able to do a repeated measures comparison, all subjects performed the three experimental conditions. The subjects were instructed to try to reach the cecum quickly with minimum patient discomfort, and to carefully inspect the colonic mucosa while retracting. They were instructed to use their left hand for steering the tip (using either the endoscope controls or the haptic device), and their right hand for feeding the endoscope. This configuration was chosen since

it is identical to the way conventional endoscopic procedures are performed.

For each control method, they were given 15 minutes practice time, followed by the measurement session where the evaluation criteria were recorded. During the practice time, instructions were given on the use of the simulator and the control method. No instructions were given during the measurement session. All three experimental conditions were tested in succession without a break in between. This took approximately 1-1.5 hours per subject.

We have counterbalanced the order of the measurements i.e., each of the six possible orders of the three conditions is performed equally often. This was done in order to minimize the influence of any learning effects and fatigue on the evaluation in both subject groups.

2.2.9 Subjects

A total of 18 subjects were recruited for the experiment, 6 experienced gastroenterologists (this is the experts group) and 12 Technical Medicine students¹. All experts had performed over 1000 colonoscopies. All students had recently completed a flexible endoscopy course, in which they performed several colonoscopies using the same simulator that was used in the experiment.

None of the subjects had previous experience with similar experiments. The subjects participated on voluntary basis, and signed an informed consent form. The subjects in the students group received financial compensation for their participation (€15).

During the experiment, two students caused a colon perforation during the introduction phase while using the *steering with haptics* method. This is a serious complication, which caused the simulator to abort the procedure. Hence, there are no results for these two subjects. In order to maintain a counterbalanced experiment design, two additional subjects participated to replace the original subjects. Of course, the fact that the two colon perforations took place, needs to be considered when comparing the three control methods.

It should be noted that perforations generally do not take place at the endoscope tip. Instead, they are caused by excessive looping of the endoscope in the sigmoid colon (Fig. 2.9). Preventing looping is a major challenge in colonoscopy, which is learnt mainly by experience. By adequately retracting and/or rotating the endoscope during the procedure, looping can be minimized [60]. When a loop is formed, it is very difficult to move the endoscope tip forward, and an inexperienced subject may use excessive force when trying to move the tip despite of the loop, resulting in perforation.

The student subject group that was used for the analysis consisted of 4 females and 8 males, aged 21-24 years, with an average age of 22 years. All were right-handed.

Within the experts group, there was one subject who did not succeed in reaching the cecum (the end of the colon) using the *steering without haptics* method. This

¹Technical Medicine is a Master's level program at the University of Twente where students study to integrate advanced technologies within the medical sciences to improve patient care.

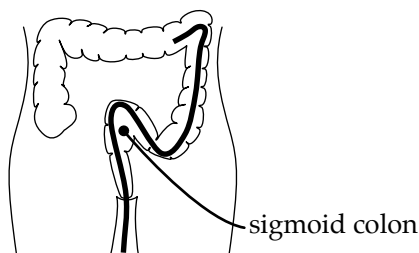


Figure 2.9: A loop formed in the sigmoid colon may cause perforation during introduction.

subject was replaced with another expert subject. Here too, we need to take the fact that the original subject did not reach the cecum into account when evaluating the results.

The expert subjects that were used for the analysis were all male, aged 39-66 years, with an average age of 51 years. All were right-handed.

2.3 Results

The results of the experimental study are shown in Fig. 2.10. These graphs show the average introduction time, discomfort, and visualization for each of the three experimental conditions, for both the students and the experts.

Three two-way mixed Analyses of Variance (ANOVA) were performed for the whole group of subjects. These were done on the introduction time, the discomfort, and the visualization, with the control method (*conventional, without haptics, with haptics*) as a factor and expertise (student, expert) as a between-subjects factor. Only significant effects ($p < 0.05$) will be reported.

The analysis showed a significant control method \times expertise interaction ($p = 0.013$) for the introduction time. This means that the influence of the method on the introduction time is different for the two groups. As seen in Fig. 2.10, students are on average slower when using the *conventional* method as compared to the other methods, while the experts are on average faster when using this method.

The analysis also showed a significant influence of the factor expertise on the introduction time ($p = 0.002$). As seen in Fig. 2.10, the experts are on average faster than the students.

Furthermore, a significant influence of the control method on the patient discomfort was found ($p = 0.039$). Subsequent pairwise comparisons with Bonferroni corrections showed no significant results. As seen in Fig. 2.10, this result probably indicates that the *without haptics* method causes most discomfort.

Additionally, three repeated measures ANOVAs were performed separately on the students and the experts groups. For the introduction time, a significant

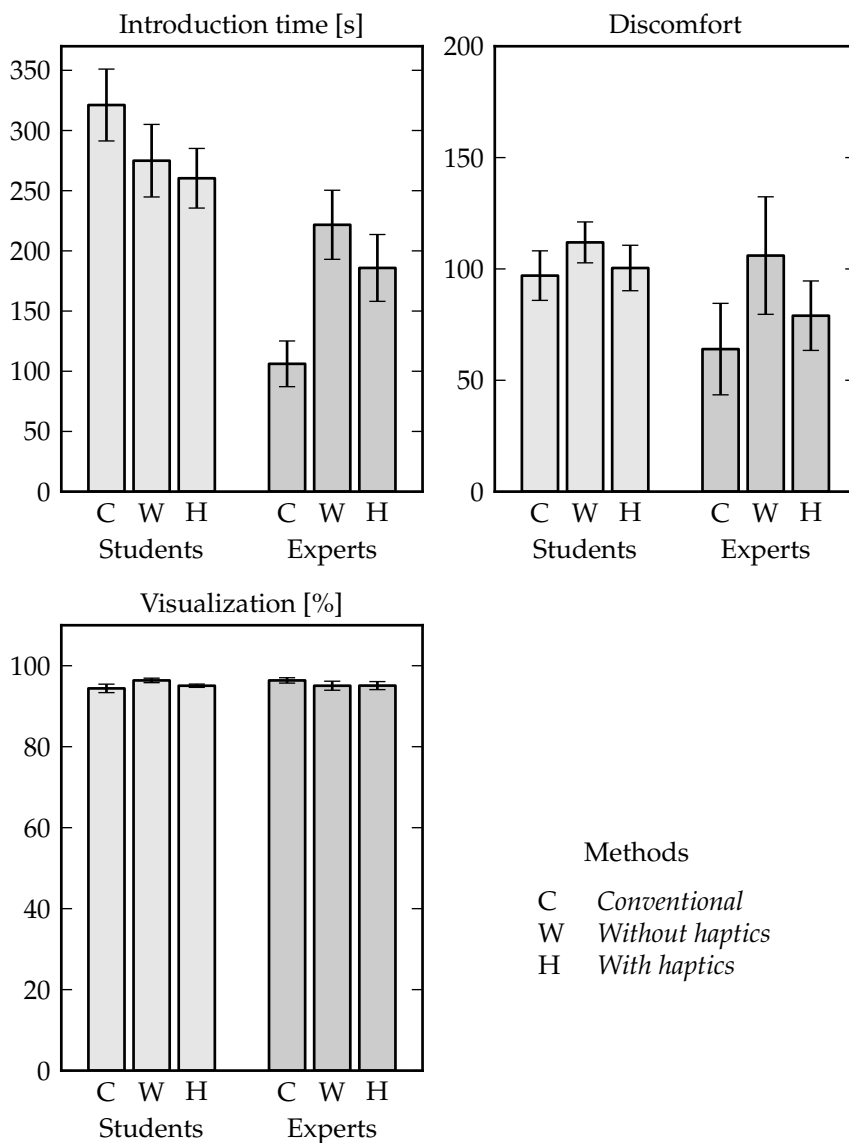


Figure 2.10: Results of the experimental study: The experts are significantly faster when using the conventional method compared to the other two methods. For the subject group as a whole, the *with haptics* method appears to result in less discomfort than the *without haptics* method. The error bars indicate the standard error.

influence of the control method was found for the experts group ($p = 0.007$). Subsequent pairwise comparisons with Bonferroni corrections showed that *conventional steering* differed significantly from *without haptics* ($p = 0.042$) and from *with haptics* ($p = 0.013$). As seen in Fig. 2.10, the experts are faster with the *conventional* method than with the other two methods.

2.4 Discussion

Within the experts group, the subjects perform significantly faster when using the *conventional* method as compared to the other two methods. Additionally, one of the original expert subjects did not succeed in reaching the cecum in the *without haptics* experimental condition. It is not remarkable that the experts perform better using the *conventional* method, since they have an experience of over 1000 procedures using this method, versus an experience of 15 minutes with the other two methods. Thus, their performance in the *without haptics* and *with haptics* conditions may improve with learning, possibly beyond their performance using the *conventional steering*.

For the whole group of subjects, there was no significant influence of the method on the introduction time. However, there was a significant influence on the patient discomfort. The results suggest that *with haptics* the discomfort is reduced compared to *without haptics*. Thus, if a haptic device is used for endoscope steering, haptic cues may improve the performance.

For the students group, the results show no significant difference between the three methods. However, two students in the original subjects group caused a colon perforation while using the *with haptics* method. They mentioned that they felt over-confident because of the haptic guidance. The risk of colonic perforation may be reduced by better training.

The results show some trends that are not statistically significant. It could be reasoned that adding more subjects to the experiment would increase the significance of the results. However, the number of available subjects is limited. The experiment requires 1-1.5 hours per subject, and not many gastroenterologists have this amount of time available. The number of available student subjects is also limited, since we chose to select only students who had recently completed a flexible endoscopy course. Adding student subjects who did not recently complete this course would reduce the homogeneity of the group.

The results suggest that the 'new' steering methods that were implemented are better than steering using a joystick, as implemented by Allemann *et al.* [2]. Their evaluation showed that both experienced and novice subjects required more time when using a joystick as compared to using conventional control. In their study, endoscopists took almost 10 times longer, while surgeons and students required approximately twice as much time. In our experiments, the experts required on average 43% more time, but students are on average 23% faster when using the *with haptics* method as compared to the *conventional steering* (although the latter result is not significant).

The results for the 'new' steering methods may be improved by using a different haptic device. The device that was used is a common off-the-shelf product, and was not designed specifically for the task. The results may have been affected in a negative sense because of the limited output force and the limited motion range. Furthermore, the mapping between the movement of the haptic device and the movement of the endoscopic camera can be optimized to improve the performance.

Conclusion

The results show that the experts are faster when using the *conventional steering* method compared to the 'new' steering methods. For the students, no significant differences were found. However, in new NOTES endoscopes, the *conventional steering* method will not be practical. The use of a multi-DOF input device may be a viable approach to controlling these endoscopes. The results suggest that in this case the implementation of haptic guidance may reduce patient discomfort. Since the performance of experts is likely to increase as they gain more experience, this methods may be a viable alternative to the conventional method.

In the next chapters, the focus will be on the control of the instruments of the endoscope.

Acknowledgments

We would like to thank Esther Rozeboom for conducting the pilot study, and Nicole Kuperij for assisting with the survey and the experiments.

3D position estimation of flexible instruments

Endoscopic images can be used to realize accurate flexible endoscopic instrument control. This can be implemented using a pose estimation algorithm, which estimates the actual instrument pose from the endoscopic images. In this chapter, two pose estimation algorithms are compared: a marker-less and a marker-based method. The marker-based method uses the positions of three markers in the endoscopic image to update the state of a kinematic model of the endoscopic instrument. The marker-less method works similarly, but uses the positions of three feature points instead of the positions of markers. The algorithms are evaluated inside a colon model. The endoscopic instrument is manually operated while an X-ray imager is used to obtain a ground-truth reference position.

The marker-less method achieves an RMS error of 1.5mm, 1.6mm, and 1.8mm in the horizontal, vertical, and away-from-camera directions, respectively. The marker-based method achieves an RMS error of 1.1mm, 1.7mm, and 1.5mm in the horizontal, vertical, and away-from-camera directions, respectively. The differences between the two methods are not found to be statistically significant. The proposed algorithms are suitable to realize accurate robotic control of flexible endoscopic instruments, which will be described in chapter 4.

3.1 Introduction

Conventional endoscopes and their instruments can only be used to perform relatively simple interventions such as taking biopsies or removing small sections of malignant tissue. In order to broaden the range of possible interventions, advanced flexible endoscopes are currently being developed, such as the EndoSAMURAI (Olympus Corp., Tokyo, Japan) and the ANUBIS (Karl Storz GmbH & Co. KG, Tuttlingen, Germany). These endoscopes both allow multiple instruments to be used simultaneously, and their instruments can be operated in multiple degrees of freedom (DOFs). This gives the physician the dexterity that is required to perform more advanced interventions, such as the removal of larger sections of mucosal tissue, and Natural Orifice Transluminal Endoscopic Surgery (NOTES, [27]).

However, the aforementioned flexible endoscopes are difficult to operate. Multiple physicians are required to operate all DOFs [36]. Since optimal coordination between the physicians is difficult, and because of the increased costs, this is undesirable. In addition, the control of the endoscope and the instruments is not intuitive, since there is no one-to-one mapping between the movement of the controls and the movement of the instrument. Intuitive control is also hindered by the presence of hysteresis due to friction and compliance in the mechanical control system of the instrument.

In order to overcome the aforementioned problems associated with current advanced flexible endoscopes, a robotic actuation system could be employed. If all DOFs of the endoscope and the instruments can be actuated, a telemanipulation setup can be constructed (Fig. 3.1). In such a system, a single physician controls the complete system, like in the daVinci surgical system (Intuitive Surgical Inc, Sunnyvale, CA, USA). Because the coupling between the movement of the physician and the movement of the actuators is implemented in software, it can be designed to allow intuitive control.

There exists a significant amount of friction and compliance between the tip of the instrument and its control handle (where it is actuated), resulting in hysteresis. Abbott *et al.* and Bardou *et al.* have proposed compensation of the hysteresis in the case that the amount of hysteresis is known in advance (i.e., determined pre-operatively) [1,5,7]. However, because the friction and compliance vary with the (unknown) shape of the endoscope, feedback of the actual tip position is required in order to be able to control it accurately. Adding extra sensors to the instruments to measure this tip position will be expensive, because the space at the tip of the instrument is very limited. Therefore, it would be beneficial if the tip position can be measured without adding extra sensors. This can be accomplished by using the endoscopic images as a feedback.

Pose estimation of laparoscopic instruments has been studied by Doignon *et al.* [20], using both marker-based and marker-less techniques. They considered a general pose-estimation problem, which has no model of the kinematics of the instrument. Moreover, for the marker-less estimation, the instrument was assumed to be straight, which is true for laparoscopy, but not for flexible endoscopy. In

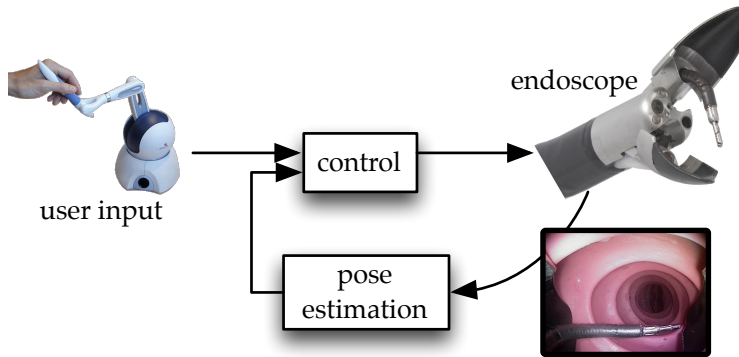


Figure 3.1: Instrument control using visual feedback: The images that are captured by the endoscope are used by the pose estimation algorithm to find the actual instrument pose. The control actuates the endoscopic instrument such that it moves to the pose that is commanded by the user.

the case of flexible endoscopy, where the instrument has only three degrees of freedom, the use of a kinematics model significantly reduces the solution space, improving the accuracy.

In this study, we compare two methods that use the endoscopic images to estimate the pose of a flexible endoscopic instrument. The first method uses feature points that are detected on the instrument tip (marker-less). The second method uses markers that are attached to the instrument (marker-based). The contributions of this study as compared to our previous work [48,51] are the following:

- In the current study, we perform a comparison of the marker-less and marker-based methods under equal experimental conditions.
- We have used an X-ray imager to reconstruct the ground-truth position of the instrument tip. This allows for an accurate evaluation of the estimation algorithm over the entire workspace.
- For the marker-based approach, we have developed a more robust method to match the marker regions that are found in the image to the markers in the model.

This chapter is structured as follows: In Section 3.2, the marker-less and marker-based estimation methods are presented, and the experimental setup for evaluation of these methods is described. The experimental results are presented in Section 3.3. Finally, Section 3.4 concludes with the discussion.

3.2 Materials and Methods

Our approach for the pose estimation is based on virtual visual servoing [35]. In this approach, the actual state of the estimator is used to find the estimated posi-

tions of certain feature points. This is done using a kinematics model of the instrument and a model of the camera. These estimated positions are compared to the positions of feature points that are observed in the endoscopic image. Based on the difference between the estimated and the actual positions, the state of the estimator is updated such that the estimated feature point positions move towards the actual feature point positions. From the state of the estimator, the pose (position and orientation) of the instrument tip can be derived using the kinematics model of the instrument.

This section describes the kinematics model of the instrument, the model of the camera, the detection of the features from the endoscopic images, and the state estimation algorithms. Finally, the experimental setup that was used to evaluate the performance is presented.

3.2.1 Kinematics model of the instrument

The kinematics model of the instrument describes the positions of points on the instrument in the three-dimensional (3D) Euclidian space. The model consists of a straight section, a bendable section, and the tip (Fig. 3.2). This model is similar to that of Bardou et al. [6]. The model assumes that there are no significant forces acting on the instrument, resulting in a constant curvature along the bending section. This assumption is valid in our experiments. However, in clinical practice, external forces are present, which may have to be accounted for. These can be modeled as external disturbances to the model.

The state of our model (denoted \mathbf{q}) has three components: translation (q_1), rotation (q_2), and bending (q_3). We define three reference points, denoted A , B , and C , on the center line of the instrument. A and B are located midway and at the end of the bendable section, respectively, while C is located at the tip. The model allows us to compute the positions of $A \cdots C$, denoted $\mathbf{p}_A \cdots \mathbf{p}_C$ using the forward kinematics function, denoted $f(\mathbf{q})$:

$$\begin{bmatrix} \mathbf{p}_A \\ \mathbf{p}_B \\ \mathbf{p}_C \end{bmatrix} = f(\mathbf{q}) . \quad (3.1)$$

Additionally, we can compute the relation between the change of the state $\dot{\mathbf{q}}$ and the changes of the positions of the points $\dot{\mathbf{p}}_A \cdots \dot{\mathbf{p}}_C$:

$$\begin{bmatrix} \dot{\mathbf{p}}_A \\ \dot{\mathbf{p}}_B \\ \dot{\mathbf{p}}_C \end{bmatrix} = \mathbf{J}_f(\mathbf{q})\dot{\mathbf{q}} , \text{ where } \mathbf{J}_f(\mathbf{q}) := \begin{bmatrix} \frac{\partial \mathbf{p}_A}{\partial \mathbf{q}} \\ \frac{\partial \mathbf{p}_B}{\partial \mathbf{q}} \\ \frac{\partial \mathbf{p}_C}{\partial \mathbf{q}} \end{bmatrix} . \quad (3.2)$$

In (3.2), \mathbf{J}_f denotes the analytical Jacobian of f . The detailed calculation of \mathbf{J}_f is in appendix A.

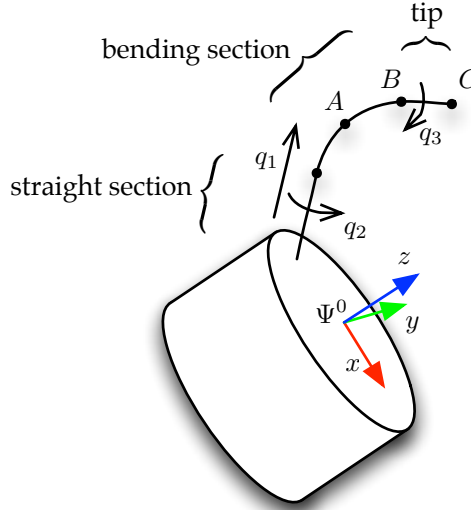


Figure 3.2: The endoscopic instrument has three degrees of freedom: translation q_1 , rotation q_2 and bending q_3 . Points A and B are positioned midway and at the end of the bendable section, respectively. Point C is at the end of the tip. Frame Ψ^0 denotes the camera frame of the endoscopic camera.

3.2.2 Endoscopic camera model

We have modeled the endoscopic camera using the pinhole camera model, with additional radial distortion. Since endoscopes have a wide-angle lens, the radial distortion is quite significant. The camera model $g(\mathbf{p})$ maps each point \mathbf{p} in the 3D space to a point \mathbf{x} in the 2D image space:

$$\mathbf{x} = g(\mathbf{p}) . \quad (3.3)$$

For the marker-based method, the 2D image space positions of marker positions $A \dots C$ are combined into the measurement vector \mathbf{s} :

$$\mathbf{s} = \begin{bmatrix} \mathbf{x}_A \\ \mathbf{x}_B \\ \mathbf{x}_C \end{bmatrix} = \begin{bmatrix} g(\mathbf{p}_A) \\ g(\mathbf{p}_B) \\ g(\mathbf{p}_C) \end{bmatrix} . \quad (3.4)$$

Similar to (3.2), the derivative relation of (3.4) can be computed, showing the relation between the change of the feature point positions in 3D space $\dot{\mathbf{p}}$ and the change of the feature point positions in the 2D image space $\dot{\mathbf{x}}$:

$$\dot{\mathbf{s}} = \begin{bmatrix} \dot{\mathbf{x}}_A \\ \dot{\mathbf{x}}_B \\ \dot{\mathbf{x}}_C \end{bmatrix} = \begin{bmatrix} \mathbf{J}_g(\mathbf{p}_A) \dot{\mathbf{p}}_A \\ \mathbf{J}_g(\mathbf{p}_B) \dot{\mathbf{p}}_B \\ \mathbf{J}_g(\mathbf{p}_C) \dot{\mathbf{p}}_C \end{bmatrix} , \text{ where } \mathbf{J}_g(\mathbf{p}) := \frac{\partial g(\mathbf{p})}{\partial \mathbf{p}} \quad (3.5)$$

Equations (3.2) and (3.5) can be combined so as to obtain the relation between the change of the state $\dot{\mathbf{q}}$ and the change of the measurement vector $\dot{\mathbf{s}}$:

$$\dot{\mathbf{s}} = \mathbf{L}\dot{\mathbf{q}}, \quad (3.6)$$

where \mathbf{L} is the (state-dependent) interaction matrix [16]. \mathbf{L} is used by the state estimation algorithm as will be described in Section 3.2.4.

For the marker-less method, the computation of the interaction matrix is similar to the marker-based method. For the marker-less method, the marker locations $A \cdots C$ are replaced by the locations of feature points $f_1 \cdots f_3$, as described in the next section.

3.2.3 Feature detection

For the estimation of the instrument state, features are extracted from the acquired endoscopic images. For the marker-less method, three points on the instrument tip are used as the features. For the marker-based method, the features are the positions of the centroids of the markers in the image.

Marker-less feature detection

For the estimation without markers, three feature points are extracted from the endoscopic images. These are the tip of the instrument and two points on either side. It should be noted that the method could easily be expanded to take more feature points into account for increased accuracy and robustness. The extraction of the feature points is done as illustrated in Fig. 3.3. First, the endoscopic image is filtered using a Gaussian kernel with a scale of $\sigma=3$ pixels (Fig. 3.3b). This reduces the effects of noise in the image. Then, the image is segmented using Fishers linear discriminant method [21], applied to the RGB color space. This results in a binary image of the centre line of the instrument tip (Fig. 3.3c). Using the same method, but with different parameters, a binary image of the complete instrument (Fig. 3.3d) is extracted.

The orientation of the instrument tip is computed using the singular value decomposition of the covariance matrix of the x - and y - coordinates of all points belonging to the instrument tip centre line region [48]. The largest singular value corresponds to the direction of the tip in the image. Using this principal direction, the point that is most towards the tip is selected as the first feature point f_1 , as shown in Fig. 3.3c.

The tip direction is also used to define a line L , which is perpendicular to the tip direction, and intersects the instrument at the beginning of the tip region. L is shown in Fig. 3.3c and 3.3e. L is positioned such that it touches the binary image of the tip centre line. Using L , the instrument region (Fig. 3.3d) is separated, resulting in the instrument tip region (Fig. 3.3e). From this region, feature points f_2 and f_3 are derived.

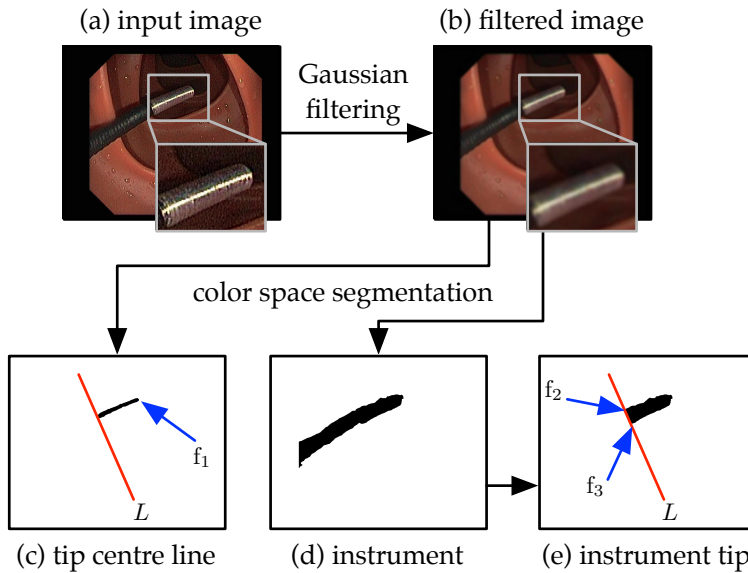


Figure 3.3: Feature detection for the marker-less method: The input image (a) is filtered using a Gaussian filter kernel in order to remove noise. This results in image (b). This image is color-space segmented twice using different parameters, resulting in the tip centre line (c) and the instrument (d) regions. From the tip centre line, the tip position is found, which is the first feature point (denoted f_1). Then, the line L is determined, which is perpendicular to the tip centre line. This line is used to separate the instrument tip (e) from the instrument region (d). From the resulting instrument tip (e), two other feature points (f_2 and f_3) are detected.

Marker-based feature detection

The markers were green so as to have a high contrast with the background of the image. As a result, the markers can be separated from the background relatively easily. As in the marker-less method, the endoscopic image is first filtered using a Gaussian filter. Then, color space segmentation is used to obtain a binary image of the markers [23]. The regions in this binary image are labeled using the `ndimage` module of the `scipy` package [53]. For every region, its centroid and its area are measured.

3.2.4 State estimation

The goal of the state estimation algorithm is to update the state of the instrument model, such that the feature points from the model match the actual features that were detected from the endoscopic images. The state estimation algorithm is similar for the marker-less and marker-based methods. However, since the features

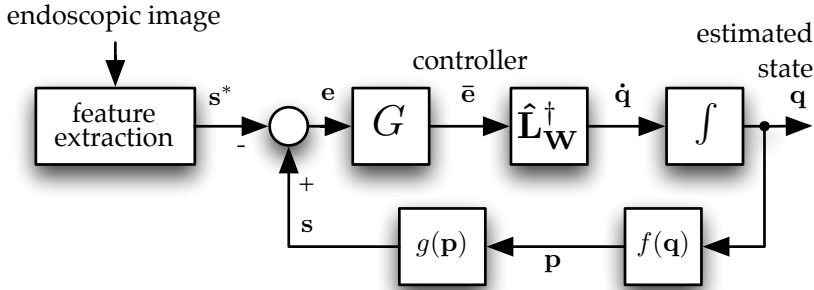


Figure 3.4: Marker-less state estimation: For a given state q , the kinematic model f and camera model g are used to compute the expected positions of the feature points in the image space, denoted s . These are compared to s^* , which are the positions of the feature points in the endoscopic image, as determined by the feature extraction algorithm. The difference $s - s^*$, denoted e , is input to the controller, which computes the state change \dot{q} to bring the model closer to the observed instrument.

that are used are different, there are some differences in the state estimation algorithm between the two methods.

Marker-less state estimation

The algorithm of the estimator is illustrated in Fig. 3.4. The current state q of the estimator is used to compute the estimated positions of the feature points in the image space, denoted s . This is done using the kinematic model f and the camera model g that were described in Section 3.2.1 and 3.2.2. Using the feature detection described in Section 3.2.3, the three feature points in the endoscopic image are found. These are denoted s^* in Fig. 3.4. The error e is defined as the difference between s and s^* . e is the input to the controller, which is implemented as a multiplication by constant gain G and \hat{L}_W^\dagger , the pseudo-inverse of the interaction matrix L . The computation of \hat{L}_W^\dagger is described at the end of this section. The output of the controller is \dot{q} , the desired change of state q that brings s closer to s^* .

Marker-based state estimation

For the marker-based method, the estimation algorithm is illustrated in Fig. 3.5. For this method, the features are the positions of the centroids of the markers in the image. Due to occlusion effects, these are in general not equal to the projection of the geometrical center of each marker. Therefore, in order to obtain accurate feature measurements from the model, a 3D rendering of the endoscopic

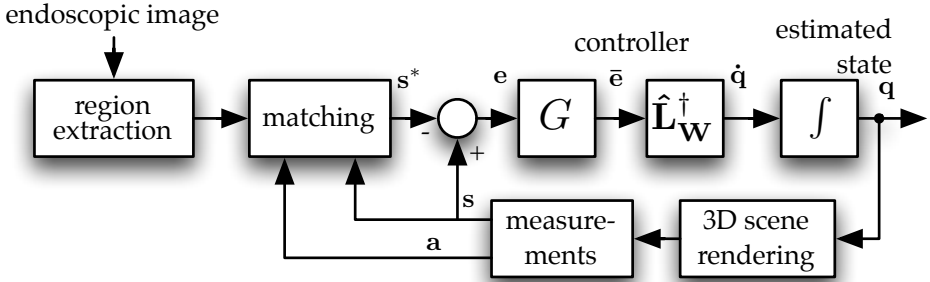


Figure 3.5: Marker-based state estimation: The structure of the estimator is similar to the marker-less method, but the main difference is the extra matching step, in which the regions that are extracted from the endoscopic image are matched to the markers. For a given state q , a 3D rendering of the scene is created. From this scene, the centroids (denoted s) and areas (denoted a) of the rendered markers are computed. s is compared to s^* , which are the centroids of the markers in the endoscopic image. The difference $s - s^*$, denoted e , is input to the controller, which computes the state change \dot{q} to bring the model closer to the observed instrument.

instrument is created using OpenGL [39]. This ensures that occlusion effects that occur in the actual scene are also present in the model. The 3D rendering uses a camera model that replicates the severe lens distortion that is present in the endoscopic camera system. The camera parameters are obtained using the Camera Calibration Toolbox for Matlab [11]. The lens distortion and the movement of the instrument are computed on the Graphics Processing Unit (GPU) using vertex shaders. This improves the computational efficiency. The measurements s , which are the positions of the centroids of the markers in the rendered scene, are obtained from the rendered scene. Additionally, the areas of the markers, denoted a in Fig. 3.5, are measured. These are used by the matching algorithm as will be described below.

Due to shadows and specular reflections, the feature detection algorithm may sometimes fail to detect a marker, or detect regions which actually are not markers. Also, in clinical practice, markers may sometimes be invisible due to occlusions. In order to provide a robust matching between the regions that are found by the feature detection algorithm and the markers of the model, a maximum-likelihood approach is used [25].

We will use k to denote the number of regions found by the feature detection algorithm. We define the likelihood function $\mathcal{L}(i, j)$ as the likelihood that marker i ($i = 1 \dots 3$) corresponds to region j ($j = 0 \dots k$). $\mathcal{L}(i, 0)$ is defined as the likelihood that marker i is missing (i.e., not detected by the feature detection algorithm).

Given the individual likelihoods $\mathcal{L}(i, j)$, the total likelihood \mathcal{L}_T that the three

markers in the model are represented by respectively regions r , s , and t is given by:

$$\mathcal{L}_T(r, s, t) = \mathcal{L}(1, r)\mathcal{L}(2, s)\mathcal{L}(3, t), \quad (3.7)$$

where r , s , and t ($0 \dots k$) denote the regions that are selected as representing the first, the second, and the third marker, respectively.

The state estimator matches the regions to the markers by finding the maximum $\mathcal{L}_T(r, s, t)$ under the condition

$$r \neq s, \quad s \neq t, \quad r \neq t. \quad (3.8)$$

The maximum likelihood is found using an exhaustive search. The positions of the centroids of the resulting regions r , s and t are combined into measurement vector \mathbf{s}^* . \mathbf{s}^* is used as an input to the virtual visual servoing loop just as in the marker-less approach.

The likelihood function $\mathcal{L}(i, j)$ was chosen to be a function of the Euclidian distance between the position of the region and the position of the marker in the image space, and the ratio between the area of the region and the area of the marker:

$$\mathcal{L}(i, j) := \begin{cases} \mathcal{L}_M(i), & j = 0 \\ \mathcal{L}_D(i, j) \mathcal{L}_A(i, j), & j \neq 0 \end{cases}. \quad (3.9)$$

In (3.9), $\mathcal{L}_D(i, j)$ denotes a likelihood function that is dependent on the Euclidian distance between the position of marker i and region j ($j = 1 \dots k$). $\mathcal{L}_A(i, j)$ denotes a likelihood function that depends on the ratio between the area of marker i and region j ($j = 1 \dots k$). $\mathcal{L}_M(i)$ denotes the constant likelihood that marker i is missing (i.e., it was not detected by the feature detection algorithm). \mathcal{L}_D and \mathcal{L}_A were chosen as exponential functions, since this matched the distributions that were observed during the actual experiment.

The distance-dependent likelihood function \mathcal{L}_D is

$$\mathcal{L}_D(i, j) := \exp\left(-\frac{\|\mathbf{x}_m(i) - \mathbf{x}_r(j)\|}{\sigma_D}\right), \quad (3.10)$$

where $\mathbf{x}_m(i)$ and $\mathbf{x}_r(j)$ denote the position of the centroid of marker i and region j in the image, respectively (subscript m for marker and r for region). $\|\cdot\|$ denotes the Euclidian distance. σ_D is a parameter that controls the decay of the exponential function.

The area-dependent likelihood function \mathcal{L}_A is

$$\mathcal{L}_A(i, j) := \exp\left(-\frac{\left|\log\left(\frac{a_m(i)}{a_r(j)}\right)\right|}{\sigma_A}\right), \quad (3.11)$$

in which $a_m(i)$ and $a_r(j)$ denote the area of marker i and region j in the image, respectively. σ_A is a parameter that controls the decay of the exponential function.

Note that $\mathcal{L}_A(i, j)$ can alternatively be written as:

$$\mathcal{L}_A(i, j) = \begin{cases} \left(\frac{a_r}{a_m}\right)^{\frac{1}{\sigma_A}} & , \quad a_r < a_m \\ \left(\frac{a_m}{a_r}\right)^{\frac{1}{\sigma_A}} & , \quad a_r \geq a_m \end{cases} . \quad (3.12)$$

This shows that $\mathcal{L}_A(i, j)$ is an exponential function with the ratio between a_m and a_r as its base.

The likelihood functions \mathcal{L}_D and \mathcal{L}_A , and the parameters σ_D , σ_A and $\mathcal{L}_M(i)$ were chosen so as to represent the distribution of the distances and area ratios that were observed during the actual experiment.

Controller

For both the marker-less and the marker-based method, the visual servo loop contains a controller consisting of a proportional gain G and the pseudo-inverse of the interaction matrix, denoted \mathbf{L}_W^\dagger . For the marker-based approach, the matrix \mathbf{L} in (3.6) is an approximation. \mathbf{L} relates to the positions of the center of each of the markers, while actually the centroids of the projections of the markers are used as measurements. Note that this approximation is only used for the computation of the interaction matrix, not in the actual virtual visual servo control loop.

For a given error \mathbf{e} between \mathbf{s} and \mathbf{s}^* , the proportional gain G yields the desired change of error \mathbf{e} (denoted $\bar{\mathbf{e}}$) that will cause \mathbf{e} to decrease: $\bar{\mathbf{e}} = G\mathbf{e}$, with G a negative scalar constant.

Since the dimension of $\bar{\mathbf{e}}$ (six) is higher than the dimension of \mathbf{q} (three), it is in general not possible to find a $\dot{\mathbf{q}}$ that will result in the desired change of error (i.e. that results in $\dot{\mathbf{e}} = \bar{\mathbf{e}}$). Therefore, we use the weighted Moore–Penrose pseudo-inverse of the approximated interaction matrix to obtain the state change \mathbf{q} that minimizes the weighted error $\|\mathbf{W}(\dot{\mathbf{e}} - \bar{\mathbf{e}})\|_2$, where \mathbf{W} denotes a weighting matrix [38]:

$$\hat{\mathbf{L}}_W^\dagger := (\mathbf{L}^T \mathbf{W}^T \mathbf{W} \mathbf{L})^{-1} \mathbf{L}^T \mathbf{W}^T \mathbf{W} . \quad (3.13)$$

For the marker-less method, the identity matrix is used for \mathbf{W} . For the marker-based method, we take advantage of the likelihoods that were computed for the matching between the regions and the markers. We use a weighting matrix:

$$\mathbf{W} = \text{diag}(\mathcal{W}(1, r), \mathcal{W}(1, r), \mathcal{W}(2, s), \mathcal{W}(2, s), \mathcal{W}(3, t), \mathcal{W}(3, t)) , \quad (3.14)$$

with

$$\mathcal{W}(i, j) := \begin{cases} 0 , & j = 0 \\ \mathcal{L}(i, j) , & j \neq 0 \end{cases} . \quad (3.15)$$

The definition of $\mathcal{W}(i, j)$ ensures that if there was no match found for a given marker ($j = 0$), a weight of 0 is used. If a match was found ($j \neq 0$), markers with a higher likelihood are weighted more than those with a lower likelihood. Because of inequality (3.8), only one of the markers can have a zero weight. This ensures the term $\mathbf{L}^T \mathbf{W}^T \mathbf{W} \mathbf{L}$ in (3.13) remains full rank and therefore invertible.

Since the estimation methods are iterative, an initialization is required. Currently, this initialization is done by starting the experiment with the instrument in a known position. In our proposed application, where the instrument is robotically actuated, the (known) state of the actuators may be used to initialize the estimation to a state that is close to the actual state.

3.2.5 Experimental evaluation

In order to evaluate the pose estimation system that was described in the previous sections, experiments were conducted. A flexible endoscopic instrument was operated inside a colon model, and the tip position was estimated. This was compared to a reference tip position which was obtained using an X-ray imager. Although the proposed methods can also estimate the orientation of the tip, the orientation was not evaluated since an accurate ground-truth orientation was not available.

Fig. 3.6 shows the experimental setup that was constructed to evaluate the performance of the marker-less and marker-based methods. The endoscope was stationary during the experiment. An endoscope attachment was designed to locate the endoscopic instrument near the endoscope tip (Fig. 3.7). In order to obtain a reference measurement of the tip position, an X-ray imaging setup was used (Fig. 3.8). The X-ray imager was positioned such, that a top view of the scene was obtained. The X-ray imager and the endoscopic camera were used as a stereo camera rig, enabling reconstruction of the tip position in 3D. The acquired images of the X-ray imager were 1024×768 pixels, resulting in a resolution of 0.25 mm per pixel. The resolution of the endoscopic images was 720×576 pixels. The X-ray imager was synchronized to the endoscopic camera, using the synchronization information that is available in the composite video output of the endoscopic camera unit. Both image sequences were stored for the processing, which was performed off-line.

For both the endoscopic image and the X-ray images, the tip position was manually annotated in each frame. From the 2D tip position in the X-ray and the endoscopic images, the 3D tip position was reconstructed using the Camera Calibration Toolbox for Matlab [11]. The stereo rig had been calibrated before the experiment. A punched metal sheet was used for the calibration as a substitute for the more commonly used checkerboard pattern, because this sheet could be clearly imaged using both imaging modalities (Fig. 3.9).

A conventional colonoscope (Exera, Olympus Imaging Corp, Tokyo, Japan) was used in the experiment. The images were captured using the FireWire output of the colonoscope imaging unit. The Anubis endoscopic instruments (Karl

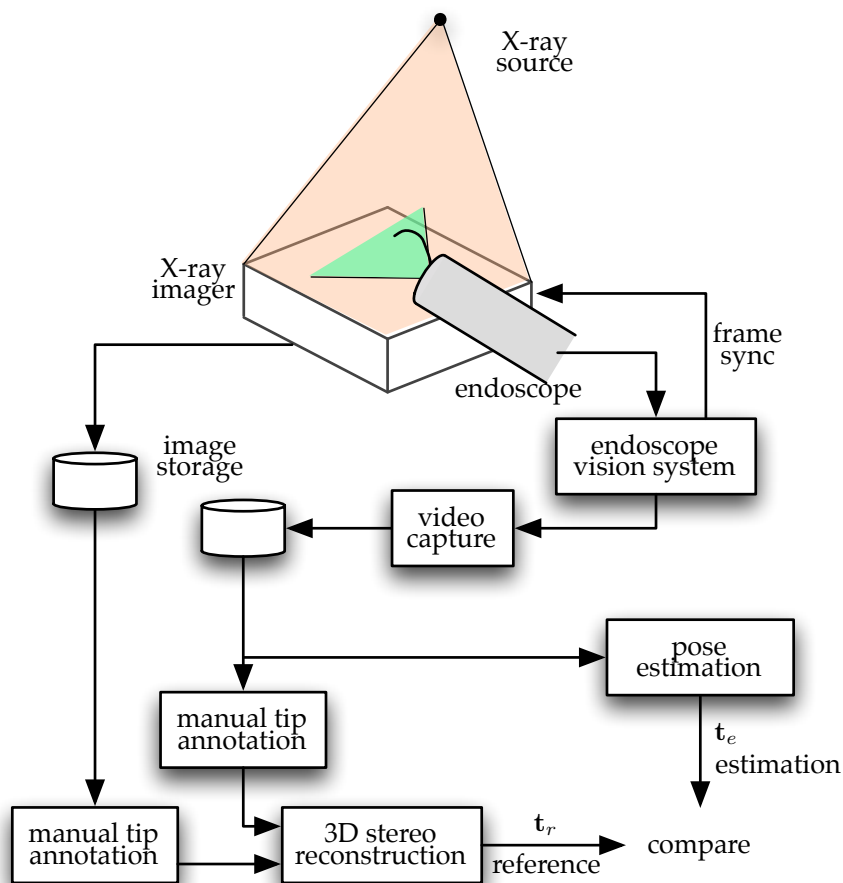


Figure 3.6: The estimator was evaluated using an X-ray imaging setup. Images from the endoscopic camera and the X-ray imager were synchronously acquired and stored. In both the X-ray images and the endoscopic images, the tip position was manually annotated. From these positions, the 3D reference position t_r was constructed. This was compared to the estimated 3D position t_e as obtained from the pose estimation. During the experiment, the endoscope and the instrument were inside a colon model. The colon model is not shown in the figure for clarity.

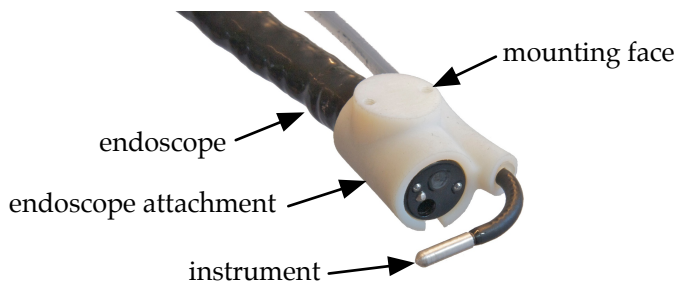


Figure 3.7: An endoscope attachment was designed to let the endoscopic instrument emerge near the endoscopic camera, similar to the Anubis endoscope. The attachment also has a mounting face, which enables the endoscope to be fixed inside the X-ray imaging setup.

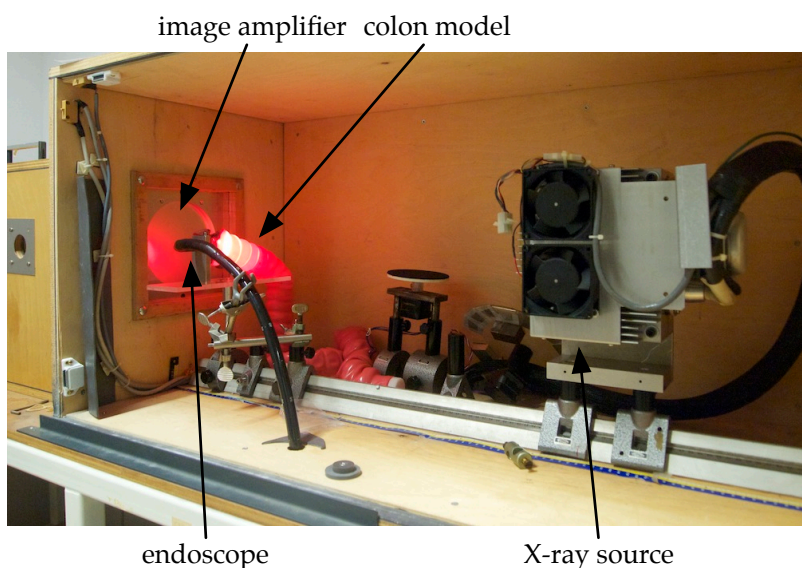


Figure 3.8: A custom-built X-ray imaging setup was used for the experiment. The X-ray source generates the X-rays which are captured by the image amplifier. The images are digitized by a digital camera (not visible in the image). The endoscope is positioned inside a colon model during the experiment.

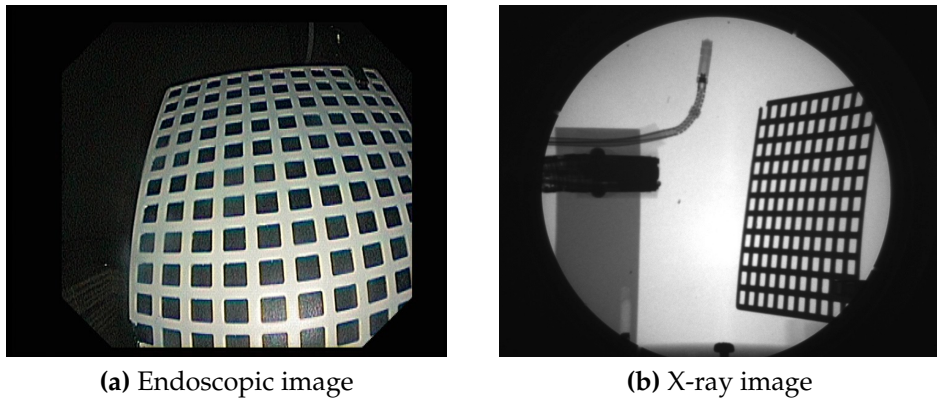


Figure 3.9: The stereo rig composed of (a) the endoscope camera and (b) the X-ray imager is calibrated by imaging a reference object using both image modalities. In (a), it can be observed that severe barrel distortion is present in the endoscopic images.

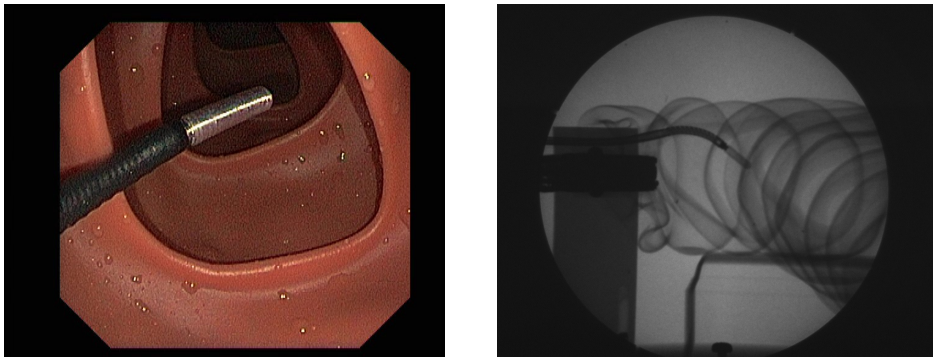
Storz GmbH & Co. KG, Tuttlingen, Germany) were manually operated. The experiment was performed inside a colon model (KKM40, Kyoto Kagaku, Kyoto, Japan) that is commonly used for colonoscopy training. A viscous fluid was used to coat the inside of the model as per the manufacturers instructions, in order to replicate the lighting conditions of clinical images. Specifically, this fluid causes specular reflections which are also commonly present in clinical images.

3.3 Results

Fig. 3.10a and 3.10b show endoscopic and X-ray images of the instrument while it was operated inside the colon model during the marker-less experiment, respectively. Fig. 3.10c shows the results of the marker-less pose estimation. It shows the x -, y -, and z - components of the estimated tip position, and the reference as obtained by the 3D reconstruction from the X-ray and endoscopic images. The positions are expressed in the camera frame Ψ^0 (Fig. 3.2). The root-mean-square (RMS) differences between the estimated and the reference position were 1.5mm, 1.6mm, and 1.8mm in the x -, y -, and z - directions, respectively.

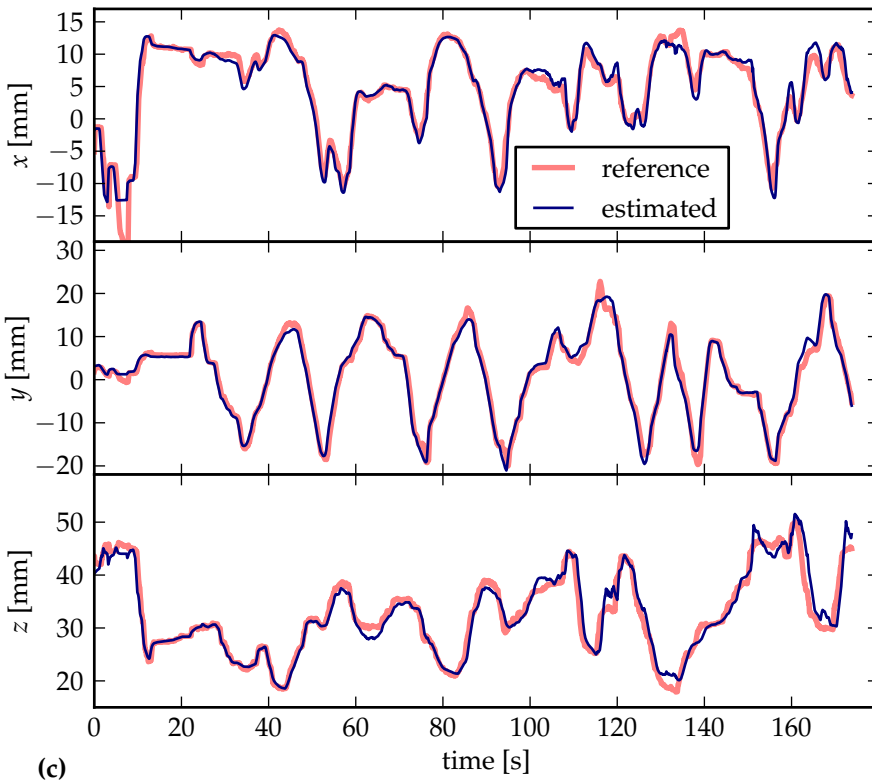
Fig. 3.11a and 3.11b show endoscopic and X-ray images for the marker-based estimation experiment, respectively. Fig. 3.11c shows the position estimation results for the marker-based estimation. For the marker-based method, the RMS differences between the estimated and the reference position were 1.1mm, 1.7mm and 1.5mm in the x -, y -, and z - directions, respectively.

The two methods were compared statistically using the Mann–Whitney–Wilcoxon test [34]. The experimental data was subsampled at 5 second intervals in order to prevent unacceptable dependence between the samples, resulting in



(a) Endoscopic image

(b) X-ray corresponding to (a)



(c)

Figure 3.10: Marker-less estimation results: (a) and (b) show the marker-less instrument in the endoscopic and X-ray images, respectively. (c) shows the x -, y - and z -coordinate of the estimated tip position, and the reference that was obtained using the X-ray imager. The RMS errors were 1.5mm, 1.6mm, and 1.8mm in the x -, y -, and z - directions, respectively.

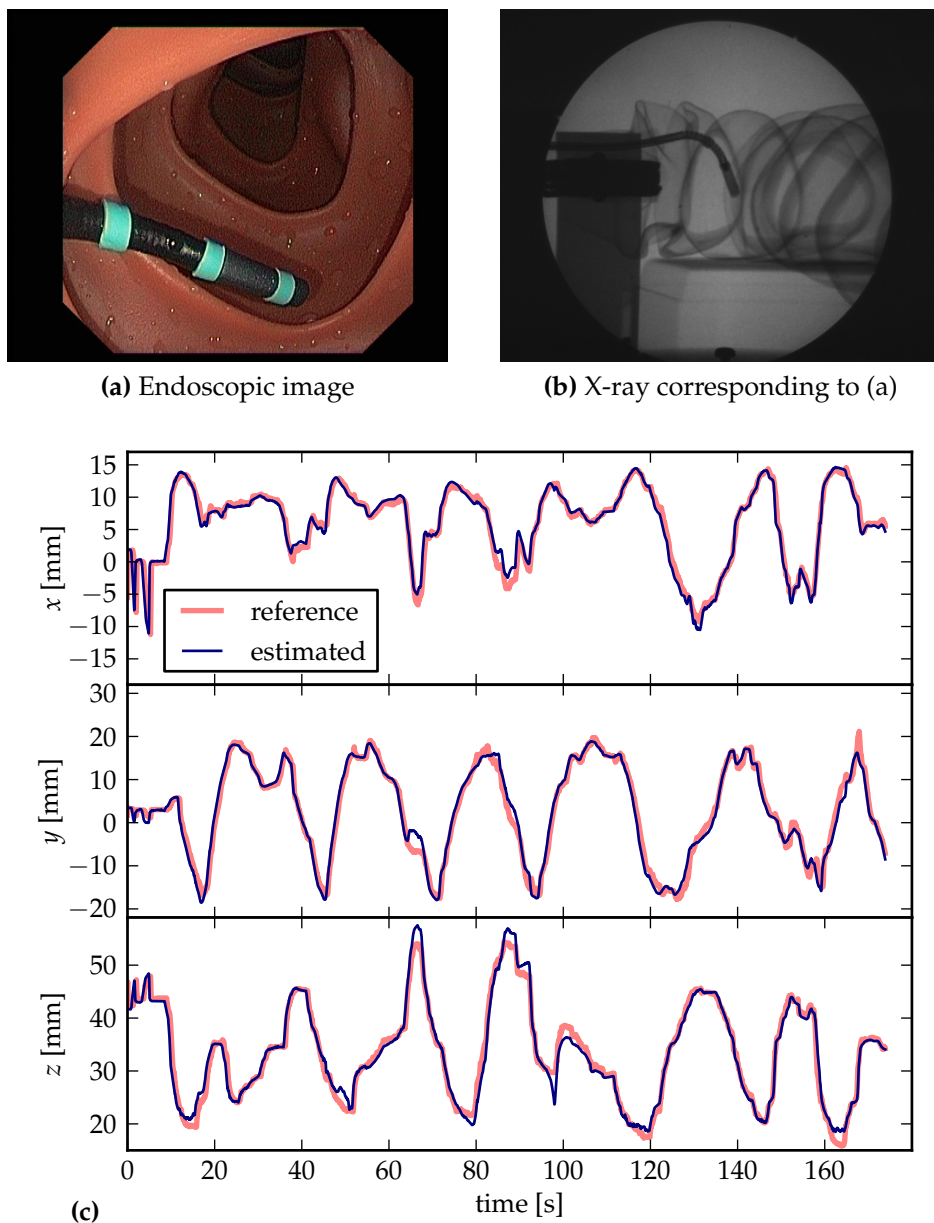


Figure 3.11: Marker-based estimation results: (a) and (b) show the instrument with markers in the endoscopic and X-ray images, respectively. The accuracy for the marker-based estimation is similar to the accuracy for the marker-less method. The RMS errors were 1.1mm, 1.7mm and 1.5mm in the x -, y -, and z -directions, respectively.

35 samples for each method. No significant differences between the methods were found ($p = 0.2$).

3.4 Discussion

Two methods were compared for estimating the pose of an endoscopic instrument, one with and one without markers on the instrument. The methods were tested inside a colon model, and the accuracy of the estimated tip position was evaluated using an X-ray imager to provide a ground-truth value. Both methods were able to track the motions of the endoscopic instrument, and performed similarly in terms of tip position accuracy. No significant difference between the methods was found in terms of accuracy. The kinematics model can also be used to derive the tip orientation. However, this was not evaluated in this study.

For the marker-based method, a maximum-likelihood approach was used to match the regions in the endoscopic image to the markers of the model of the endoscopic instrument. This approach makes the state estimator robust against missing markers that may be caused by e.g., occlusions or shadows. This is a potential advantage over the marker-less method. However, we have not evaluated the robustness of the two methods in the current study. Also, the computed likelihood value gives a measure of how reliable the estimated position is. An alternative control method for the instrument could be used as a backup if the likelihood is too low. This would create the robustness that is required for the system to be implemented in clinical practice. Another advantage of the marker-based method is that the apparent size of the markers could be used as a cue for the z -position of each marker. In this case, the area of each marker would be included in the vector s in (3.4). This could improve the estimation accuracy, especially in the z -direction.

An advantage of the marker-less method is that current instruments can be used without adding any markers. However, it might be necessary to adapt the feature detection algorithm depending on the type of instrument that is used.

In the following chapter, the marker-based position estimation algorithm will be used to compensate the hysteresis that is present in the endoscopic instrument.

Image-based hysteresis reduction for the control of flexible instruments

The limited dexterity of conventional flexible endoscopic instruments restricts the clinical procedures that can be performed by flexible endoscopy. Advanced instruments with a higher degree of dexterity are being developed, but are difficult to control manually. Adding actuators to these instruments may make them easier to control. However, the intrinsic hysteresis that is present between the actuators and the tip of the instrument needs to be reduced in order to allow accurate control. We present an estimation algorithm that determines the hysteresis between the actuators and the instrument tip in all three degrees of freedom of the instrument: insertion, rotation, and bending. The estimation is performed on-line. The endoscopic images are used as the only feedback, and no additional sensors are placed on the instrument, which is beneficial for application in clinical practice. This is done using the marker-based pose estimation approach that was described in the previous chapter. The estimated parameters are used to reduce the hysteresis that is present. Experimental validation showed a hysteresis reduction of 75%, 78% and 73% for the insertion, rotation, and bending degrees of freedom, respectively.

4.1 Introduction

Improving the dexterity of the endoscopic instruments will enable physicians to perform interventions using a flexible endoscope, that would otherwise be done laparoscopically. This can reduce the patient trauma. Improved dexterity will also be required for efficient Natural Orifice Translumenal Endoscopic Surgery (NOTES) procedures [27, 40, 43]. Currently, advanced endoscopic instruments and endoscopes with improved dexterity are being developed. Examples of these include the ANUBIS (Karl Storz GmbH & Co. KG, Tuttlingen, Germany) and the EndoSAMURAI (Olympus Corp., Tokyo, Japan). Unfortunately, the control of these endoscopes requires multiple physicians [36]. This is undesirable, since optimal coordination is difficult, and because of associated costs.

In order to control advanced endoscopes and instruments in an optimal way, it is required that a single physician can control all degrees of freedom. This can be realized by a teleoperated robotic setup, where the physician interacts with a master console, which in turn controls the instruments. Such an approach requires adding actuators to the endoscope and the instruments. However, there will be significant hysteresis between the actuator motion and the actual tip motion due to friction and compliance within the instrument. This hysteresis will prohibit accurate control of the instrument tip, and must therefore be reduced.

Hysteresis reduction for flexible endoscopic instruments has been studied by Abbott *et al.* [1] and by Bardou *et al.* [5, 7, 8]. Two approaches are included in these works: off-line hysteresis estimation [1, 5, 7] and on-line feedback using an external sensor [5, 8]. In the case of off-line hysteresis estimation, the hysteresis is characterized pre-operatively. The characterization is used to perform the intra-operative hysteresis reduction. However, the hysteresis between the actuation of the instrument and the actual instrument tip motion will depend on several unknown factors which vary during the intervention. These include the friction and compliance of the instrument, and the actual shape of the endoscope. Thus, for optimal hysteresis reduction, the hysteresis cannot be determined pre-operatively, but should be estimated on-line.

In order to perform the on-line hysteresis estimation, the actual position of the instrument tip must be known. Adding extra sensors to the instrument is difficult, since the available space is limited, and because of added costs and sterilization issues. Bardou *et al.* evaluated compensation using an external sensor [5, 8]. However, their proposed setup is not suitable for clinical procedures due to the requirement for an external sensor.

Instead, we propose to use the endoscopic camera images in order to determine the instrument tip position intra-operatively without adding any additional sensors to the endoscope system. In previous chapter, we have used virtual visual servoing techniques to estimate the position and orientation of an endoscopic instrument from endoscopic images [48, 51]. In the current study, these techniques are employed to determine the tip position of the endoscopic instrument. In order to increase the robustness of the vision algorithms, markers are used. Additionally, the position of the actuators is used as prior knowledge for the tip position

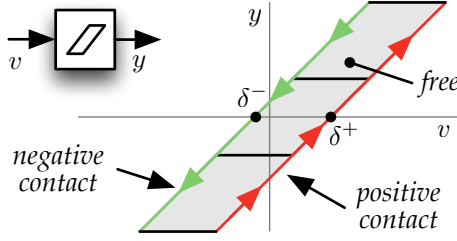


Figure 4.1: The hysteresis model has three modes. In the *free* mode, the output stays constant independent of the input. In the *negative contact* and *positive contact* modes, the output follows the input. Parameters δ^- and δ^+ represent the *negative contact* and the *positive contact* positions, respectively.

estimation. From the estimate of the actual tip position and the (known) actuator movements, the hysteresis in the endoscopic instrument is estimated on-line. This estimate is then used to compensate the hysteresis.

This chapter is outlined as follows: Section 4.2 describes the modeling of the hysteresis and the compensation and estimation algorithms. Section 4.3 provides the models of the kinematics of the instrument and the endoscopic camera. These models are used by the image-based state estimation that is discussed in Section 4.4. Section 4.5 describes the experimental evaluation of the proposed method. Section 4.6 concludes the chapter.

4.2 Hysteresis Compensation and Estimation

The hysteresis in the endoscopic instruments is modeled similar to Lagerberg and Egardt [31]. The model is hybrid with three discrete modes:

- *free*: The output is decoupled from the input
- *negative contact*: The output follows the input as it decreases
- *positive contact*: The output follows the input as it increases

We will denote the input of the hysteresis model as v and the output as y . We will denote the time derivatives of v and y as \dot{v} and \dot{y} , respectively. The model output is given by

$$\dot{y} = \begin{cases} \min(\dot{v}, 0), & y = v + \delta^- & (\text{negative contact}) \\ 0, & v + \delta^- < y < v + \delta^+ & (\text{free}) \\ \max(\dot{v}, 0), & y = v + \delta^+ & (\text{positive contact}) \end{cases}, \quad (4.1)$$

where δ^- and δ^+ represent the negative and positive contact positions, respectively ($\delta^- < \delta^+$). The behavior of the model is illustrated in Fig. 4.1. The magnitude of the hysteresis (the permissible change in v without any change in y) is given by $\delta^+ - \delta^-$.

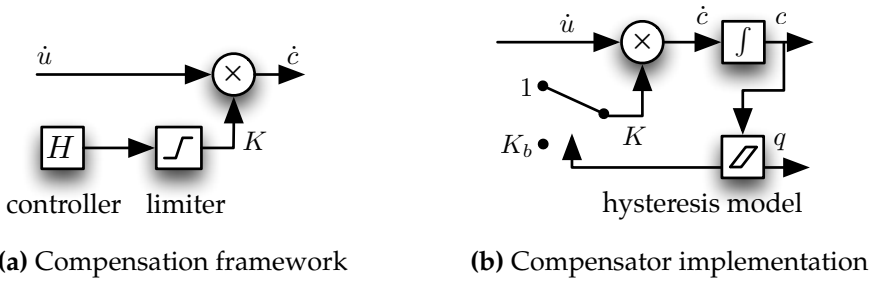


Figure 4.2: Hysteresis compensation: The limited-gain compensation approach (a) has an output rate \dot{c} that is a multiple of the input rate \dot{u} . The gain K is limited, preventing undesired ‘nervous’ behavior of the system. Fig. (b) shows the implementation of controller H . Gain K is selected as either 1 or K_b , depending on whether the hysteresis model is in *contact* mode or in *free* mode.

4.2.1 Compensation

In order to compensate the hysteresis effect, the actuator must be commanded to transverse the free region whenever the direction of motion is reversed. There exist several approaches to transversing this free region. A common approach is to use a fixed motion profile that is executed whenever the direction of motion is reversed [5,31]. However, when the hysteresis is over-estimated, this will result in high-velocity movements of the tip every time this motion profile is executed. Also, in a teleoperated setting, the direction of motion may change often due to tremor of the physician when performing small movements. This would result in a ‘nervous’ behavior of the system, i.e., undesired high-velocity movements of the actuator that result in no or little tip movement.

Therefore, we use a limited-gain compensation approach that limits the actuator velocity to a multiple of the input velocity. This approach is illustrated in Fig. 4.2a. The hysteresis controller determines the desired input-to-actuator velocity gain, denoted K , which is limited to an upper bound, denoted L :

$$0 \leq K \leq L \quad . \quad (4.2)$$

The actuator velocity, denoted \dot{c} , is given by:

$$\dot{c} = K\dot{u} \quad , \quad (4.3)$$

where \dot{u} denotes velocity of the reference input u .

The implementation of the hysteresis controller is illustrated in Fig. 4.2b. The controller uses a model of the hysteresis. If the model predicts that the system is in the *contact* mode, a gain of 1 is used. In the *free* mode, a gain of K_b ($K_b > 1$) is used. The resulting behavior is that the actuator moves K_b times faster than the input in the *free* mode, and thus the observed size of the hysteresis is decreased by a factor K_b . The output position of the hysteresis model is denoted q .

4.2.2 Estimation

The hysteresis estimator has two state variables, denoted δ_k^- and δ_k^+ , which are the estimates of δ^- and δ^+ after the k^{th} estimation update, respectively. An estimation update is performed each time the input has moved a given threshold distance (denoted τ) since the previous estimation update. Using this approach, the update of the estimation is independent of time, and thus independent of the rate of v and y .

The change in v since the last estimation update will be denoted Δv , the change in y will be denoted Δy . When an estimation update is performed, the estimated positive contact position, δ_k^+ , is updated when either

- Δv is positive (i.e., the input moved in the positive direction), and Δv and Δy are equal up to a given error margin (denoted ϵ):

$$|\Delta v - \Delta y| < \epsilon \Delta v \quad , \quad (4.4)$$

or,

- output y is larger than possible according to the model:

$$y > v + \delta_k^+ . \quad (4.5)$$

The updating of δ_k^+ and δ_k^- is illustrated in the flow chart in Fig. 4.3. The inequality condition (4.5) causes the updates of δ_k^+ to take place even when the output y is not yet changing. This speeds up the initial estimation of δ_k^+ on startup of the estimator.

If either condition (4.4) or (4.5) is true, the estimation is updated according to

$$\delta_{k+1}^+ = (1 - \alpha)\delta_k^+ + \alpha(v - y) , \quad (4.6)$$

where α denotes a constant that determines the update speed ($0 < \alpha < 1$). The update of δ_k^- is done in the same way.

4.3 Kinematics and Camera Models

In order to estimate the hysteresis parameters δ^+ and δ^- , the actual position of the endoscopic instrument is required. This actual position will be estimated from the endoscopic images as described in Section 4.4. In order to improve the accuracy of this estimation, two markers are placed on the instrument. The estimation requires a model of the kinematics of the instrument and a model of the endoscopic camera in order to predict the positions of these markers in the endoscopic image. These models are described in this section.

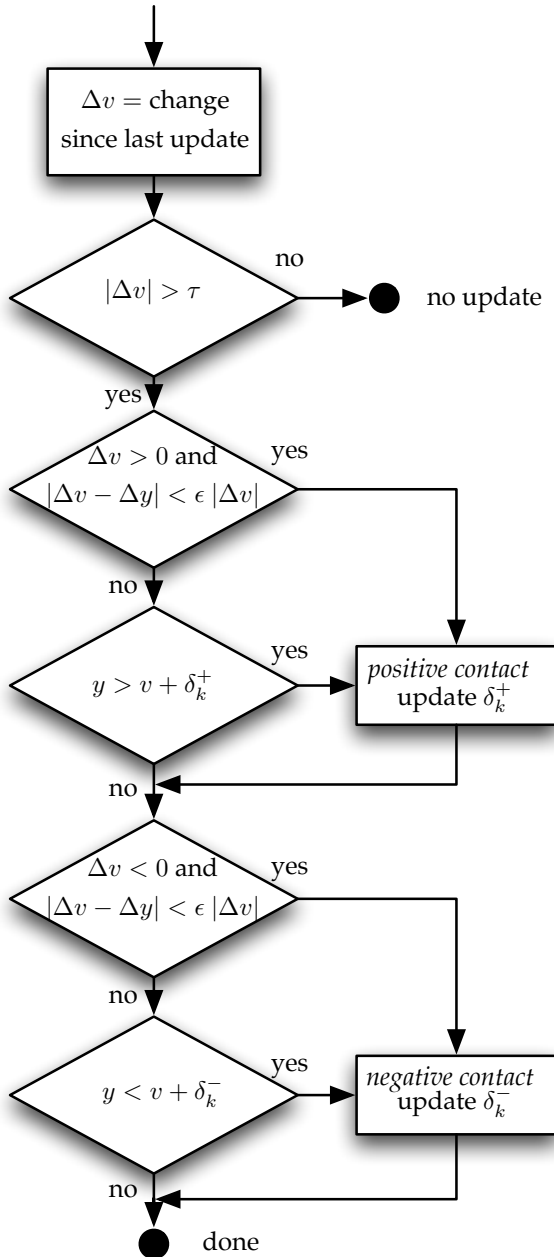


Figure 4.3: Hysteresis estimation: Based on the input motion v and the observed output motion y , *positive contact* and *negative contact* is detected. Estimated hysteresis parameters δ_k^+ and δ_k^- are updated during *positive contact* and *negative contact*, respectively.

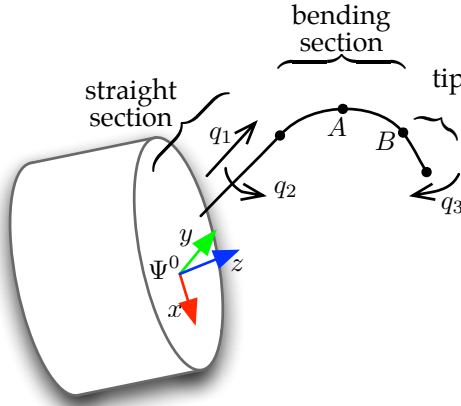


Figure 4.4: The instrument model consists of a straight section, a bending section and the tip. The instrument can be inserted/retracted (q_1), rotated (q_2) and bent (q_3). The model gives the position of the marker points A and B , as a function of q_1 , q_2 , and q_3 .

4.3.1 Kinematics Model of the Instrument

The endoscopic instrument is modeled as a straight section, a bendable section, and a tip (Fig. 4.4). This model is similar to the one used by Bardou et al. [8]. The bendable section is assumed to have a constant radius of curvature along the path. This assumption is valid as long as the forces that are acting on the instrument are limited. The kinematics model predicts the positions of the two markers that are fixed to the instrument:

$$\begin{bmatrix} \mathbf{p}_A \\ \mathbf{p}_B \end{bmatrix} = f(\mathbf{q}), \quad (4.7)$$

where \mathbf{p}_A and \mathbf{p}_B denote the three-dimensional (3D) position of the markers, \mathbf{q} denotes the model state and f denotes the forward kinematics function. The model state \mathbf{q} has three components describing the three degrees of freedom (DOFs) of the instrument: insertion (q_1), rotation (q_2) and bending (q_3). This is illustrated in Fig. 4.4.

4.3.2 Camera Model

The endoscopic camera is modeled as a pinhole camera, with added radial distortion. The camera projection function, denoted $g(\mathbf{p})$, maps a point \mathbf{p} from the 3D world space to the 2D camera image plane:

$$\mathbf{x} = g(\mathbf{p}), \quad (4.8)$$

where \mathbf{x} denotes the position of the point in the 2D camera image.

The kinematics model $f(\mathbf{q})$ and the camera model $g(\mathbf{p})$ can be combined to form a single function (denoted h) that gives the marker positions in the 2D camera image for a given state \mathbf{q} :

$$h(\mathbf{q}) := \begin{bmatrix} g(\mathbf{p}_A) \\ g(\mathbf{p}_B) \end{bmatrix}, \quad (4.9)$$

in which \mathbf{p}_A and \mathbf{p}_B depend on \mathbf{q} according to f as given in (4.7). The resulting vector containing the 2D coordinates of the markers is the measurement vector, denoted \mathbf{s} :

$$\mathbf{s} := h(\mathbf{q}). \quad (4.10)$$

From the kinematics and the camera models, the interaction matrix \mathbf{L} can be derived. \mathbf{L} describes the relation between the change in the state $\dot{\mathbf{q}}$ and the change in the measurement vector $\dot{\mathbf{s}}$:

$$\dot{\mathbf{s}} = \mathbf{L}\dot{\mathbf{q}}, \text{ where } \mathbf{L} := \frac{\partial h}{\partial \mathbf{q}}. \quad (4.11)$$

The interaction matrix \mathbf{L} will be used to estimate the tip position from the endoscopic images.

4.4 Image-based State Estimation

In order to estimate the hysteresis of the endoscopic instrument on-line, the actual state of the endoscopic instrument is required. We will use the endoscopic images to estimate the state of the endoscopic instrument. This is done by first finding the locations of the markers on the instrument in the endoscopic image, and then reconstructing the state of the instrument from these marker locations. As opposed to the approach described in the previous chapter, the reconstruction algorithm is not iterative. The algorithm uses the current position of the actuators as prior knowledge.

4.4.1 Image Processing

The positions of the markers are obtained from the endoscopic image as illustrated in Fig. 4.5. First, the markers are separated from the background by color space segmentation using Fishers linear discriminant method [21]. Subsequently, connected component labeling is applied to the resulting binary image in order to obtain the two marker regions. Finally, the centroid is computed for each marker region. The resulting centroid coordinates form the vector \mathbf{s}^* :

$$\mathbf{s}^* := \begin{bmatrix} c_{1x} \\ c_{1y} \\ c_{2x} \\ c_{2y} \end{bmatrix}, \quad (4.12)$$

where c_{nx} and c_{ny} denote the x and y coordinates of the centroid of the n^{th} marker, respectively ($n = 1, 2$).



Figure 4.5: Endoscopic image processing: From the endoscopic image, the marker regions are extracted and their centroids are computed.

4.4.2 State Estimation

Given the extracted 2D marker positions, the state of the instrument is estimated using a linearization of the function $h(\mathbf{q})$. We will use \mathbf{q}^* to denote the state of the actual instrument (as opposed to \mathbf{q} which denotes the state of the model). Thus, the marker locations are:

$$\mathbf{s}^* = h(\mathbf{q}^*) \quad (4.13)$$

Using a Taylor expansion, (4.13) can be rewritten as:

$$\mathbf{s}^* = h(\mathbf{q}^*) = h(\mathbf{q}) + \frac{\partial h}{\partial \mathbf{q}}(\mathbf{q}) \cdot (\mathbf{q}^* - \mathbf{q}) + o(\|\mathbf{q}^* - \mathbf{q}\|^2), \quad (4.14)$$

where $o(\|\mathbf{q}^* - \mathbf{q}\|^2)$ denotes the higher order terms. In the linearization, these terms are ignored. Replacing \mathbf{q}^* by $\hat{\mathbf{q}}$ to denote the approximation, and using (4.11), (4.14) can be written as:

$$\mathbf{s}^* - \mathbf{s} = \mathbf{L}(\hat{\mathbf{q}} - \mathbf{q}). \quad (4.15)$$

The estimated state $\hat{\mathbf{q}}$ is found using the unweighted pseudo-inverse of \mathbf{L} , denoted \mathbf{L}^\dagger :

$$\hat{\mathbf{q}} = \mathbf{q} + \mathbf{L}^\dagger (\mathbf{s}^* - \mathbf{s}). \quad (4.16)$$

Note that the unweighted pseudo-inverse minimizes the norm $\|\mathbf{s}^* - h(\hat{\mathbf{q}})\|_2$. The estimated state is used to complete the hysteresis reduction system as depicted in the block diagram in Fig. 4.6. The user input \mathbf{u} is translated into actuator movement \mathbf{c} by the hysteresis compensation. From the endoscopic images, the marker locations \mathbf{s}^* are obtained, which are used to compute the estimated state of the model, $\hat{\mathbf{q}}$. Using $\hat{\mathbf{q}}$ and \mathbf{c} , the hysteresis is estimated. This estimate is used to update the hysteresis compensation.

4.5 Evaluation

The hysteresis estimation and compensation system was evaluated experimentally. For the experiment, a conventional colonoscope was used (Exera, Olympus Imaging Corp, Tokyo, Japan). A custom-built instrument guide was fitted on the

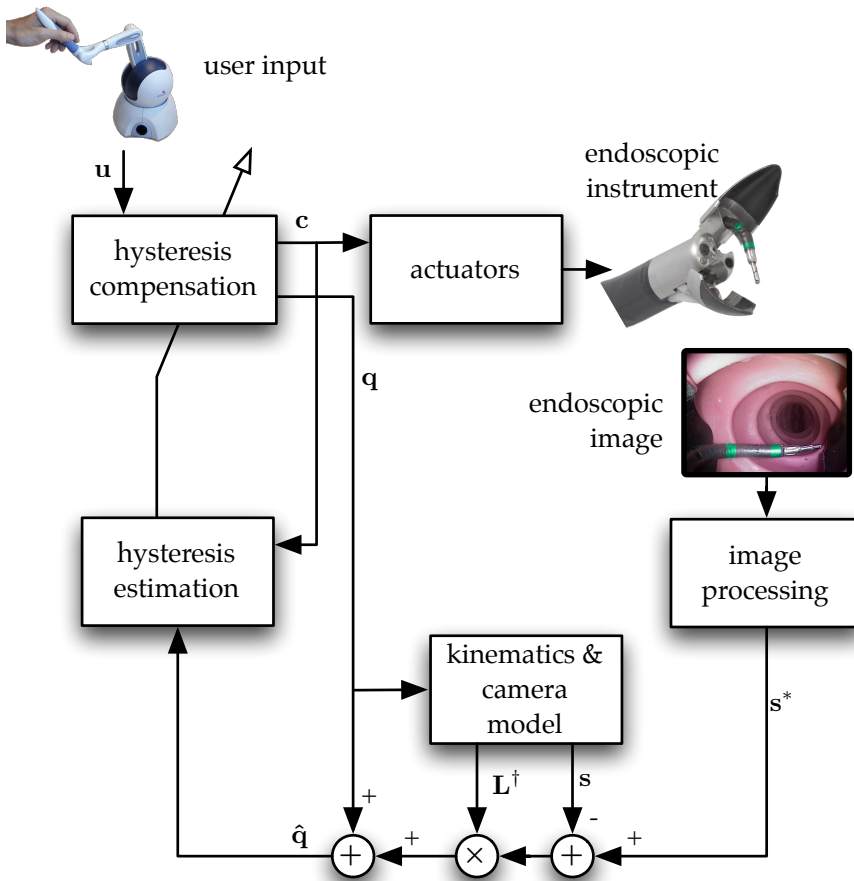


Figure 4.6: Block diagram of the image-based hysteresis reduction system: From the user input u , the hysteresis compensation computes actuator signal c . The actuators move the endoscopic instrument, which is observed in the endoscopic image. Using image processing, the markers are segmented from the image. The marker positions s^* are compared to the marker positions from the combined kinematics and camera model s . The difference is used to compute the estimated instrument state \hat{q} . Using \hat{q} and c , the hysteresis is estimated, and the estimation is used to update the parameters of the hysteresis compensation.

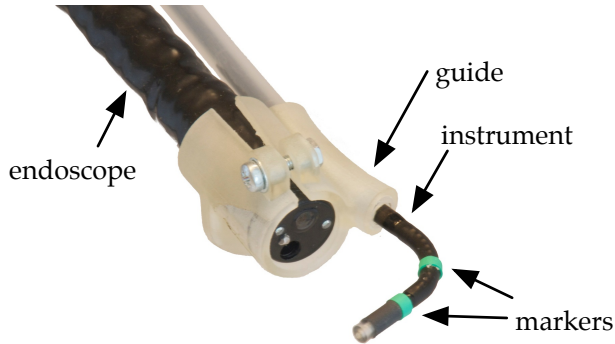


Figure 4.7: Endoscope tip: An instrument-guide was mounted onto the tip of a conventional flexible endoscope in order to properly locate the endoscopic instrument. Two green marker bands were fitted to the instrument.

tip of this colonoscope, in order to let the instrument emerge at the tip in a similar position and orientation as the Anubis endoscope (Fig. 4.7). An instrument of the Anubis endoscope system was used (Karl Storz GmbH & Co. KG, Tuttlingen, Germany).

4.5.1 Experimental Setup

An experimental setup was built that enables actuation of all three DOFs of the instrument. It consists of a linear stage for the insertion and retraction of the instrument, a rotational degree of freedom and a unit that controls the Bowden-cables of the instrument for the bending. A picture of this setup is shown in Fig. 4.8. Three DC motors (A-Max 22, Maxon, Sachseln, Switzerland) were used to actuate all DOFs. They were controlled by Elmo Whistle servo amplifiers (Elmo Motion Control, Petach-Tikva, Israel).

The FireWire output of the colonoscope imaging unit was used to capture the endoscopic images. The processing of the images and the computation of the control algorithms was done on a laptop computer (Macbook Pro 2GHz Core i7, Apple, Cupertino, USA).

4.5.2 Experimental Plan

In order to evaluate the hysteresis estimation and compensation, a pre-determined reference trajectory u was used. A sinusoidal reference input of five periods was applied for each of the DOFs in succession. The initial hysteresis estimation parameters δ_0^+ and δ_0^- were set to 0. This allowed an evaluation of the startup behavior of the estimation. During the experiment, the endoscope tip was fixed and the instrument was moving freely.

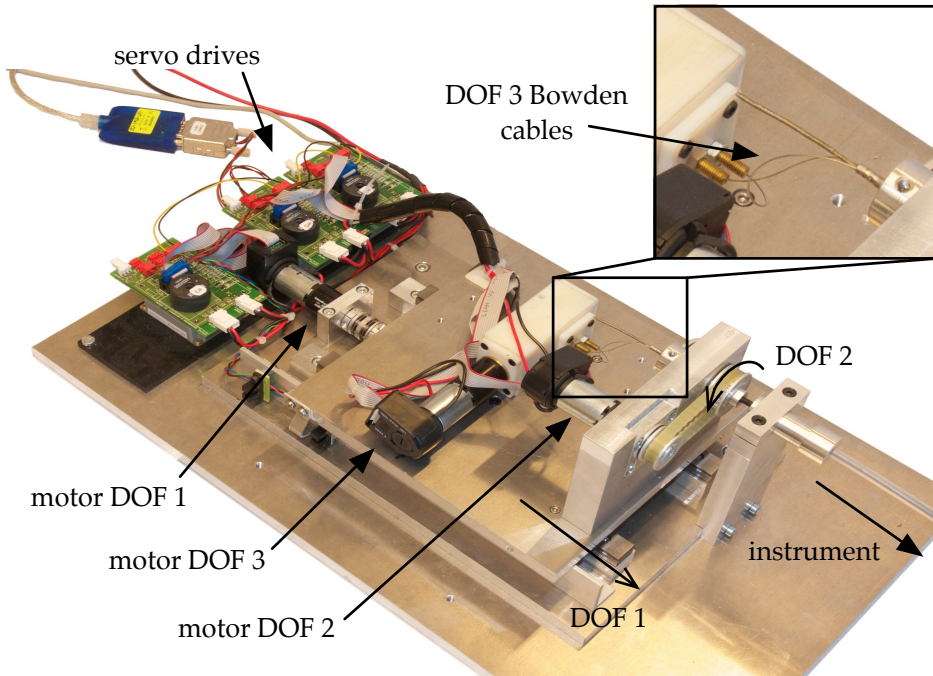


Figure 4.8: An experimental setup was built to actuate the three DOFs of the endoscopic instrument. DOF 3 (bending) is actuated by two miniature Bowden cables that run through the instrument (inset). The servo drives control the three DC motors. The instrument is fed to the tip of the endoscope through a flexible tube.

4.5.3 Results

The results are shown in Fig. 4.9. For each DOF, two graphs are shown. Graphs (a)-(c) show the reference trajectory u , the actuator motion c , and the resulting position \hat{q} that is estimated from the observed instrument. They also show the evolution of the estimated hysteresis parameters δ^+ and δ^- . Graphs (d)-(f) show the uncompensated and the compensated hysteresis. The uncompensated hysteresis graphs show the instrument position \hat{q} versus the actuator position c . The compensated graphs show the instrument position \hat{q} versus the reference position u .

In graphs (a)-(c), it can be seen that the estimated hysteresis parameters δ^+ and δ^- are updated each time the hysteresis comes into the *contact* mode. Graph (b) shows clearly that in the first cycle, the movement of the instrument \hat{q} is significantly smaller than the movement of the reference input u , while in the following cycles the difference in amplitude becomes smaller due to the hysteresis compensation. It can also be observed that the actuator c follows the reference input u if it is in *contact* mode, while it moves quicker when the hysteresis is transversed.

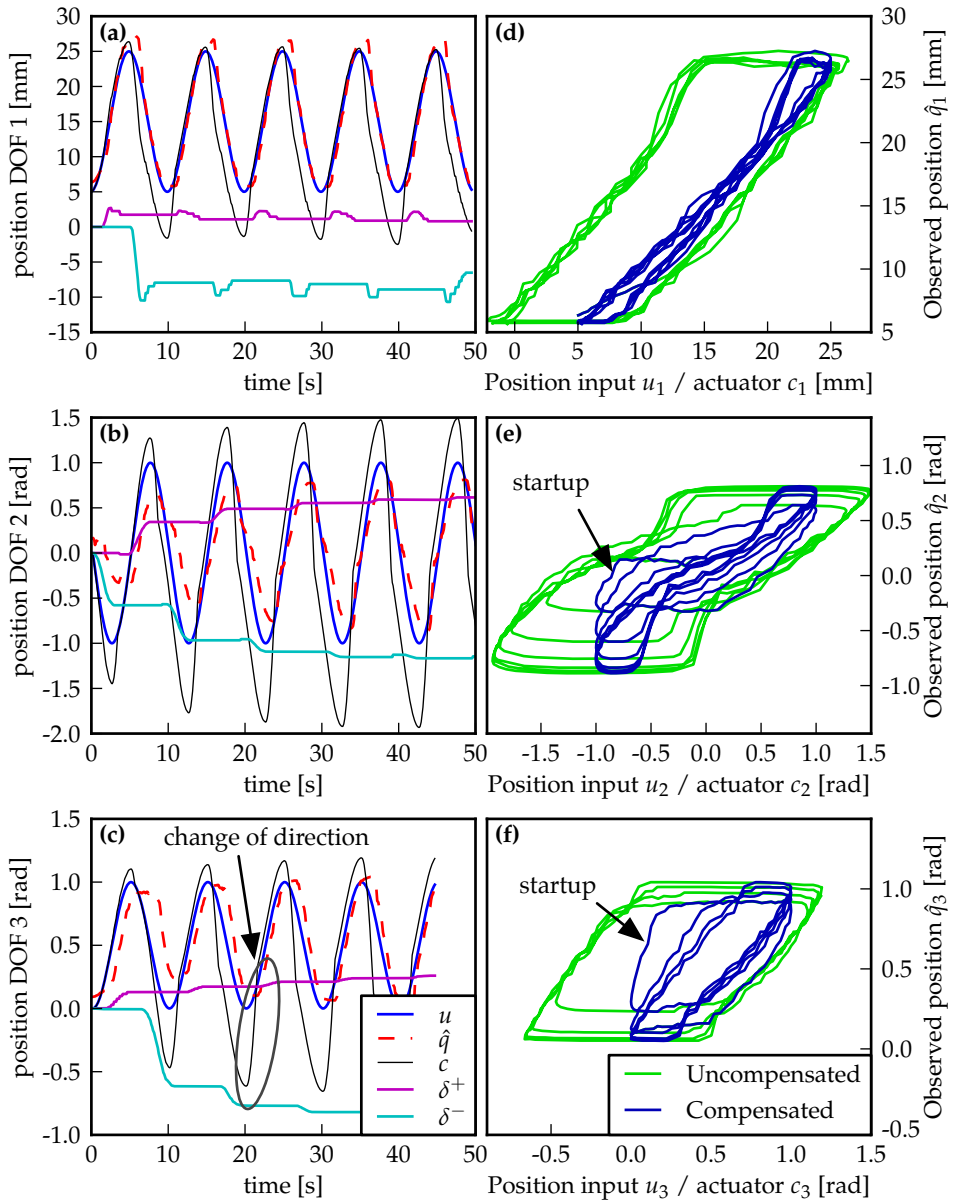


Figure 4.9: Evaluation of the hysteresis reduction: Graphs (a)-(c) show for each DOF the reference position u , the actuator motion c , and the resulting position \hat{q} that is estimated from the observed instrument. They also show the estimated hysteresis parameters δ^+ and δ^- . Graphs (d)-(f) show the original (uncompensated) hysteresis loop for each DOF (\hat{q} vs. c), together with the compensated hysteresis loop (\hat{q} vs. u). It can be seen that after the startup, the observed hysteresis is reduced significantly by the compensation.

	DOF 1	DOF 2	DOF 3
Uncompensated	10 mm	1.8 rad	1.1 rad
Compensated	2.5 mm	0.4 rad	0.3 rad
Reduction	75 %	78 %	73 %

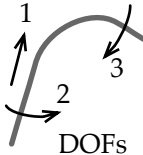


Table 4.1: Results of the hysteresis reduction: The observed hysteresis is significantly reduced by the compensation for each of the DOFs.

The quantitative results are presented in Table 4.1. It shows that the observed hysteresis is reduced significantly by the compensation: 75%, 78%, and 73% for the insertion, rotation, and bending of the instrument, respectively.

4.6 Conclusion

We have developed a hysteresis reduction system that allows accurate control of the endoscopic instruments without adding any additional sensors to the endoscope system. This system uses the endoscopic images to estimate the motions of the actual instrument and to determine the hysteresis between the actuator movement and the movement of the tip of the instrument. The system was experimentally evaluated, and showed a hysteresis reduction of 75%, 78%, and 73% for the insertion, rotation, and bending DOFs of the instrument, respectively. This may enable clinicians to perform advanced flexible endoscopic procedures with higher accuracy as compared to manual operation of the instruments. This comparison of robotic versus manual operation of the instruments is presented in the following chapter.

Evaluation of robotically controlled advanced endoscopic instruments

Advanced flexible endoscopes and instruments with multiple degrees of freedom enable physicians to perform challenging procedures such as the removal of large sections of mucosal tissue. However, these advanced endoscopes are difficult to control and require several physicians to cooperate. In the previous chapter, a robotic system was presented that allows accurate control of the instrument of an advanced flexible endoscope. In this chapter, we will use this system to allow a user to control the instrument in an intuitive way using a haptic device. The hysteresis in the robotic system is reduced using the algorithms that were described in the previous chapter. Performance with the robotic and the conventional control methods are compared in a human subjects experiment. Subjects use both methods to tap a series of targets. For each method, they perform four trials while looking at the endoscopic monitor, and two trials while looking at the instrument directly. They are significantly faster using the robotic method, 54s vs. 164s. Their performance in the second trial is significantly improved with respect to the first trial. This study provides evidence that the robotic control method can be implemented to improve the performance of physicians using advanced flexible endoscopes.

5.1 Introduction

Flexible endoscopy allows for small interventions such as biopsies and polyp removal. However, more advanced procedures such as the removal of larger sections of mucosal tissue are challenging due to the limited dexterity of the endoscopic instruments. In order to overcome this limitation, advanced endoscopic instruments are currently being developed. These advanced instruments have a greater dexterity. This includes the Karl Storz ANUBIS endoscope (Karl Storz GmbH & Co. KG, Tuttlingen, Germany) and the Olympus EndoSamurai (Olympus Corp., Tokyo, Japan). These endoscope systems have the dexterity that would also make them suitable for Natural Orifice Transluminal Endoscopic Surgery (NOTES) [36].

However, the aforementioned endoscopes are difficult to use. Multiple physicians are required to control the endoscope and the instruments [36]. This is undesirable since coordination is difficult, and because of associated costs. Furthermore, the control of the endoscope and the instruments is not intuitive, their interface is not ergonomic and there is significant hysteresis present in the controls which limits the accuracy. A teleoperated setup, in which a single physician controls all degrees of freedom (DOFs) of the endoscope system, could overcome these issues [1, 6]. In order to control the instruments accurately, the hysteresis that is present in these instruments needs to be reduced. This can be done using an external sensor [8], by measuring the hysteresis pre-operatively as described by Abbott *et al.* [1] and Bardou *et al.* [7], or by online estimation based on the endoscopic images as described in the previous chapter. The latter method is advantageous because no external sensors are required, and it can adapt to variations in the hysteresis parameters that may occur during the intervention.

The aforementioned works show that it is possible to control an endoscopic instrument accurately. However, it is not evaluated if there is a performance gain for the physician, i.e. whether the proposed methods are better than conventional control of the instruments in the sense of the task that needs to be performed. In this study, we present a human-subjects experiment that compares robotic teleoperated control of flexible instruments with conventional control (Fig. 5.1).

This chapter is structured as follows. Section 5.2 describes the robotic and the conventional control methods, and the experimental evaluation. The results of the experimental evaluation are presented in Section 5.3. Section 5.4 concludes with a discussion.

5.2 Materials and Methods

In order to evaluate the robotically actuated instruments, a human subject experiment is performed. This section describes the endoscopic instruments, and the robotic control of these instruments. Furthermore, the experimental procedure is also described.

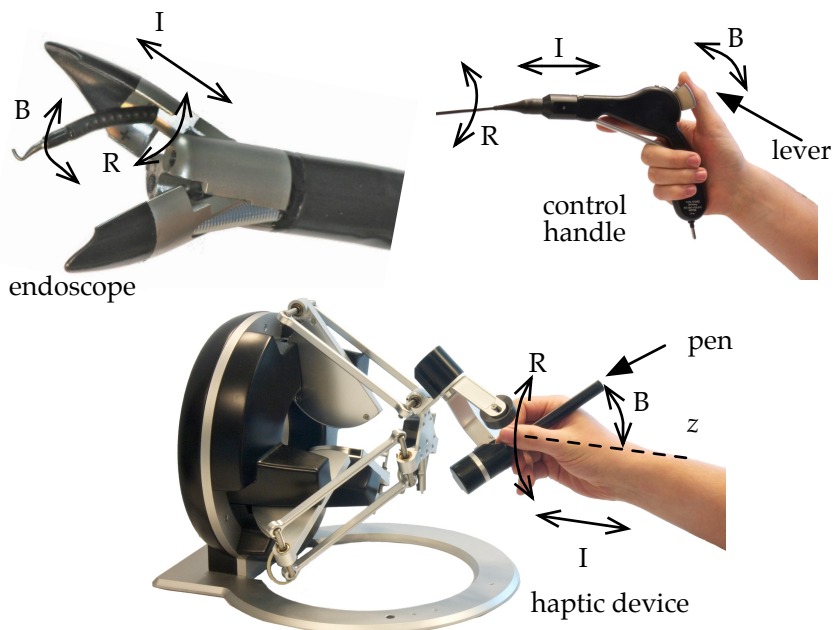


Figure 5.1: The Anubis endoscopic instruments have three degrees of freedom: insertion (I), rotation (R) and bending (B). For the conventional method, these are controlled by moving the control handle forwards and backwards (I), by rotating the control handle (R), and by using the bending lever (B). For the robotic method, these are controlled by moving the haptic device forwards and backwards (I), by rotating the pen around the z -axis (R), and by rotating the pen away from the z -axis (B).

5.2.1 Advanced flexible endoscopic instruments

For this study, an instrument of the Anubis endoscope system (Karl-Storz GmbH & Co. KG) is used. It has three degrees of freedom, as indicated in Fig. 5.1: insertion (I), rotation (R), and bending (B). The instrument is designed to be operated manually. The control handle can be moved forwards and backwards to insert and retract the instrument, and it can be rotated to rotate the instrument around its axis. The bending of the instrument is controlled by a lever that is operated by the thumb.

5.2.2 Robotic control of the endoscopic instrument

A setup is used that allows actuation of all three DOFs of the endoscopic instrument. This setup is depicted in Fig. 5.2. The DOFs are driven by three DC motors (A-Max 22, Maxon, Sachseln, Switzerland), which are controlled by Elmo Whis-

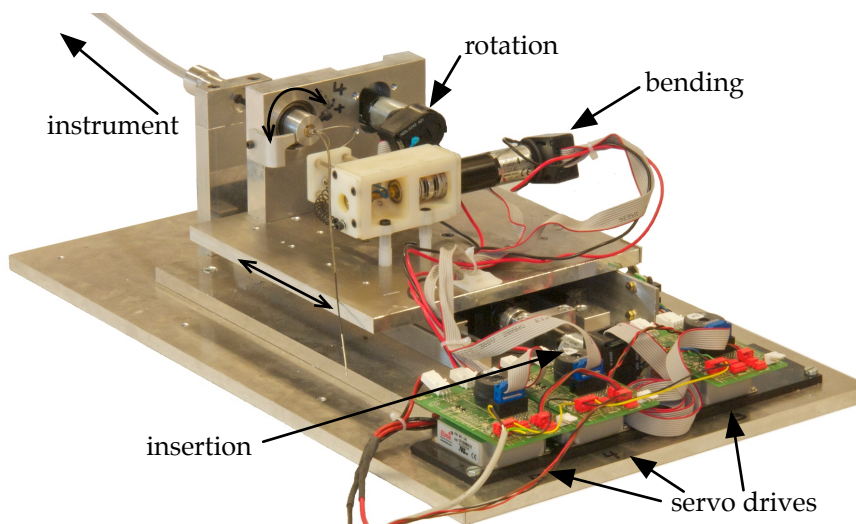


Figure 5.2: Actuation of the instrument: Three motors actuate the insertion, rotation, and bending DOFs of the instrument. The motors are controlled by servo drives.

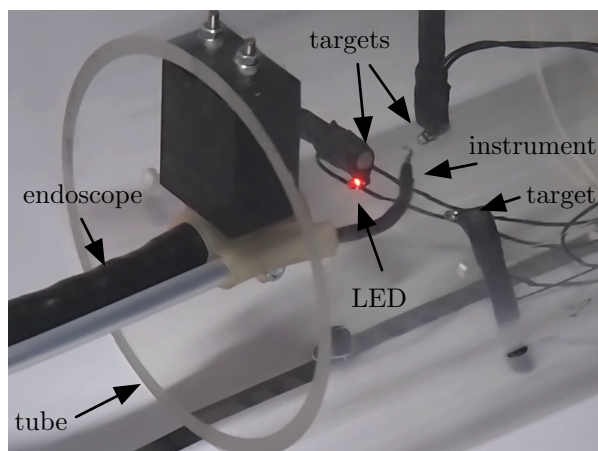


Figure 5.3: The environment for the experiment consisted of a transparent tube with three targets. The endoscope was fixed to the tube. LEDs were used to signal the subject which target was to be tapped.

the servo amplifiers (Elmo Motion Control, Petach-Tikva, Israel). The set-points for the DOFs are generated by a laptop computer (Macbook Pro, 2 GHz Core i7, Apple, Cupertino, USA).

When the instrument is controlled robotically, the hysteresis that is present in the instrument can be reduced to improve the performance. This is done as described in the previous chapter, section 4.2.1. For the current study, we have used

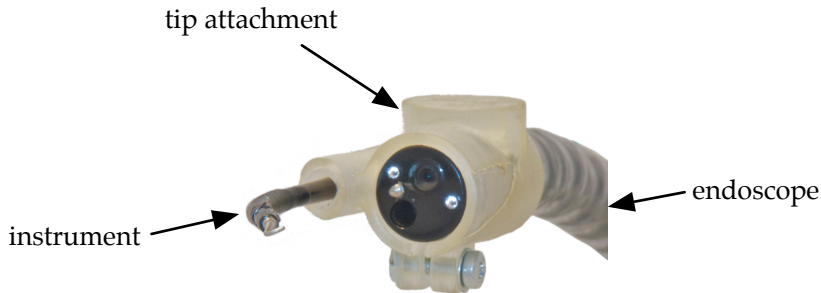


Figure 5.4: A tip attachment is fitted to the tip of the endoscope in order to guide the instrument.

pre-identified values for the hysteresis. However, since in clinical practice these values may change during the procedure, alternatively online estimation of these values could be implemented. The hysteresis can be estimated by comparing the actuator motion and the motion of the instrument tip. The motion of the instrument tip can be obtained from the endoscopic images as described in chapter 4. This method requires no external sensors to be added to the instrument.

5.2.3 Experimental methods

The robotic instrument control method that was described in the previous section was compared to conventional control using a tapping experiment. In the experimental evaluation, subjects used both methods to tap on fixed targets. As opposed to Golenberg *et al.* [22], who used a flat surface with targets, we have constructed a three-dimensional environment that contains the targets. This environment was constructed from a plexiglass tube of 110mm diameter. The endoscope was rigidly attached to this tube, as shown in Fig. 5.3. Three targets were located in the workspace of the endoscopic instrument. They were positioned such that the subjects would need to manipulate all three DOFs of the instrument in order to reach from one target to the next. Each target consisted of a metal bolt of 4mm diameter. The sides of the bolt were covered, to force the subjects to actually tap the top of the target, as opposed to sliding the instrument tip along the side of the target. An orange light emitting diode (LED) next to each target was used to show which target to tap. A circuit was built to detect electrical conductance between the tip of the instrument and the target in order to register when a tap was successful.

A conventional colonoscope was used for the experiment (Exera, Olympus Corp., Tokyo, Japan). A tip attachment was designed to guide the instrument (Fig. 5.4). The position and orientation of the instrument with respect to the endoscope are identical to the Anubis endoscope system.

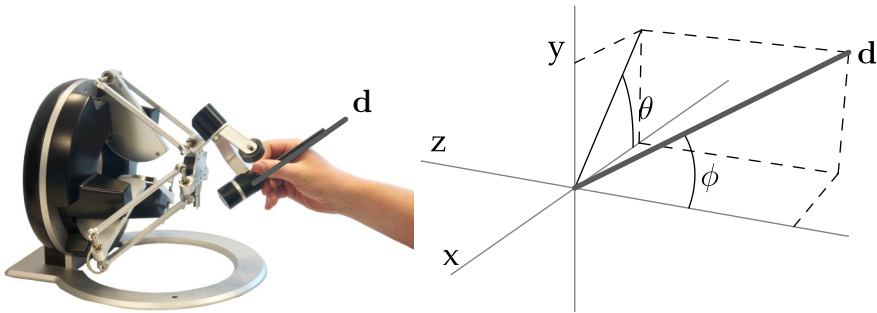


Figure 5.5: The direction of the pen of the haptic device (indicated \mathbf{d}) controls the bending and rotation DOFs. The angle ϕ controls the bending. The angle θ controls the rotation.

5.2.4 Experimental conditions

The control of the endoscopic instruments was evaluated using four experimental conditions. These four conditions are the combinations of two methods and two ways of viewing the environment. The two methods are *robotic* and *conventional*. The two ways of viewing the experimental environment are *endoscopic view* and *direct view*. These methods and views are described below.

Robotic method

In the *robotic* method, the endoscopic instrument is controlled by an Omega 6 haptic device (Force Dimension, Nyon, Switzerland). Insertion (I) is controlled by moving the pen of the Omega 6 forward and backward. The orientation of the pen controls the rotation (R) and bending (B), such that the orientation of the instrument tip will match the orientation of the Omega 6 pen. This is realized as follows. The direction vector of the pen is indicated by \mathbf{d} (Fig. 5.5). The bending is controlled by the angle between \mathbf{d} and the z -axis, denoted ϕ . The rotation is controlled by the rotation around the z -axis, that is, the angle between the x -axis and the projection of \mathbf{d} onto the xy -plane. This angle is denoted θ .

The force-feedback capabilities of the Omega 6 are used to limit the translation of the device to the forward/backward (z) direction. Translations away from the z -axis are counteracted by virtual springs. Fig. 5.6 shows the setup in use with the *robotic* method.

Conventional method

In the *conventional* method, the endoscopic instrument is controlled using the conventional control handle, as shown in Fig. 5.1. Fig. 5.7 shows the experimental setup in use with the *conventional* method. The instrument is inserted into a flexible outer tube that guides the instrument into the endoscope tip attachment. The

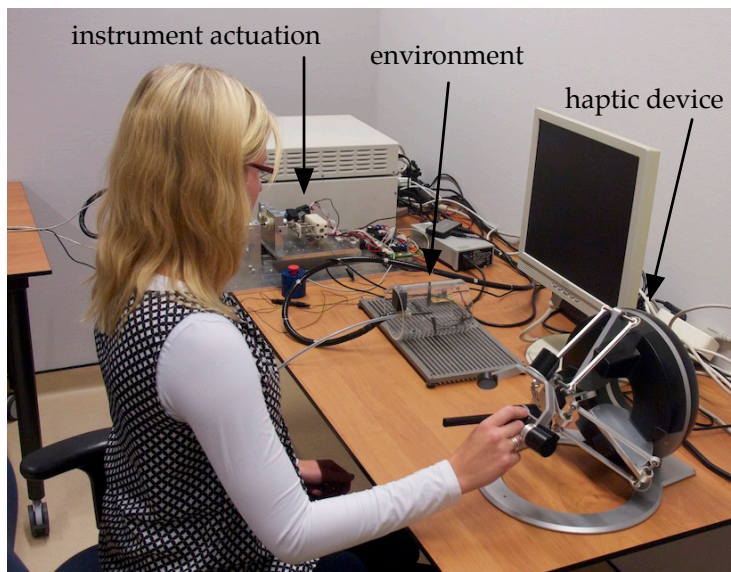


Figure 5.6: Subject performing the experiment using the *robotic* method under the *direct view* condition.

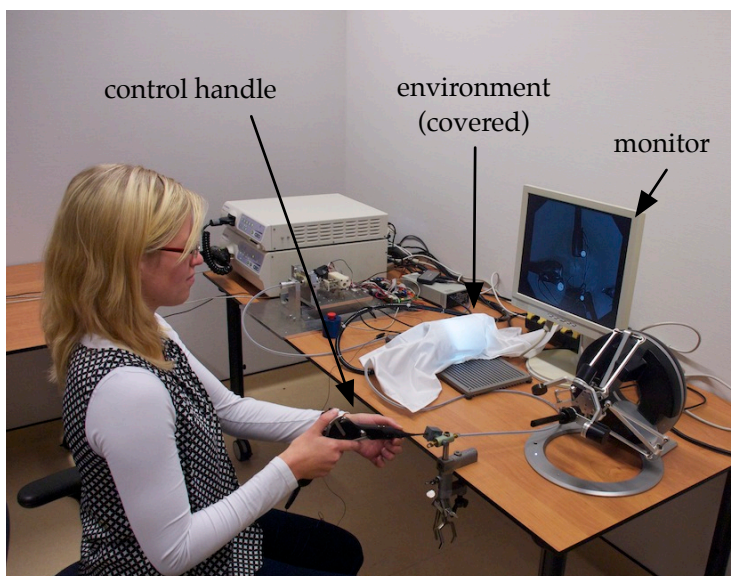


Figure 5.7: Subject performing the experiment using the *conventional* method under the *endoscopic view* condition.

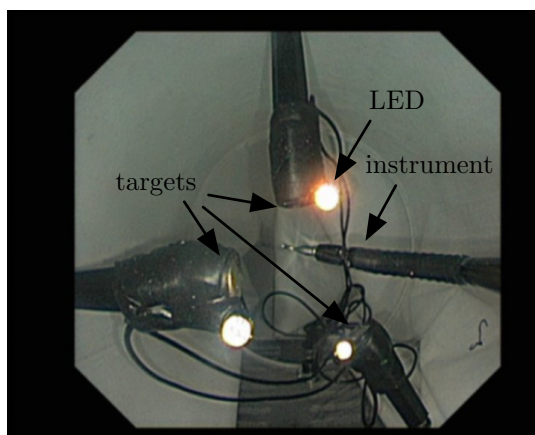


Figure 5.8: This endoscopic image shows the environment as seen on the endoscopic monitor. It shows the instruments, the three targets, and the LED that is illuminated to show which target needs to be tapped.

proximal end of this tube is fixed to the table. Insertion (I) is controlled by inserting the instrument into the outer tube. Rotation (R) is controlled by rotating the control handle. Bending (B) is controlled by a lever on top of the handle that is operated by the thumb.

Endoscopic view

In the *endoscopic view* condition, the scene is captured by the flexible endoscope. The subject observes the scene on a flat screen monitor. The plexiglass tube is covered by a white cloth to ensure the subject cannot see the scene directly. Also, this ensures that the endoscopic view does not contain anything that is outside the plexiglass tube. Furthermore, the white cloth improves the lighting of the scene and thus, the image quality. The *endoscopic view* condition is shown in Fig. 5.7. Fig. 5.8 shows the endoscopic image that is displayed on the monitor.

Direct view

In the *direct view* condition, the subject looks at the scene directly. The endoscope camera system is switched off. This allows the subject to observe the scene stereoscopically, as opposed to the monoscopic (two-dimensional) view that is shown on the monitor in the *endoscopic view* condition. Although the *direct view* condition is not of clinical relevance, it was included to find out whether the lack of stereoscopic vision in the *endoscopic view* condition was of significant influence. The *direct view* condition is shown in Fig. 5.6.

5.2.5 Procedure

Each subject was instructed using a pre-recorded video. This ensured all subjects received the same instructions. The video showed the subject how to manipulate the instruments using both the *robotic* and the *conventional* method, and showed a successful tapping sequence.

After watching the instruction video, the subject performed an experimental session using each of the two methods, while viewing the environment on an endoscopic monitor (Fig. 5.8). The orders in which the methods were used were counterbalanced over the subjects. Each session was composed of four trials consisting of seven taps each, with a small break between the trials. There are six possible paths from one target to the next (from target 1 to 2, from 2 to 3 etc.). The tapping sequences were such that after the first tap, each of the six possible paths was transversed exactly once. In each subsequent trial, the order of the taps was different to ensure that the subjects would not know in advance which would be the next target. The orders were the same for each subject.

When the subject made contact with the target, they were given audible feedback. In order to obtain a successful tap, they needed to remain in contact for 400ms. This was done to prevent accidental touches from being registered as a successful tap. After the 400ms period, another audible feedback signal was given. After the two methods were evaluated using the *endoscopic view*, the subjects repeated the sessions while observing the environment directly (*direct view*). In this case they performed two trials of seven taps for each of the two methods. The complete experiment took 30-45 minutes per subject.

All subjects started with the *endoscopic view* condition, because this one is the most clinically relevant. Of course, this may create a bias towards lower completion times for the *direct view* condition due to learning effects. However, the hypothesis is that subjects will perform better with the *direct view* condition due to the presence of stereoscopic vision. Thus, if indeed subjects do perform better with the *direct view* condition, it cannot be concluded whether this is due to learning or due to the presence of stereoscopic vision. If there are no significant differences between the two view conditions, this will suggest that the presence of stereoscopic vision is not of major influence.

5.2.6 Subjects

16 subjects participated in the experiment. The subjects were senior Technical Medicine students¹ who had completed a training in rigid and flexible endoscopy. As such, they were acquainted with instrument manipulation and the lack of stereoscopic vision during the procedure. There were 4 male and 12 female subjects, aged 22-26 years, with an average age of 24 years. All subjects were right-handed. All subjects had normal stereopsis, as was confirmed by a stereopsis test prior to the experiment [56]. The subjects participated on voluntary basis,

¹Technical Medicine is a Master's level program where students study to integrate advanced technologies within the medical sciences to improve patient care.

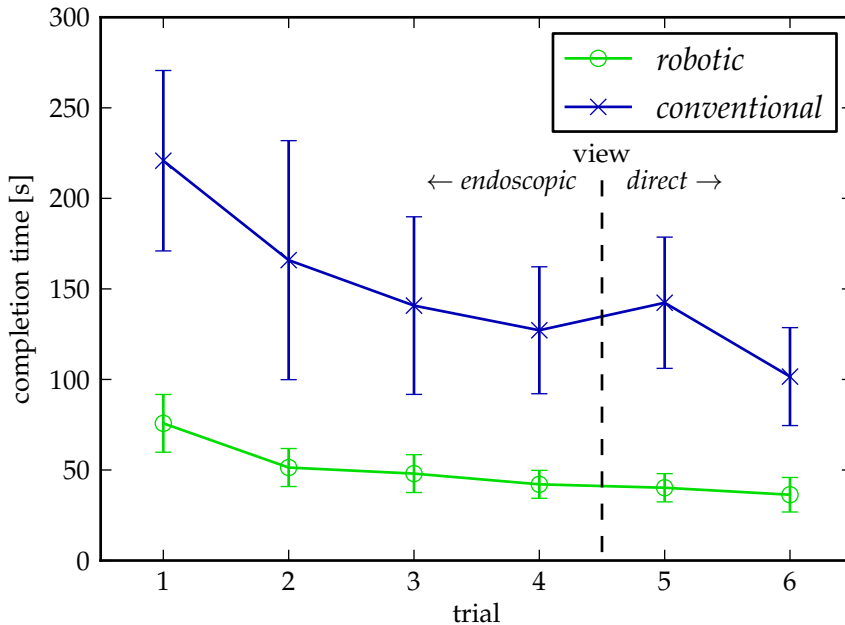


Figure 5.9: Results: The *robotic* method has a lower average completion time than the *conventional* method for each trial. There is a significant learning effect between the first and the second trial. Trials 1 to 4 are performed under the *endoscopic view* condition, while trials 5 and 6 are performed under the *direct view* condition. The error bars indicate the 95% confidence interval.

and signed an informed consent form. They received financial compensation for their participation (€10).

5.3 Results

Fig. 5.9 shows the average completion time for each trial per method. The completion times for each trial were compared using a repeated measures ANOVA (analysis of variance). For the *endoscopic view* condition, significant effects were found for method ($p < 0.001$), trial ($p < 0.001$) and method \times trial interaction ($p = 0.02$). The *robotic* method has a significantly lower average completion time than the *conventional* method, 54s and 164s respectively. Subsequent pairwise comparisons with Bonferroni correction for multiple comparisons showed that the first trial is significantly slower than the other trials ($p < 0.05$). There were no significant differences found between the second and subsequent trials.

Fig. 5.9 suggest that the rate at which the completion times decrease for

each trial is different for the two methods. This is supported by the significant method \times trial interaction effect. Therefore, we have performed a linear least squares fit of the completion time results. For each subject, and for both methods, the four trial completion times were fitted to the linear model

$$t_c = \alpha n + \beta, \quad (5.1)$$

where t_c denotes the completion time, n indicates the trial number ($n = 1 \dots 4$), and α and β are fitting constants. We have done a repeated measures analysis on the resulting slopes α . A significant influence of the method on α was found ($p = 0.03$). The mean α was -10 s/trial for the *robotic* method and -30 s/trial for the *conventional* method. Thus, there was a significantly faster improvement in the *conventional* method than in the *robotic* method.

The *endoscopic view* and the *direct view* conditions were compared using a repeated measures ANOVA on the completion time of the last trial of each method (i.e., trial 4 for the endoscopic view and trial 6 for the direct view). No significant differences were found.

5.4 Discussion

Two methods for control of advanced multi-DOF endoscopic instruments were compared using a tapping experiment. It was found that the average task completion time was significantly lower for the *robotic* method than for the *conventional* method. It was found that for the *conventional* method, the improvement in completion times was higher than for the *robotic* method. This is probably due to the fact that with the robotic method, the learning process is already nearly finished after a few trials, and thus there is hardly any room for further improvement.

From the current experiment, the lowest completion time that the subjects could achieve after performing many trials cannot be determined. Possibly, subjects are able to achieve similar completion times using both methods if they learn more by performing additional trials. To determine the ultimate performance would require another experiment in which the subjects perform more trials. However, even if similar completion times could be achieved using both methods, it would still be favorable to use *robotic* control. It is more intuitive and its ergonomics can be optimized by tuning the mapping between the haptic device and instrument motions. Furthermore, *robotic* control is more suitable to be used in an integrated system in which both the endoscope and the instruments can be controlled by a single physician.

No significant differences were found between the *endoscopic view* and the *direct view* conditions. Thus, the lack of stereoscopic vision seems of little influence during this experiment. All subjects performed the *endoscopic view* condition first, and then the *direct view* condition. This could create a bias towards lower completion times for the *direct view* condition due to learning effects. However, the presence of stereoscopic vision in the *direct view* condition was hypothesized to

also lower the completion time for the *direct view* condition. Yet, no significant differences in completion time were found, and thus there is no indication that the *direct view* condition lowers the completion time. It was noticed that the subjects, which already had experience with (simulated) endoscopic procedures, were well capable to deal with the lack of stereoscopic vision. When they moved the instrument in front of or behind one of the targets, they could correct this quickly and then hit the target.

The objectives of the work described in this thesis were to realize intuitive steering of the endoscope and the endoscopic instruments, and to evaluate the performance of the developed steering methods. Several aspects of the steering of advanced flexible endoscopes and their instruments were covered. The conclusions are summarized in this chapter, and possible directions for future work are provided.

Steering of the endoscope tip

For the steering of the endoscope tip, the use of a haptic device was evaluated using a simulated colonoscopy procedure. The results showed that the experienced physicians were significantly faster when using the conventional control method, and there was no significant difference in completion time for the novice subjects. Of course, the physicians had much more experience with the conventional control method as compared to the 'new' steering methods that were proposed. From the experiment that was conducted, it cannot be concluded whether the two subject groups will perform better with the 'new' steering methods as their experience grows. However, for the purpose of steering of advanced flexible endoscopes, the conventional steering method will not be practical. Since the performance of the physicians is likely to increase with experience, the use of a haptic device to steer the endoscope may be a viable alternative to the conventional steering method. In this setting, haptic guidance can be implemented, since the results of the experiment indicate that this may reduce patient discomfort.

Steering of the endoscopic instruments

For the intuitive and accurate steering of the endoscopic instruments, the hysteresis that is present is a major issue. The hysteresis should thus be compen-

sated. Since the hysteresis may vary during the procedure, on-line estimation is desirable. In order to perform this estimation without adding external sensors to the instrument, a method has been developed that estimates the instrument tip position based on the endoscopic images. The method uses a 'virtual visual servoing' estimation that adjusts the actual state of a model of the instrument so as to match the model to the observed instrument. Two approaches were compared: with and without adding visual markers to the instrument. Both approaches performed similarly, with an RMS estimation error of less than 1.8mm in the horizontal, vertical, and away-from-camera directions. This method provides a way to estimate the position of the instrument tip without any modifications to the existing endoscope or instrument.

A hysteresis estimation and compensation algorithm has been developed that uses the marker-based position estimation approach to estimate the hysteresis in the endoscopic instruments, and to compensate it. A robotic actuation for the instrument was developed to evaluate this algorithm. The experimental validation showed that this algorithm can reduce the hysteresis by approximately 75% in all degrees of freedom of the instrument.

Tele-manipulation of the hysteresis-compensated instruments was compared to conventional control of the instruments in a human-subject experiment. This comparison showed that the subjects were significantly faster using robotically actuated instruments, with a 67% shorter completion time than the conventional control. This shows that tele-operation of the hysteresis-compensated instruments is a viable method to steer the endoscopic instruments accurately.

Recommendations for future work

The results of the studies that were described in this thesis show that intuitive tele-operation of an advanced flexible endoscope and the instruments can be realized. However, for the steering of the endoscope as described in chapter 2, it was found that the experienced subjects still performed significantly better using the conventional method. It would be interesting to see if the performance with the 'new' steering methods that were described can approach or even exceed the conventional method with more training. This will require a more elaborate experiment in which the performance of several trials using both methods is recorded to monitor the learning effect.

Furthermore, a complete setup should be realized that implements the steering of the endoscope and the instruments as described in this thesis. This involves actuation of all DOFs of the endoscope and all instruments. Also, a master console needs to be realized. This master console will contain a monitor on which the physician can observe the endoscopic image, and the haptic devices that control the endoscope and the instruments. Using this setup, clinically relevant experiments can be performed, such as *ex-vivo* cutting and suturing. Those experiments will show whether tele-operated control can be used to

perform clinical tasks effectively. If this is indeed the case, the next steps towards actual implementation in clinical practice can be made.

Before implementation in clinical practice, an important issue to be addressed is the robustness of the system. For the image processing algorithms that were described in this thesis, the robustness has not been studied thoroughly. Yet, robustness against e.g. lighting variations and occlusions is essential if these algorithms are to be used in clinical practice. Thus, this is an issue that still needs to be investigated.

For the estimation of the 3D instrument tip position that was described in chapter 3, an alternative approach may be to use Fiber Bragg Grating (FBG) sensors in the tip and the bending section of the instruments [33]. These optical strain gauges are well suited to miniaturization, and can withstand the high temperatures that occur during the sterilization of the instruments. From the measured strains, the shape of the instrument may be reconstructed, and this may be used as an input for the hysteresis estimation algorithm that was described in chapter 4. A major advantage of the FBG sensors over the image-based position estimation would be that the FBG sensors are not influenced by lighting variations or occlusions. Possible drawbacks of FBG sensors are the added costs and complexity.

Using either FBG or image-based measurements, it may be possible to determine the forces that are acting on the tip of the instruments. These external forces will lead to a deviation of the measurements from the prediction that can be made using a model. From the deviations that are observed, the forces may be inferred. This can be used to provide haptic feedback to the physician, which can help to improve his performance.

Robotic flexible endoscopy

In rigid endoscopic surgery, the da Vinci surgical system by Intuitive Surgical, Inc. is a successful robotic surgical platform that has changed the way interventions are performed. For flexible endoscopy, no such system is available for clinical use, but research prototypes are under development, as outlined in the introduction. These have the potential to enable clinicians to perform interventions more efficiently and less invasively. The flexibility that is present in the endoscope presents new challenges that are to be solved in order to create a surgical platform that can be controlled intuitively and accurately. Solutions to some of these challenges were presented in this thesis.

Appendix A

Derivation of the forward kinematics of the instrument model

Here we show the derivation of the analytical Jacobian $\mathbf{J}_f(\mathbf{q})$ of the forward kinematics function $f(\mathbf{q})$ in (3.2). We define five frames on the instrument (Fig. A.1). Frame Ψ^0 is the camera frame, with the z -axis in the direction of the camera optical axis. Frame Ψ^1 is located at the point where the instrument emerges from the endoscope, with the z -axis aligned with the instrument direction. Frame Ψ^2 is at the end of the straight section, rotating with the instrument rotation q_2 . Frame Ψ^3 is midway the bending section, and frame Ψ^4 is at the end of the bending section.

We first derive the unit twists of frames Ψ^2 , Ψ^3 and Ψ^4 associated with each of the three DOFs. We denote the motion of frame Ψ^l with respect to frame Ψ^m , expressed in frame Ψ^k as the infinitesimal twist $\mathbf{T}_l^{k,m}$. We denote the unit twist of frame Ψ^l associated with q_j , with respect to frame Ψ^0 , expressed in frame Ψ^0 as $\hat{\mathbf{T}}_{l,j}$. From the unit twists, the Jacobian $\mathbf{J}_f(\mathbf{q})$ is derived.

Straight section

The pose of frame Ψ^2 , located at the end of the straight section, is defined by q_1 and q_2 , which are a translation along the z -axis of frame Ψ^1 and a rotation around the same axis, respectively. Thus, the pose of frame Ψ^2 with respect to frame Ψ^1 is given by:

$${}^1_2\mathbf{H} = \begin{bmatrix} 0 & & & \\ \mathbf{R}_z(q_2) & 0 & & \\ & q_1 & & \\ 0 & 0 & 0 & 1 \end{bmatrix}, \quad (\text{A.1})$$

where $\mathbf{R}_z(\cdot)$ denotes the 3-by-3 rotation matrix around the z -axis. The pose of frame Ψ^1 with respect to frame Ψ^0 is determined by the geometry of the endoscope, and is thus fixed.

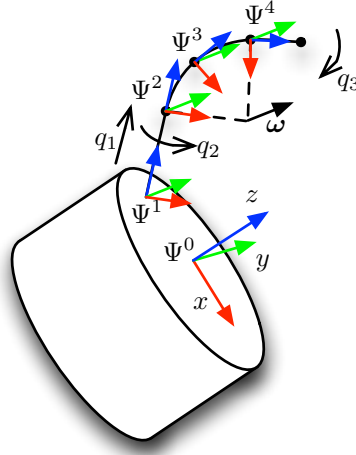


Figure A.1: Five frames are defined: frame Ψ^0 and Ψ^1 are fixed to the endoscope, while frame Ψ^2 , Ψ^3 and Ψ^4 are fixed along the instrument. q_1 , q_2 , and q_3 denote the three DOFs: insertion, rotation, and bending, respectively.

The motion of frame Ψ^2 with respect to frame Ψ^0 is described by the infinitesimal twist:

$$\mathbf{T}_2^{0,0} = \hat{\mathbf{T}}_{2,1}\dot{q}_1 + \hat{\mathbf{T}}_{2,2}\dot{q}_2, \quad (\text{A.2})$$

where $\hat{\mathbf{T}}_{2,1}$ and $\hat{\mathbf{T}}_{2,2}$ represent a translation along the z -axis of frame Ψ^1 and a rotation around that z -axis, respectively. They are:

$$\hat{\mathbf{T}}_{2,1} = \text{Ad}_{\mathbf{0}_1^{\mathbf{H}}} [0 \ 0 \ 0 \ 0 \ 0 \ 1]^T \quad (\text{A.3})$$

$$\hat{\mathbf{T}}_{2,2} = \text{Ad}_{\mathbf{0}_1^{\mathbf{H}}} [0 \ 0 \ 1 \ 0 \ 0 \ 0]^T, \quad (\text{A.4})$$

where $\text{Ad}_{\mathbf{0}_1^{\mathbf{H}}}$ denotes the Adjoint operator that changes the coordinates of the twist from frame Ψ^1 to frame Ψ^0 .

Bending section

The bending section is modeled as a constant curvature. It can be defined by a finite twist around axis $\omega = [0 \ \omega \ 0]^T$ (Fig. A.1), where ω is the angle of the arc. The axis ω is in the y -direction of frame Ψ^2 , located at $[\rho \ 0 \ 0]^T$ in frame Ψ^2 , where ρ denotes the curve radius. The chord length, denoted ℓ , is given by $\ell = \omega\rho$. q_3 is defined as $q_3 := \omega$. This results in the finite twist describing the

bending section:

$$\mathbf{S}_4^{2,2} = \begin{bmatrix} \rho & \boldsymbol{\omega} \\ 0 & \wedge & \boldsymbol{\omega} \\ 0 & & \end{bmatrix} = \begin{bmatrix} 0 \\ q_3 \\ 0 \\ 0 \\ 0 \\ \ell \end{bmatrix}, \quad (\text{A.5})$$

where $\mathbf{S}_4^{2,2}$ denotes the finite twist of frame Ψ^4 with respect to frame Ψ^2 expressed in frame Ψ^2 . The infinitesimal twist $\mathbf{T}_4^{2,2}$ can be derived from the finite twist $\mathbf{S}_4^{2,2}$ using the definition of the twist in matrix form (denoted by the tilde: $\tilde{\mathbf{T}}_l^{k,m}$):

$$\tilde{\mathbf{T}}_4^{2,2} := \frac{2}{4} \dot{\mathbf{H}}_2^4 \mathbf{H} \quad (\text{A.6})$$

$$= \frac{\partial \mathbf{S}_4^{2,2}}{\partial q_3} \dot{q}_3 \exp(\tilde{\mathbf{S}}_4^{2,2}) \quad (\text{A.7})$$

$$= \begin{bmatrix} 0 & 0 & 1 & \frac{\ell}{q_3^2}(-1 + \cos q_3) \\ 0 & 0 & 0 & 0 \\ -1 & 0 & 0 & \frac{\ell}{q_3^2}(q_3 - \sin q_3) \\ 0 & 0 & 0 & 0 \end{bmatrix} \dot{q}_3. \quad (\text{A.8})$$

The unit twist $\hat{\mathbf{T}}_{4,3}$ is found by writing (A.8) in vector form, and transforming it to frame Ψ^0 :

$$\hat{\mathbf{T}}_{4,3} = \text{Ad}_{\mathbf{q}_2} \mathbf{H} \begin{bmatrix} 0 \\ 1 \\ 0 \\ \frac{\ell}{q_3^2}(-1 + \cos q_3) \\ 0 \\ \frac{\ell}{q_3^2}(q_3 - \sin q_3) \end{bmatrix} \quad (\text{A.9})$$

Since frame Ψ^3 is located midway the bending section, unit twist $\hat{\mathbf{T}}_{3,3}$ is found by substituting ℓ by $\frac{\ell}{2}$ in (A.9).

The velocity of a point \mathbf{p}_i , that is fixed to frame Ψ^l , is [55]

$$\dot{\mathbf{p}}_i = \tilde{\mathbf{T}}_l^{0,0} \mathbf{p}_i, \quad (\text{A.10})$$

with respect to frame Ψ^0 and expressed in frame Ψ^0 . Since point A (Fig. 3.2) is fixed to frame Ψ^3 , and point B and C are fixed to frame Ψ^4 , the Jacobian \mathbf{J}_f is:

$$\mathbf{J}_f = \begin{bmatrix} \tilde{\mathbf{T}}_{3,1} \mathbf{p}_A & \tilde{\mathbf{T}}_{3,2} \mathbf{p}_A & \tilde{\mathbf{T}}_{3,3} \mathbf{p}_A \\ \tilde{\mathbf{T}}_{4,1} \mathbf{p}_B & \tilde{\mathbf{T}}_{4,2} \mathbf{p}_B & \tilde{\mathbf{T}}_{4,3} \mathbf{p}_B \\ \tilde{\mathbf{T}}_{4,1} \mathbf{p}_C & \tilde{\mathbf{T}}_{4,2} \mathbf{p}_C & \tilde{\mathbf{T}}_{4,3} \mathbf{p}_C \end{bmatrix}. \quad (\text{A.11})$$

Note that $\tilde{\mathbf{T}}_{3,1} = \tilde{\mathbf{T}}_{4,1} = \tilde{\mathbf{T}}_{2,1}$ and $\tilde{\mathbf{T}}_{3,2} = \tilde{\mathbf{T}}_{4,2} = \tilde{\mathbf{T}}_{2,2}$ since the poses of frame Ψ^3 and Ψ^4 with respect to frame Ψ^2 are independent of q_1 and q_2 .

Bibliography

- [1] D. Abbott, C. Becke, R. Rothstein, and W. Peine. Design of an endoluminal NOTES robotic system. In *Proc. IEEE/RSJ Int'l Conf. on Intelligent Robots and Systems (IROS)*, pages 410–416, San Diego, CA, USA, 2007.
- [2] P. Allemann, L. Ott, M. Asakuma, N. Masson, S. Perretta, B. Dallemagne, D. Coumaros, M. De Mathelin, L. Soler, and J. Marescaux. Joystick interfaces are not suitable for robotized endoscope applied to notes. *Surg Innov*, 16(2):111–116, 2009.
- [3] K. V. Asari. A fast and accurate segmentation technique for the extraction of gastrointestinal lumen from endoscopic images. *Medical Engineering & Physics*, 22(2):89–96, 2000.
- [4] J. A. Astudillo, E. Sporn, S. Bachman, B. Miedema, and K. Thaler. Transgastric cholecystectomy using a prototype endoscope with 2 deflecting working channels (with video). *Gastrointestinal Endoscopy*, 69(2):297 – 302, 2009.
- [5] B. Bardou. *Développement et étude d'un système robotisé pour l'assistance à la chirurgie transluminale*. PhD thesis, Université de Strasbourg, 2011.
- [6] B. Bardou, F. Nageotte, P. Zanne, and M. de Mathelin. Design of a telemanipulated system for transluminal surgery. In *31st Annual International Conference of the IEEE EMBS*, 2009.
- [7] B. Bardou, F. Nageotte, P. Zanne, and M. De Mathelin. Improvements in the control of a flexible endoscopic system. In *Proc. IEEE Int'l. Conf. on Robotics and Automation (ICRA)*, pages 3725–3732, St. Paul, MN, USA, May 2012.
- [8] B. Bardou, P. Zanne, F. Nageotte, and M. de Mathelin. Control of a multiple sections flexible endoscopic system. In *Proc. IEEE/RSJ Int'l Conf. on Intelligent Robots and Systems (IROS)*, pages 2345–2350, Taipei, Taiwan, Oct. 2010.
- [9] A. Bettini, P. Marayong, S. Lang, A. Okamura, and G. Hager. Vision-assisted control for manipulation using virtual fixtures. 20(6):953 – 966, 2004.
- [10] J. Bluteau, S. Coquillart, Y. Payan, and E. Gentaz. Haptic guidance improves the visuo-manual tracking of trajectories. *PLoS ONE*, 3(3), 2008.
- [11] J.-Y. Bouguet. Camera calibration toolbox for Matlab, URL: http://www.vision.caltech.edu/bouguetj/calib_doc.
- [12] I. A. M. J. Broeders and S. S. Kalisingh, editors. *Handboek endoscopische chirurgie*. Bohn Stafleu van Loghum, 2009.

- [13] C. Cao, M. Zhou, D. Jones, and S. Schwaitzberg. Can surgeons think and operate with haptics at the same time? *Journal of Gastrointestinal Surgery*, 11:1564–1569, 2007.
- [14] F. J. Carter, M. P. Schijven, R. Aggarwal, T. Grantcharov, N. K. Francis, G. B. Hanna, J. J. Jakimowicz, and Work Group for Evaluation and Implementation of Simulators and Skills Training Programmes. Consensus guidelines for validation of virtual reality surgical simulators. *Surg Endosc*, 19(12):1523–32, Dec. 2005.
- [15] R. S. Chamberlain and S. V. Sakpal. A comprehensive review of single-incision laparoscopic surgery (sils) and natural orifice transluminal endoscopic surgery (notes) techniques for cholecystectomy. *J Gastrointest Surg*, 13(9):1733–40, Sept. 2009.
- [16] F. Chaumette and S. Hutchinson. Visual servo control. I. basic approaches. *Robotics Automation Magazine, IEEE*, 13(4):82–90, Dec. 2006.
- [17] T. R. Coles, D. Meglan, and N. W. John. The role of haptics in medical training simulators: A survey of the state-of-the-art. *IEEE Transactions on Haptics*, 2010, In Press.
- [18] D. Coombs, M. Herman, T.-H. Hong, and M. Nashman. Real-time obstacle avoidance using central flow divergence, and peripheral flow. 14(1):49–59, 1998.
- [19] B. Dallemagne and J. Marescaux. The ANUBIS™ project. *Minimally Invasive Therapy & Allied Technologies*, 19(5):257–261, 2010. PMID: 20868298.
- [20] C. Doignon, F. Nageotte, B. Maurin, and A. Krupa. Pose estimation and feature tracking for robot assisted surgery with medical imaging. In D. Kragic and V. Kyrki, editors, *Unifying Perspectives in Computational and Robot Vision*, pages 79–101. Springer US, 2008.
- [21] R. Fisher. The use of multiple measurements in taxonomic problems. *Annals of Eugenics*, 7(2):179–188, 1936.
- [22] L. Golenberg, A. Cao, R. D. Ellis, M. Klein, G. Auner, and A. K. Pandya. Hand position effects on precision and speed in telerobotic surgery. *Int J Med Robot*, 3(3):217–23, Sept. 2007.
- [23] R. C. Gonzalez and R. E. Woods. *Digital Image Processing*. Prentice Hall, 2002.
- [24] G. C. Harewood. Relationship of colonoscopy completion rates and endoscopist features. *Digestive Diseases and Sciences*, 50(1):47–51, 2005.
- [25] J. Harris and H. Stocker. *Handbook of Mathematics and Computational Science*. Springer-Verlag, 1998.

- [26] K. Ikeda, K. Sumiyama, H. Tajiri, K. Yasuda, and S. Kitano. Evaluation of a new multitasking platform for endoscopic full-thickness resection. *Gastrointestinal Endoscopy*, 73(1):117 – 122, 2011.
- [27] A. N. Kalloo et al. Flexible transgastric peritoneoscopy: a novel approach to diagnostic and therapeutic interventions in the peritoneal cavity. *Gastrointestinal Endoscopy*, 60(1):114–117, 2004.
- [28] V. Karimyan, M. Sodergren, J. Clark, G.-Z. Yang, and A. Darzi. Navigation systems and platforms in natural orifice transluminal endoscopic surgery (notes). *International Journal of Surgery*, 7(4):297 – 304, 2009.
- [29] N. Kuperij, R. Reilink, M. P. Schwartz, S. Stramigioli, S. Misra, and I. A. M. J. Broeders. Design of a user interface for intuitive colonoscope control. In *Proc. IEEE/RSJ Int'l. Conf. on Intelligent Robots and Systems (IROS)*, pages 937 –942, Sept. 2011.
- [30] C. K. Kwok, G. N. Khan, and D. F. Gillies. Automated endoscope navigation and advisory system from medical imaging. In *Physiology and function from multidimensional images*, San Diego, CA, USA, Feb. 1999.
- [31] A. Lagerberg and B. S. Egardt. Estimation of backlash with application to automotive powertrains. In *Proc. 42nd IEEE Conf. on Decision and Control*, pages 4521–4526, Maui, Hawaii USA, Dec. 2003.
- [32] M. Liedlgruber and A. Uhl. Endoscopic image processing - an overview. In *Proc. 6th Int'l Symp. on Image and Signal Processing and Analysis*, pages 707 – 712, 2009.
- [33] Z. Lunwei, Q. Jinwu, S. Linyong, and Z. Yanan. Fbg sensor devices for spatial shape detection of intelligent colonoscope. In *Proc. IEEE Int'l. Conf. on Robotics and Automation (ICRA)*, volume 1, pages 834 – 840 Vol.1, 2004.
- [34] H. B. Mann and D. R. Whitney. On a test of whether one of two random variables is stochastically larger than the other. *Annals of Mathematical Statistics*, 18(1):50–60, 1947.
- [35] É. Marchand and F. Chaumette. Virtual visual servoing: a framework for real-time augmented reality. *Eurographics*, 21(3):289–298, 2002.
- [36] J. Marescaux, B. Dallemagne, S. Perretta, A. Wattiez, D. Mutter, and D. Coumaros. Surgery without scars: report of transluminal cholecystectomy in a human being. *Archives of Surgery*, 142(9):823–826, 2007.
- [37] C. McCarthy and N. Barnes. Performance of optical flow techniques for indoor navigation with a mobile robot. volume 5, pages 5093–5098, New Orleans, LA, USA, Apr. 2004.
- [38] Y. Nakamura. *Advanced Robotics, Redundancy and Optimization*. Addison-Wesley, 1991.

- [39] OpenGL: The industry standard for high performance graphics, URL: www.opengl.org.
- [40] J. P. Pearl and J. L. Ponsky. Natural orifice transluminal endoscopic surgery: a critical review. *J Gastrointest Surg*, 12(7):1293–300, July 2008.
- [41] S. J. Phee, K. Y. Ho, D. Lomanto, S. C. Low, V. A. Huynh, A. P. Kencana, K. Yang, Z. L. Sun, and S. C. S. Chung. Natural orifice transgastric endoscopic wedge hepatic resection in an experimental model using an intuitively controlled master and slave transluminal endoscopic robot (master). *Surg Endosc*, 24(9):2293–8, Sept. 2010.
- [42] S. J. Phee, S. C. Low, Z. L. Sun, K. Y. Ho, W. M. Huang, and Z. M. Thant. Robotic system for no-scar gastrointestinal surgery. *The International Journal of Medical Robotics and Computer Assisted Surgery*, 4(1):15–22, 2008.
- [43] D. Rattner and A. Kalloo. ASGE/SAGES working group on natural orifice transluminal endoscopic surgery. *Surg Endosc*, (20):329–333, 2006.
- [44] R. Reilink, G. de Bruin, M. Franken, M. A. Mariani, S. Misra, and S. Stramigioli. Endoscopic camera control by head movements for thoracic surgery. In *Proc. 3rd IEEE RAS/EMBS Int'l. Conf. on Biomedical Robotics and Biomechatronics (BioRob)*, pages 510–515, Tokyo, Japan, Sept. 2010.
- [45] R. Reilink, A. M. L. Kappers, S. Stramigioli, and S. Misra. Evaluation of robotically controlled advanced endoscopic instruments. *International Journal of Medical Robotics and Computer Assisted Surgery*, 2013. Accepted for publication.
- [46] R. Reilink, S. Stramigioli, A. M. L. Kappers, and S. Misra. Evaluation of flexible endoscope steering using haptic guidance. *International Journal of Medical Robotics and Computer Assisted Surgery*, 7(2):178–186, 2011.
- [47] R. Reilink, S. Stramigioli, and S. Misra. Image-based flexible endoscope steering. In *Proc. IEEE/RSJ Int'l. Conf. on Intelligent Robots and Systems*, pages 2339–2344, Taipei, Taiwan, Oct. 2010.
- [48] R. Reilink, S. Stramigioli, and S. Misra. Three-dimensional pose reconstruction of flexible instruments from endoscopic images. In *Proc. IEEE/RSJ Int'l. Conf. on Intelligent Robots and Systems (IROS)*, pages 2076–2082, San Francisco, USA, Sept. 2011.
- [49] R. Reilink, S. Stramigioli, and S. Misra. 3D position estimation of flexible instruments: marker-less and marker-based methods. *International Journal of Computer Assisted Radiology and Surgery*, 2012. Published online.
- [50] R. Reilink, S. Stramigioli, and S. Misra. Image-based pose estimation of an endoscopic instrument. In *Proc. IEEE Int'l. Conf. on Robotics and Automation (ICRA)*, pages 3555–3556, May 2012.

- [51] R. Reilink, S. Stramigioli, and S. Misra. Pose reconstruction of flexible instruments from endoscopic images using markers. In *Proc. IEEE Int'l. Conf. on Robotics and Automation (ICRA)*, pages 2939–2943, St. Paul, MN, USA, May 2012.
- [52] R. Reilink, S. Stramigioli, and S. Misra. Image-based hysteresis reduction for the control of flexible endoscopic instruments. *Mechatronics*, 2013. Under review.
- [53] SciPy: scientific tools for Python, URL: www.scipy.org.
- [54] R. E. Sedlack and J. C. Kolars. Validation of a computer-based colonoscopy simulator. *Gastrointest Endosc*, 57(2):214–8, Feb. 2003.
- [55] S. Stramigioli and H. Bruyninckx. *Geometry and Screw Theory for Robotics*. Seoul, Korea, 2001.
- [56] TNO. *TNO test for stereoscopic vision*. Laméris Ootech BV, 1972.
- [57] E. Trucco and A. Verri. *Introductory Techniques for 3-D Computer Vision*. Prentice Hall, 1998.
- [58] N. van der Stap, R. Reilink, S. Misra, I. A. M. J. Broeders, and F. van der Heijden. The use of the focus of expansion for automated steering of flexible endoscopes. In *Proc. 4th IEEE RAS/EMBS Int'l. Conf. on Biomedical Robotics and Biomechanics (BioRob)*, pages 13–18, June 2012.
- [59] P. Wang, S. Krishnan, Y. Huang, and N. Srinivasan. An adaptive segmentation technique for clinical endoscopic image processing. In *Proc. 24th Annual Conf. and the Annual Fall Meeting of the Biomedical Engineering Society*, volume 2, pages 1084–1085, 2002.
- [60] J. Waye, D. Rex, and C. B. Williams. *Colonoscopy: principles and practice*. Wiley-Blackwell, 2003.
- [61] S. Xia, S. M. Krishnan, M. P. Tjoa, and P. M. Goh. A novel methodology for extracting colon's lumen from colonoscopic images. *Journal of Systemics, Cybernetics and Informatics*, 1:7–12, 2003.
- [62] B. P. M. Yeung and T. Gourlay. A technical review of flexible endoscopic multitasking platforms. *Int J Surg*, 10(7):345–354, 2012.
- [63] S. Zhai. *Human Performance in Six Degree of Freedom Input Control*. PhD thesis, University of Toronto, 1995.

Nawoord

Tijdens mijn afstuderen heb ik meermaals gezegd: “ik ga niet promoveren”. Vooral het feit dat het mij niet genoeg praktijkgericht leek stond mij tegen. Dat ik toch aan een promotietraject ben begonnen is grotendeels te danken aan de opdracht die voor mij beschikbaar was: ontwerp een robotisch systeem om intuïtief een geavanceerde flexibele endoscoop te bedienen. Een opdracht waar naast theoretische ook ruim voldoende praktische uitdagingen in zaten, en met een duidelijke toepassing in de klinische praktijk. Voor het onderzoek dat in dit proefschrift is beschreven heb ik uiteindelijk enkel proefopstellingen gebruikt die nog ver van praktische toepassing zijn. Echter, de opstelling waarin alle verschillende modules van het onderzoek gecombineerd worden nadert op het moment van schrijven zijn voltooiing. Deze opstelling is al veel dichterbij toepassing in de klinische praktijk, en dat is toch waar het uiteindelijk om gaat.

Natuurlijk heb ik mijn resultaten niet in mijn eentje bereikt. Ik ben dankbaar dat Stefano mij destijds heeft overgehaald om deze uitdaging aan te nemen, en mij tijdens het project ook steeds wist te inspireren om weer de volgende stappen te maken. Sarthak kwam bij de groep toen ik ongeveer een jaar onderweg was. De eerste paar keer dat ik mijn papers terug kreeg schrok ik flink van de strepen en opmerkingen. Terugkijkend zie ik dat dit me wel veel heeft geholpen om mijn vindingen kort en duidelijk op te schrijven. Zonder de nodige druk om te schrijven zou ik nu niet zoveel gepubliceerd hebben. De klinische motivatie voor mijn onderzoek kwam van Ivo. De bezoeken aan het Meander ziekenhuis en het bijwonen van verschillende interventies was erg nuttig. Niet alleen inhoudelijk, maar het gaf mij ook motivatie, omdat het mij liet zien dat er met robotica echt winst te halen is in de zorg. Astrid hielp bij het ontwerp van de ‘human-subject’-experimenten en de evaluatie van de resultaten hiervan. Bedankt voor je medewerking en voor je adviezen. Voor discussie over beeldbewerking kon ik terecht bij Ferdi. Bedankt dat je altijd je deur open had voor advies.

Mijn collega’s wil ik bedanken voor de leuke tijd op de vakgroep, in het bijzonder mijn kamergenoten Bayan, Maarten en Jeroen. Carla en Jolanda, Gerben, Marcel en Alfred, bedankt voor jullie ondersteuning.

Ik heb tijdens mijn promotie mogen werken met maar liefst vier studenten: Gart, Nicole, Nanda en Esther. ‘Mogen’, want jullie hebben alle vier een waardevolle bijdrage geleverd aan mijn werk. Bedankt daarvoor! Daarnaast was het natuurlijk ook gewoon gezellig, op de vakgroep, bij de IROS in San Francisco en tijdens een weekendje duiken in Utrecht.

Michel, jij schreef het subsidievoorstel dat ten grondslag lag aan mijn promotieplaats. Daarvoor ben ik je dankbaar, alsook voor de ervaringen op de IROS conferentie in Taiwan, gevolgd door onze mooie roadtrip. Ik ben je excuses verschuldigd voor de vele keren dat ik commentaar had op jouw soldeerkunsten en andere praktische vaardigheden in het lab.

Ludo, jij hebt de afgelopen periode laten zien dat mijn commentaar op jouw praktische vaardigheden tijdens ons afstuderen onterecht was. Met jou en Jos de bier-Segway bouwen was een prachtig project. Ik ben je ook dankbaar voor de nuttige discussies over manifolds, tangent spaces, twists en Jacobians die mij hielpen met de theoretische onderbouwing van mijn werk, en natuurlijk ook voor de gezelligheid zowel bij de koffie op de vakgroep als buiten werktijd. Dikwijls kwam in zo'n gezellige discussie ook wel weer één of ander wiskundig concept voorbij wat mij soms ook weer nieuwe inzichten gaf voor mijn onderzoek.

Samen met Almar zijn we met z'n drieën nu alweer twee jaar actief met IEP en Python. Ons gezamenlijke programmeerwerk, nu ook met Science Applied, geeft mij steeds weer voldoening. Het gebruik van IEP en Python heeft mij enorm geholpen bij mijn onderzoek. Ludo en Almar, bedankt hiervoor!

Sjoerd, ik wil jou bedanken voor de vele leerzame en gezellige zaterdagen dat we samen aan ons videosysteem 'Ethercam' gewerkt hebben. Ook al zijn we er dan (nog) niet rijk mee geworden, de kennis over embedded Linux, video-bewerking en gstreamer is mij tijdens mijn onderzoek nog veelvuldig van pas gekomen. Ook de Latex-kennis die we samen opdeden tijdens het schrijven van het Compendium heeft me nog vaak geholpen.

Gelukkig is er meer dan werken alleen. Ontspanning is belangrijk en waar kun je dat nou beter doen dan onder water. Het is niet voor niets dat mijn laatste stelling luidt: 'wie wil duiken moet niet drijven'. Bedankt Erik en Saskia voor jullie gezelligheid de afgelopen jaren, niet alleen bij het duiken maar ook tijdens samen eten en een spelletje spelen of bij het klussen waarbij Saskia oplet dat Erik en ik voorzichtig doen. Anneke, Xavier, Hanna, Patrick, Steven, Renske, Siebren, Robbert, Bas, Ingmar, Charlotte, Marijn, Fokke, Tom, Ester, Claire en alle anderen, bedankt voor jullie gezelligheid zowel rond het duiken als daarbuiten.

Tijdens mijn promotie was ik ook altijd welkom bij de familie Koorn. Joke, Ruud, Marthijn en Wouter, bedankt voor jullie gastvrijheid. Ik heb me steeds weer uitstekend vermaakt met klussen in en om de boerderij en aan de Fiat. Iets doen met je handen was een welkome afwisseling van een week voornamelijk met je hoofd werken.

Derk en Karin, ook bij jullie kon ik altijd goed even ontspannen. Bedankt voor alles. Derk, jou ben ik in het bijzonder dankbaar voor de leuke en nuttige elektronica-knutsel-sessies en de leuke tijd dat we in Enschede samen woonden.

Pap en mam, bedankt voor jullie voortdurende steun en interesse. De liefde voor wetenschap en techniek die ik met de paplepel kreeg ingegoten heeft mij in staat gesteld dit te bereiken.

Lieve Evelien, jij hebt de laatste periode van mijn promotie zoveel leuker gemaakt. Bedankt voor je ondersteuning, zo af en toe een duwtje in de rug en bovenal je liefde.

Rob
Enschede, februari 2013

About the author

Rob Reilink was born in Waspik, the Netherlands on October 6th, 1983. After completing high school at Het Assink in Haaksbergen, he started his study Electrical Engineering at the University of Twente in 2001. During his study, he joined the Solar Team Twente in 2004 in designing and building a solar-powered vehicle. In 2005 the team competed in the World Solar Challenge, crossing the Australian continent. In 2006, he visited the Massachusetts Institute of Technology (MIT), joining over 60 international students in designing and building four environmentally friendly vehicles at the MIT vehicle design summit. He received the B.Sc. degree in 2007.



For his M.Sc. studies, he returned to Australia for his internship at Tritium Pty. Ltd., Brisbane, where he developed a battery balancing system for electric vehicles. After returning to The Netherlands, he did his M.Sc. research at the Robotics and Mechatronics group of the University of Twente. The topic was the design the vision system for a humanoid head. He received the M.Sc. degree with honors in 2008.

Following his M.Sc. studies, he started his Ph.D. research at the same group. Within the Teleflex project, his focus was on the control of flexible endoscopes and instruments. His research interests are on robotics, computer vision, and visual servoing.

